

ALBERT-LUDWIGS-UNIVERSITÄT, FREIBURG IM BREISGAU
FAKULTÄT FÜR PHYSIK

DIPLOMARBEIT / DIPLOMA THESIS

The calibration of the vector polarimeter POLIS

CHRISTIAN BECK



angefertigt am
Kiepenheuer-Institut für Sonnenphysik, Freiburg
April 2002

Abstract

In this diploma thesis, the calibration of the new vector polarimeter POLIS will be described. The instrument is built by the Kiepenheuer-Institut für Sonnenphysik (KIS, Freiburg, Germany) in cooperation with the High Altitude Observatory (HAO, Boulder, USA). It will be operated at the German Vacuum Tower Telescope (VTT) in Tenerife.

The instrument yields simultaneously the polarization state of light in two spectral ranges at 396 nm and 630 nm. The measurement is performed with a rotating retarder, which modulates the incident polarization. The modulation is transformed into a varying intensity through polarizing beamsplitters. The demodulation uses a weighted integration scheme to obtain the full Stokes vector of the radiation.

To achieve a sufficient polarimetric accuracy of 0.1 % of the continuum intensity, it is necessary to calibrate the polarimeter and remove the instrumental polarization due to the telescope.

The calibration of the polarimeter is performed through the evaluation of the calibration data set. This data is produced with a calibration unit consisting of a linear polarizer and a retarder. Both elements are placed in rotatable mounts and can be steered by remote control. The calibration unit will be placed inside the vacuum tank at the VTT Tenerife.

The polarimeter response function or \mathbf{X} -matrix can be determined from a comparison between created input and measured output. The calibration data images have to be corrected for the detector properties before, which can be achieved with additional flatfield and dark current data. The application of the inverse matrix \mathbf{X}^{-1} removes the properties of the polarimeter from measured data.

The instrumental polarization of the telescope, which changes the Stokes vector incident from the sun, will be removed through the usage of a model of the polarimetric properties of the telescope. The optical elements in the telescope are modelled by appropriate Mueller matrices with free parameters. To calculate the total optical train, it is necessary to consider the specific geometry of the light path at each moment of time. For this purpose a numerical approach was developed that can be applied to other optical setups as well, if the beam path is known. The free parameters in the telescope model will be derived from a least-square-fit to telescope calibration data. Similar to the polarimeter calibration, known input states can be created with an array of polarizing sheets, which can be placed either on top of the first mirror or on top of the entrance window of the vacuum tank. The corresponding measurements should allow to obtain the required parameter values, after the polarimeter properties have been removed by the application of \mathbf{X}^{-1} .

Due to the delayed setup of POLIS, data from the Advanced Stokes Polarimeter (ASP) is used to display the calibration steps and probable results. The last chapter presents a preliminary evaluation of two data sets from the ASP.

Contents

1	Introduction	5
2	Solar physics & polarized light	7
2.1	Solar magnetism	7
2.2	The Zeeman effect	9
2.3	The theoretical description of polarized light	11
2.3.1	The Stokes formalism	12
2.3.2	The Mueller matrix calculus	13
3	Vector polarimetry	15
3.1	A dual beam polarimeter with rotating retarder	15
3.2	The measurement process	16
4	The vector polarimeter POLIS	19
4.1	The predecessor of POLIS: The Advanced Stokes Polarimeter	19
4.2	The design of POLIS	22
4.2.1	Optical layout	22
4.2.2	The modulator unit	23
4.2.3	The scan mirror	25
4.2.4	Observed spectral lines	27
4.3	Summary: Characteristics and intended usage of POLIS	28
5	The calibration of POLIS	31
5.1	Polarimeter calibration	31
5.1.1	Polarimeter calibration data	32
5.1.2	Flatfield & dark current data	32
5.1.3	Data reduction	33
5.1.4	Determination of the polarimeter response function	34
5.2	Telescope calibration	36
5.2.1	The telescope model of the vacuum tower telescope in Tenerife	36
5.2.2	Telescope calibration data	46
6	Observations with the ASP: evaluation of polarimetric data	53
6.1	Measurement data: size and content	53
6.2	Evaluation of the Stokes V signal	55
6.2.1	The zero-crossing velocity	55
6.2.2	Net circular polarization	57
	Bibliography	63
A	The Mueller matrices	65
B	Alignment of the polarimeter calibration unit	69

C	The analytical telescope model: discussion and comparison	73
C.1	The analytical solution of the telescope model	73
C.1.1	Position of the second coelostat mirror	73
C.1.2	Analytical equations	73
C.2	Mirror matrix for optical thick coatings	74
C.3	Discussion and comparison of model results	74
D	Technical characteristics	77
D.1	The grating	77
E	Many thanks to	79
F	Zusammenfassung (in german)	81
	Glossary	83

Chapter 1

Introduction

" These results leave no doubt in my mind that the doublets and triplets in the sun-spot spectrum are actually due to a magnetic field." G.E.Hale (1908)

The sun as the nearest and for us most important star is known for centuries to show activities of periodic and random character, the most prominent being the sun spots. The key feature of solar physics was already well known at the beginning of the last century, but many of the details still are far from being understood.

The only sources of information available for ground observations on earth are some of the particles in the solar wind, and a limited range of the solar spectrum, which can penetrate the atmosphere of the earth. From spectroscopic examinations of the sunlight a number of discoveries were made, for example the detection of helium through its absorption lines. The combination of spectroscopy with polarimetric measurements permitted G.E.Hale to prove the existence of magnetic fields on the solar surface and obtain the value of the field strength.

The polarimeter POLIS¹ could be regarded as a refined version of these first measurements. The basic physics of the polarization of light, the Zeeman effect and its interpretation has changed only little. Major technical improvements are increased spectral and spatial resolution, enhanced sensitivity of detectors, faster data acquisition and storage, and a more complicated calibration procedure to remove most polarization effects of non-solar origin.

The main difference to the observations at the beginning of the 20th century is the vector polarimetry, which allows the calculation of the vector magnetic field, i.e. field strength and direction. This technique has been successfully applied in a number of instruments, for example the Advanced Stokes Polarimeter (ASP). But most of these instruments have a certain drawback: the needed spectral resolution requires the restriction on one spectral line. The magnetic field configuration can then only be established in a limited height in the solar atmosphere, where this absorption line is formed.

This is the point, that makes POLIS an improvement to existing high resolution instruments. It has been designed for the simultaneous polarimetry in two spectral lines, which originate in different heights in the solar atmosphere, a FeI-line from the photosphere and a CaII-line from the chromosphere. This offers the opportunity to reconstruct the magnetic field at two heights over the same region at the same time. Moving the region of measurement on the solar image in the focal plane a data set is obtained, which contains information from all three spatial dimensions.

The additional dimension of the data, the height information, allows to build a consistent model of the magnetic field lines from the photosphere up to the chromosphere. Simultaneous observations with the Tenerife Infrared Polarimeter (TIP) will be possible in the future, adding information from the lower photosphere. But the calculation of the vector magnetic field has one requirement: the observed polarization signal has to be of only solar origin.

To achieve a sufficient polarimetric accuracy two main points are of importance. The proper polarimeter has to be considered, which is calibrated to check its response to polarization. Secondly, the instrumental

¹Polarimetric Littrow Spectrometer, built in cooperation with the High Altitude Observatory (HAO) at the Kiepenheuer Institut für Sonnenphysik, Freiburg (KIS). POLIS is intended to be used at the German Vacuum Tower Telescope (VTT) in Tenerife.

polarization due to the telescope, at which the polarimeter is used, has to be removed.

This thesis will start with a short summary on solar magnetic phenomena, and their influence on the polarization of light, in chapter 2. The Stokes formalism is introduced to describe the properties of polarized light. In connection with the Mueller matrix calculus it is the theoretical base of the measurement and the evaluation of data. Chapter 3 explains the method of the measurement of the polarization state, which is used for POLIS. The instrument and its predecessor, the ASP, are described in detail in chapter 4. The scientific goals of POLIS will be formulated in the context of theory and instrumental design. Chapter 5 develops the calibration of the polarimeter, and the model for the polarization properties of the VTT Tenerife, where POLIS will be installed. The thesis finishes with an examination of observations with the ASP in chapter 6, which are similar to a part of the data POLIS will hopefully make available.

During the thesis it got clear that the main difficulty was -and will be- the telescope model for the VTT. Unfortunately this problem can not be rigidly discussed without actual measurements with POLIS at the VTT.

To state it at least once, most of the work executed by the author was to translate the theoretical concepts and methods of the calibration into a set of program routines. The routines are supposed to almost automatically perform the calibration from the respective data sets. The routines must allow an external observer with no additional knowledge on the instrument to obtain calibrated measurement data in about half an hour after the observation. If that goal was achieved will also have to be tested in Tenerife.

Chapter 2

Solar physics & polarized light

"*Evershed's recent spectroheliographic results indicate that there is an outward flow, parallel to the photosphere, from the center of sunspots at the iron level,...*" G.E.Hale (1910)

The following description of solar magnetic phenomena is far from complete. It especially concentrates on topics, which can be displayed from the examination of polarimetric data performed by the author himself in chapter 6. For words in *italics* a short explanation can be found in the glossary on page 83.

2.1 Solar magnetism

The activities on and of the sun include a number¹ of phenomena like:

- sun spots
- flares
- coronal mass ejections
- the sun spot cycle
- the solar wind
- total solar luminosity.

Some of them are of no or little concern to us, while others like solar storms or variations of the total solar luminosity can influence the existence of life on our planet. Today most of these features are supposed to result from an interaction between the material motions of a *gas plasma* of electrons and ionized atoms and *magnetic fields*.

The basic feature most suited to display this interaction are also the most prominent structures on the sun, the sun spots. Fig. 2.1 displays a high resolution intensity image of a typical spot near the disc center.

Sun spots have been reported as early as in the 17th century after the invention of the telescope. They appear as darker areas on a bright background. The first and simplest explanation is that they are cooler than their surroundings. This has been proven by the observation of absorption lines from molecules, which dissociate at higher temperatures, in the spectra of spots. This leads to the next question, namely why are they 'cool' ?

A hint to the answer were the observations made by G.E.Hale in 1908², where the Zeeman effect was used to measure the magnetic field strength in sun spots. The existence of these fields was suspected, because photographs in the H_{α} spectral line "suggest that all sun spots are vortices"³. It is a consequence

¹For a more detailed overview see for example M.Stix, *The sun* , [26].

²G.E.Hale, *On the probable existence of a magnetic field in sun spots* , [7], ApJ **28**, 1908

³[7], p. 315

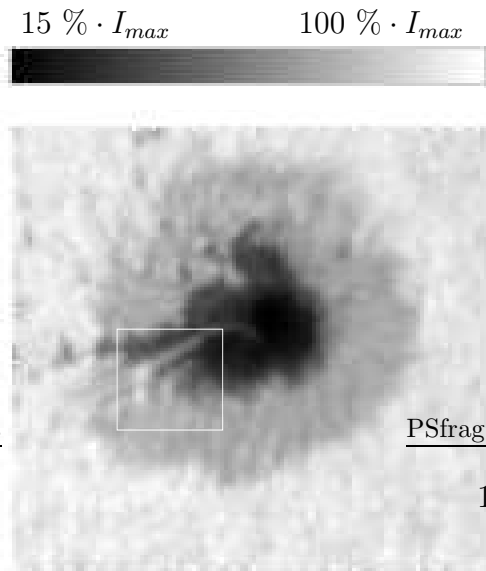


Figure 2.1: Sunspot near disc center, continuum intensity. The image area is $62'' \times 55''$, ASP data from 10.2.2000 (courtesy M.Sigwarth). The suppression of convection by the magnetic field causes a decrease in temperature and emitted intensity. Inside the spot the dark umbra can be distinguished from the brighter penumbra. The rectangle marks an area with a radial oriented substructure in the penumbra of the spot, extending into the umbra as well.

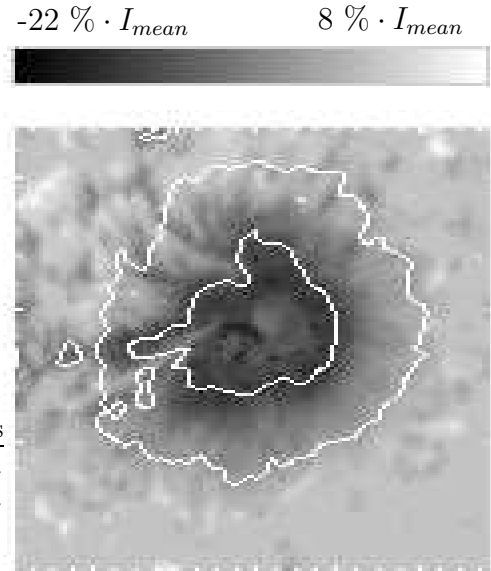


Figure 2.2: The signed Stokes-V amplitude with superimposed borders of the umbra and penumbra from the continuum image.

The Stokes-V amplitude is proportional to the line-of-sight component of the magnetic field, while the sign indicates the direction of the field to (+) or away (-) from the observer. The magnetogram is constructed from the amplitudes in the Stokes V signal, see section 6.2 for details.

of Maxwell's laws, that these moving charges, or in other words, a current, induced a magnetic field. Even as it was proven later by velocity measurements with the Doppler shift that the supposed whirling motion did not exist at all, the results from Hale's observations were non-ambiguous: in sun spots existed magnetic fields of about 2900 Gauss⁴ (or 0.29 Tesla⁵ in SI units). Fig. 2.2 displays the existence of the magnetic field, as the shown Stokes-V amplitude is proportional to the line-of-sight (LOS) component of the magnetic field.

The decrease of the temperature in sun spots is no direct result of the magnetic field, only in connection with the conditions prevailing on the sun can this be achieved. The upper layers of the sun's atmosphere transport energy mainly by *convection*, in difference to the *radiative* core. The convection can be seen as *granulation cells* on the surface of the sun. In sun spots this convection is suppressed, because the plasma can only move along the magnetic field lines and not normal to them.

Like the sun spots most other solar features are coupled to magnetic fields influencing material motions or vice versa:

- The magnetic field appearing later in sunspots is supposed to be caused by the *solar dynamo*, which generates it from convective motion and the *differential rotation* of the sun. A comparison with other active stars shows a strong dependence on the velocities of the material motions⁶.
- The structure of the *corona* is dominated by field lines, building magnetic *loops* or *filaments*. Regions with open field lines are the origin of the *solar wind*.

⁴[7], p. 325

⁵1 Tesla = 1 Vs/m² = 10000 Gauss

⁶see K.G. Strassmeier, *Aktive Sterne*, [27]

- Flares or coronal mass ejections consist of a massive energy release in a short time. The energy is assumed to result partly from *magnetic reconnection*. These outbursts lead to an acceleration of ionized material, which may eventually hit the atmosphere of the earth, causing polar lights.
- Sun spots can be stable for some weeks, while their surrounding is permanently changing. In this case the strong magnetic field dominates over other dynamical influences.
- Sun spots exhibit internal structure like the division into umbra and penumbra. The penumbra has a substructure with varying magnetic fields. On the static background field of the sun spot moving *penumbral grains* hint to mass motions.
- The *Evershed flow* as a global phenomenon in sun spots also indicates a systematic mass flow, approximately radially outwards from the spot center.

To understand the features appearing on the sun two different environment parameters have to be known: the velocity and direction of mass motions, which can be measured at least in the line-of-sight (LOS) with the *Doppler shift*, and the magnetic field. For the first part one can use a spectrograph to obtain resolved spectral lines, the second part is the task of *polarimetry*. As the magnetic field influences the shape of the intensity spectrum and the polarization of the radiation, it is possible to invert this process and reconstruct the magnetic field from polarimetric data measured by instruments like POLIS.

2.2 The Zeeman effect

G.E.Hale made use of the splitting of spectral lines due of the Zeeman effect to prove the existence of magnetic fields on the sun. This method works without taking into account any polarization effects, because in fields of sufficient strength the splitting can be seen in the spectrum of the intensity⁷. The required field strength depends magnetic sensitivity of the spectral line used. One has to use additional polarimetric information to obtain the field direction, or for weaker fields, due to the line broadening by collisions and random motions.

The Zeeman effect describes the change of the energy of atomic levels in the presence of a magnetic field⁸. Its main feature is to break the energy degeneracy of atomic levels with different quantum number m , which is the case for an undisturbed atom. The actual fields on the sun are 'weak' in the terminology of atomic physics. The so called Russel-Saunders coupling of the angular momentum⁹ \mathbf{L} and the electron spin \mathbf{S} to the total angular moment \mathbf{J} can be assumed. If the magnetic field \mathbf{B} is taken to be $(0, 0, B_z)$ ¹⁰, the problem can be solved in the following way:

- $\mathbf{J} = \mathbf{L} + \mathbf{S}$, where $|\mathbf{L} - \mathbf{S}| \leq J \leq |\mathbf{L} + \mathbf{S}|$
- the quantum number m_j can have the $(2J+1)$ values $-J, -J+1, \dots, J-1, J$ for a fixed value of J
- the energy level corresponding to m_j is corrected by a value $\Delta E_{B, m_j}$, for which perturbation theory yields

$$\Delta E_{B, m_j} = \mu_B g_j m_j B \quad (2.1)$$

where $\mu_B = \frac{e\hbar}{2m_e c}$ is Bohr's magneton and the Landé factor g_j is calculated by

$$g_j = 1 + \frac{J(J+1) + S(S+1) - L(L+1)}{2J(J+1)} \quad (2.2)$$

This result can best be visualized with an example like Fig. 2.3, using one of the spectral lines observed by POLIS. The transition is one of neutral iron (FeI) with a rest wavelength around 630.25 nm. The

⁷Hale's measurement method was the comparison with a spectral line produced with a spark and a electromagnet of known field strength, [7], p. 325f.

⁸For a detailed discussion see for example Mayer-Kuckuck, *Atomphysik*, [15], or any textbook on quantum mechanics.

⁹Both vectors and matrices will be printed bold, the context should exclude confusions.

¹⁰This is assumed everywhere in the following text, if not especially mentioned otherwise.

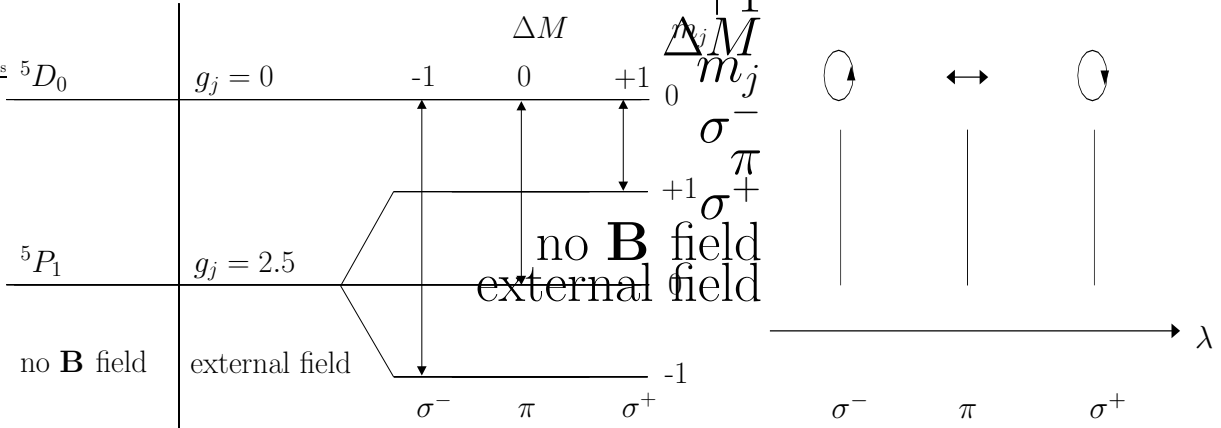


Figure 2.3: (left) Zeeman splitting of the FeI line at 630.25 nm. The notation is $^{2S+1}L_J$. (right) Resulting spectrum in the external field.

The upper level remains unaffected by the magnetic field, as $\mathbf{J} = 0$, and also the Landé factor g_j . The lower splits into three different levels. The possible dipole transitions π , σ^+ and σ^- are coupled to a fixed polarization each, corresponding to linear and left or right circular polarized light, depending on the value of ΔM . The π -component lies at the wavelength of the undisturbed transition.

lower level 5P_1 splits into three energetically different equidistant levels, while the upper level cannot split up ($\mathbf{J} = 0 \rightarrow m_J = 0$, $g_j = 0$). The three possible dipole transitions π , σ^+ and σ^- differ in wavelength¹¹ as well as in the polarization state. A transition with $\Delta M = 0$ corresponds to linear and $\Delta M = \pm 1$ to right respectively left circular polarized light. The resulting spectrum consists of three different polarized spectral lines instead of a single unpolarized one.

The case just discussed is the simplest that can happen. If the Landé factors are not zero for both levels, one has to calculate all energy levels, and use the rules for dipole transitions¹² to obtain the allowed transitions. Usually a spectral distribution results, in which lines of different polarization are mixed. Fortunately it is often possible to use an *effective* Landé factor to group lines with the same polarization to reach an analogon to the situation depicted.

The importance of the observation of the polarization does not lie in the calculation of the absolute field strength. This would for example be possible from the distance between the two circular polarized components, if they are measured separately. The circular components would lie at different wavelengths in the spectrum, even if the splitting can not be resolved in the intensity profile due to the line broadening. A classical treatment of the Zeeman effect¹³ reveals that in the strength of the different polarization components the information on the direction of the magnetic field is also included.

The motion of an electron around an atomic nucleus is considered there as an oscillation in three dimensions, with a central force given by the coulomb attraction. This system is disturbed by the presence of the magnetic field, which leads to a Lorentz force $\propto \mathbf{v} \times \mathbf{B}$. This results in three different oscillation frequencies depending on the sense of revolution in the x-y-plane, while movement parallel to the z-axis is not influenced. Figure 2.4 gives a symbolical sketch of the situation: on observation parallel to the magnetic field, i.e. looking down on the x-y-plane, only the two circular polarized components ω_1 and ω_3 can be seen, as the radiation characteristic of an electric dipole forbids emission in the oscillation direction (*longitudinal* Zeeman effect). If one observes in the x-y-plane normal to the magnetic field lines, one sees three distinct linear polarized lines at the frequencies ω_i with $i=1,2,3$ (*transversal* Zeeman effect).

From the strength of the single polarization components relative to each other and their spectral position, i.e. the displacement from the zero level of undisturbed ground state transitions, one has enough information to obtain absolute strength as well as the direction of the magnetic field. The intensity spectrum in

¹¹ $E_\gamma = h \cdot \nu = h \cdot c / \lambda$, and $E_\gamma = E_0 (\rightarrow \pi)$ respectively $E_0 \pm \Delta E_{B,m_j} (\rightarrow \sigma^\pm)$.

¹²See for example W. Demtröder, Band 3 : *Atome, Moleküle und Festkörper*, [5], p. 205f.

¹³Collett, [4], chapter 18.

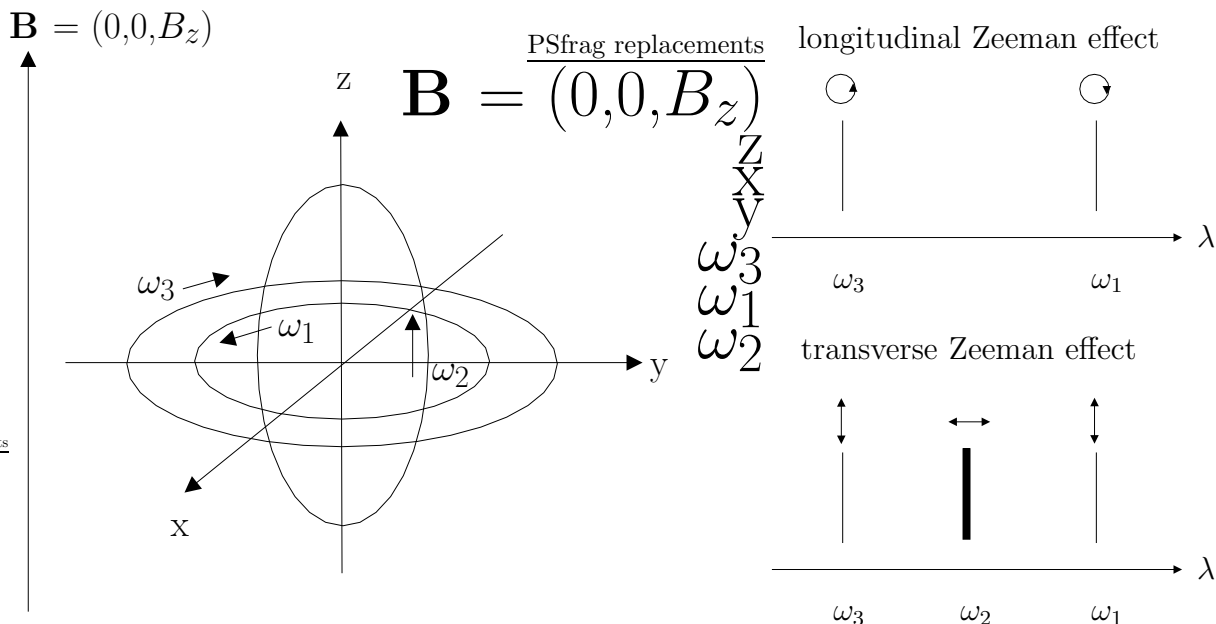


Figure 2.4: (left) A symbolic sketch of the classical treatment of the Zeeman effect.(right) Resulting spectra for observation along and perpendicular to the magnetic field.

The rotation of an electron around the atomic nucleus in an external field results in different rotation frequencies ω_i corresponding to the three wavelengths. The frequencies depend on the sense of direction of the rotation and the differences are caused by the Lorentz force $\mathbf{v} \times \mathbf{B}$, with $\omega_1 (\sigma^+) < \omega_2 (\pi) < \omega_3 (\sigma^-)$. On observation parallel to the z-axis one can only see the two circular components ω_1 and ω_3 because of the radiation characteristic of a dipole (longitudinal Zeeman effect). On observation in the x-y-plane normal to the magnetic field there are three linear polarized oscillations with the frequencies ω_i (transverse Zeeman effect). From the relative strength of the components one can, as the direction of observation is known, retrieve information on the direction of the magnetic field.

Fig. 6.1 from actual observations shows the discussed necessity of polarization measurements: even if the spectral line with the greatest Landé factor splits visibly, the position and intensity of the components can not be established accurate enough due to the doppler broadening of the line.

The usual way to obtain the magnetic field from observational data is an inversion, i.e. the comparison of observed with synthetic line profiles from a model atmosphere. The model atmosphere includes open parameters like field strength and field direction, which are adjusted until the synthetic profiles match the observation.

The effects discussed here concerning an *emission* line can be also applied on the actual measured *absorption* line.

2.3 The theoretical description of polarized light

The Zeeman effect produces linear or circular polarized light. In combination with the geometrical aspects of observation direction and inclination of the magnetic field at last an arbitrary polarization is usually obtained. The description to be used must therefore be capable of including all possible states of polarization¹⁴.

¹⁴Also totally unpolarized light, which proves to be difficult to describe, and even more difficult to artificially produce.

2.3.1 The Stokes formalism

The Stokes formalism was formulated around 1850 by Sir G.E.Stokes. The derivation given here follows Collett, [4], Chapter 2-4.

The starting point is the wave character of light, which was the only existing view at the times of Stokes. The electric and magnetic vector fields are supposed to be the solutions of a wave equation, which was only later really proven by Maxwell's laws. This empirical approach was motivated by many interference experiments, which found their natural explanation in a wave character. Most of the basic optical effects can be understood by using a wave equation taken from mechanics, namely

$$\Delta \mathbf{u}(\mathbf{r}, t) = \frac{1}{\nu^2} \frac{d^2}{dt^2} \mathbf{u}(\mathbf{r}, t) , \quad (2.3)$$

where $\Delta = \frac{d^2}{dx^2} + \frac{d^2}{dy^2} + \frac{d^2}{dz^2}$, ν is the oscillation frequency, $\mathbf{r} = (x,y,z)$, and the components u_x , u_y and u_z are three displacements dependent on place and time.

The interference experiments of Fresnel and Arago (1816) showed, that light can only perform *transversal* oscillations and no *longitudinal* ones¹⁵, which can also be derived from Maxwell's laws. If the z-axis always is parallel to the direction of the light propagation, only two field components are left.

A simple solution of equation (2.3) can be given by

$$\begin{aligned} E_x(z, t) &= E_{x,0} \cdot \cos(\omega t - kz + \delta_x) \\ E_y(z, t) &= E_{y,0} \cdot \cos(\omega t - kz + \delta_y) , \end{aligned} \quad (2.4)$$

where the displacement \mathbf{u} has been substituted by the electrical field \mathbf{E} . The longitudinal component E_z can be left out, and the solution is characterized by the values of the angular velocity, $\omega = 2\pi \cdot \nu$, the wave number, $k = 2\pi/\lambda$, the field amplitudes, $E_{i,0}$, and an arbitrary phase, δ_i .

After squaring the equations in (2.4) the equation of the polarization ellipse can be derived:

$$\boxed{\frac{E_x^2}{E_{x,0}^2} + \frac{E_y^2}{E_{y,0}^2} - 2 \cdot \frac{E_x}{E_{x,0}} \cdot \frac{E_y}{E_{y,0}} \cdot \cos \delta = \sin^2 \delta} , \quad (2.5)$$

with the phase difference, $\delta = \delta_x - \delta_y$. The argument (z,t) has been omitted.

Equation (2.5) gives the locus of points (E_x, E_y) , which are taken in the course of one oscillation, forming a general ellipse. The specific shape depends on the amplitudes $E_{x,0}$ and $E_{y,0}$, as well as on the relative phase δ . These three parameters encode the polarization state of the light beam. For example, $\delta = \frac{\pi}{2}$, and $E_{x,0} = E_{y,0}$, leads to the equation of a circle, corresponding to circular polarized light¹⁶.

With the polarization ellipse of the instantaneous field vector it is only possible to describe fully polarized light. Furthermore, it can not be used as measurement reading, as in the visible range the oscillation frequency amounts to about 10^{15} Hz, far beyond the time resolution of most instruments. The special merit of Stokes' work was the transformation of all information needed to characterize a polarization state into measurable quantities.

Without the ability to resolve the oscillation, it seems natural to imitate the measurement process possible, i.e. to average over a great number of oscillations. The time average is given by

$$\langle E_i(t), E_j(t) \rangle = \lim_{T \rightarrow 0} \frac{1}{T} \int_0^T E_i(t) E_j(t) dt . \quad (2.6)$$

If one now substitutes the time dependent values ($E_x = E_x(z, t)$) with their time averages in Eq. (2.5), one obtains after a short computation¹⁷ the equation

$$(E_{x,0}^2 + E_{y,0}^2)^2 = (E_{x,0}^2 - E_{y,0}^2)^2 + (2 \cdot E_{x,0} \cdot E_{y,0} \cdot \cos \delta)^2 + (2 \cdot E_{x,0} \cdot E_{y,0} \cdot \sin \delta)^2 . \quad (2.7)$$

¹⁵C.Beck, *Kalibration und Auswertung von ASP-Daten*, [1], Appendix C.1, or Collett, [4], Chapter 12.

¹⁶For more details compare Beck, [1], Section 2.2.2, or Collett, [4], Chapter 3.

¹⁷One can assume $z=0$. the calculation can be found in Collett, [4], p. 36.

With the terms in Eq. (2.7) the following definition of the Stokes parameters S_i , usually arranged in a vector¹⁸ for convenience, can be made:

$$\boxed{\text{Stokes parameters } \mathbf{S} = \begin{pmatrix} S_0 \\ S_1 \\ S_2 \\ S_3 \end{pmatrix} = \begin{pmatrix} E_{x,0}^2 + E_{y,0}^2 \\ E_{x,0}^2 - E_{y,0}^2 \\ 2 \cdot E_{x,0} \cdot E_{y,0} \cdot \cos \delta \\ 2 \cdot E_{x,0} \cdot E_{y,0} \cdot \sin \delta \end{pmatrix}}. \quad (2.8)$$

With different values for the phase difference ($\delta = 0, \pm\pi/2, \pi$) and the amplitudes ($E_{x,0}, E_{y,0}$), it can be seen that the Stokes parameters encompass the information on the polarization state of the light in the following way:

- S_0 is the total intensity of polarized and unpolarized light.
- S_1 is the difference of the intensity of *linear horizontal* and *vertical* polarized light.
- S_2 is the difference of the intensity of $+45^\circ$ -*linear*¹⁹ and -45° -*linear* polarized light.
- S_3 is the difference of the intensity of *right* and *left circular* polarized light.

The following Stokes vectors, which contain only one polarization state each, can be used as a base for all polarized light:

$$\mathbf{S}_{\text{unpol}} = \begin{pmatrix} 1 \\ 0 \\ 0 \\ 0 \end{pmatrix}, \quad \mathbf{S}_{\text{lin,hor/ver}} = \begin{pmatrix} 1 \\ \pm 1 \\ 0 \\ 0 \end{pmatrix}, \quad \mathbf{S}_{\text{lin},\pm 45^\circ} = \begin{pmatrix} 1 \\ 0 \\ \pm 1 \\ 0 \end{pmatrix}, \quad \mathbf{S}_{\text{circ,right/left}} = \begin{pmatrix} 1 \\ 0 \\ 0 \\ \pm 1 \end{pmatrix}. \quad (2.9)$$

In contrast to the polarization ellipse, unpolarized as well as partially polarized light is possible by linear combinations of the vectors above. The requirements on a physical sensible vector are:

$$S_0^2 \geq S_1^2 + S_2^2 + S_3^2, \quad (2.10)$$

i.e. the polarization degree $P = \frac{\sqrt{S_1^2 + S_2^2 + S_3^2}}{S_0}$ can not exceed 100 %, and of course $S_0 > 0$.

To establish the polarization state of a light beam one has to measure, with a quantitative intensity detector like a photographic emulsion or a CCD chip²⁰, the contribution of each of the polarization states in Eq. (2.9). This can be done for:

- The total intensity without any additional device.
- The linear polarizations with a polarizer under different angles, resulting in S_1 and S_2 .
- The circular polarization with a combination of polarizer and retarder²¹, resulting in S_3 .

In newer publications the notation is chosen as $\mathbf{S} = (I, Q, U, V)$. This will also be adopted here in the following.

2.3.2 The Mueller matrix calculus

Optical elements that influence the polarization state in a linear way, can be included easily into the Stokes formalism. The element is represented by a matrix $\mathbf{M} \in \mathbb{R}^{4 \times 4}$, which expresses the modifications of the base vectors performed by the device. The resulting Stokes vector \mathbf{S}' after the transmission or reflection is given by $\mathbf{S}' = \mathbf{M} \cdot \mathbf{S}$. The matrices for the commonly used optical devices can be found in

¹⁸Even though addition and a norm are defined, the Stokes vectors form no vector space in the strict mathematical sense.

¹⁹To the vertical.

²⁰A point which hindered the success of Stokes theory at first was the absence of such a detector at his time.

²¹Also called wave plate.

Appendix A. The matrix of the rotator (A.6) can be used to describe elements with an arbitrary position angle. The matrices have to be also physical sensible, i.e. they must not lead to a violation of eq. (2.10) on application, either by the introduction of negative intensities or hyper-polarization.

The calculations are simplified by the fact that most detectors can only record intensity regardless of its polarization state. A complicated optical train can be expressed by the matrix multiplication of its elements in the correct order, i.e. their place in the light path, and the selection of the intensity entry S'_0 as measurement value.

Chapter 3

Vector polarimetry

”The observer lay on his back while making the observations in the following way...” C.E.St.John (1909)

Solar magnetometry has been performed for decades now. The instruments used at the beginning differ in some respects to a vector polarimeter, as they mostly only measure the Stokes V signal. A more detailed description of such *magnetographs* can be found in M.Stix, *The sun*, [26]. This thesis also abstains from the description of the various ways to built optical elements like retarders or polarizers for the sake of shortness. The book of Shurcliff ([22]) can here be used as reference. Besides POLIS only one instrument shall be introduced in more detail in section 4.1, the vector polarimeter ASP.

To establish the full Stokes vector of a light beam always at least four intensity measurements are needed. For the 'classical' method this is the intensity produced by a linear polarizer and a retarder at four fixed angle positions. There are also various measurement methods with a single element and a continuously changing position angle¹. An extensive summary of possible methods can be found in E. Landi Degl'Innocenti, [12], (1992).

A general measurement scheme consists of two parts:

- (1) The transformation of a polarized input into a modulated intensity signal by one or more optical elements. The intensity after transmission has to be proportional to all polarization content in some way.
- (2) The demodulation, the decomposition of the modulated intensity into separate parts. Each part has to be related to
 - a single polarization state
 - a linear combination of polarization states with known coefficients.

To give only one example for an unuseable scheme: a continuously rotating polarizer would produce more than the minimal four intensity measurements, but is opaque to circular polarization, which contradicts the condition in (1).

3.1 A dual beam polarimeter with rotating retarder

POLIS² uses a rotating retarder as variable optical element. It is followed by a polarizing beamsplitter, which helps to reduce intensity loss and the influence of detector noise. The schematical design of a dual beam polarimeter with this modulation procedure is given in Fig. 3.1. The needed devices are:

¹compare [4], Chapter 6

²As the ASP is similar in many respects, it will not be especially mentioned in the following.

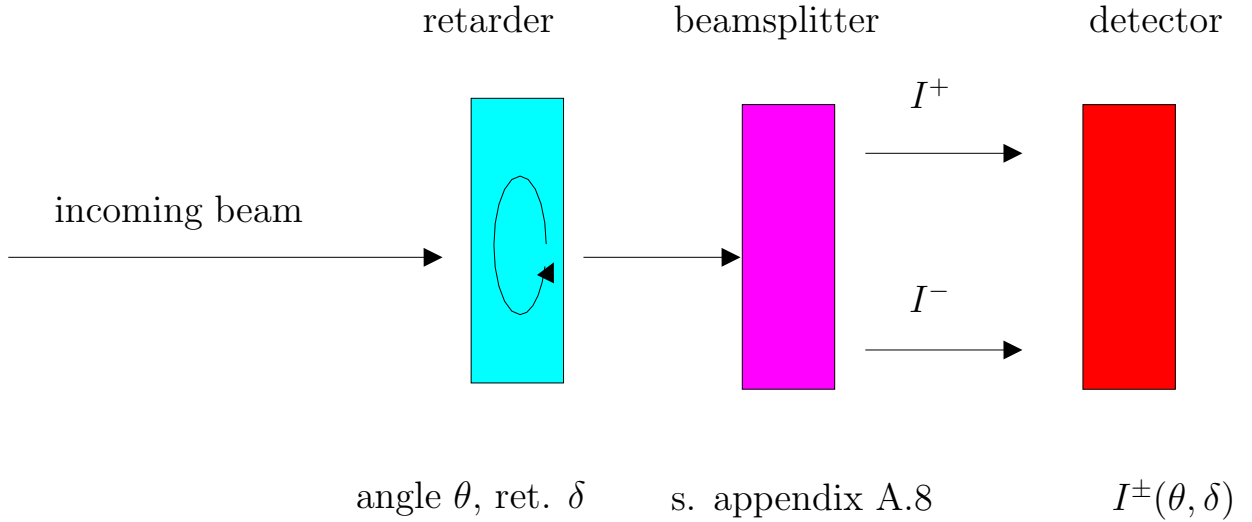


Figure 3.1: Schematic design of a dual beam polarimeter with rotating retarder.

The incoming beam from the light source hits the retarder, which is rotated continuously around the propagation direction, and modulates the polarization state. The polarizing beam splitter produces the two beams I^+ and I^- , which are registered on spatially separated regions of the detector or on two detectors. Their respective intensity $I^\pm(\theta, \delta)$ depends on the retardance, the angular position and the polarization of the incoming light.

- A retarder of known retardance, δ , which can be rotated around the direction of light propagation with the position angle of its fast axis, θ .
- A polarizing beamsplitter to produce two spatially separated beams $I^\pm(\theta, \delta)$.
- A suited set of detectors to record these intensities.

In the Mueller calculus the optical train is described by:

$$\mathbf{M}^\pm(\theta, \delta) = \mathbf{M}_{\text{beamsplitter}}^\pm \cdot \mathbf{M}_{\text{rot}}(-2\theta) \cdot \mathbf{M}_{\text{ret}}(\delta) \cdot \mathbf{M}_{\text{rot}}(2\theta). \quad (3.1)$$

The resulting intensity for the beams $I^\pm(\theta, \delta)$ can be calculated by:

$$I^\pm(\theta, \delta) = (\mathbf{S}^{\text{out}})_0^\pm = (\mathbf{M}^\pm(\theta, \delta) \cdot \mathbf{S}^{\text{in}})_0. \quad (3.2)$$

3.2 The measurement process

Executing the calculations in Eq. (3.2) the intensities I^\pm of the two beams in dependence of an incoming Stokes vector $\mathbf{S}^{\text{in}} = (I, Q, U, V)$ are obtained:

$$I^\pm(\theta, \delta) = \frac{r^\pm}{2} \{ I \pm Q \cdot (c_{2\theta}^2 + s_{2\theta}^2 c_\delta) \pm U \cdot s_{2\theta} c_{2\theta} (1 - c_\delta) \mp V \cdot s_{2\theta} s_\delta \}, \quad (3.3)$$

where $c_j = \cos j$, $s_k = \sin k$, r^\pm is the transmission coefficient for the respective beam³, and δ is the constant retardance.

Eq. (3.3) shows a constant contribution by the total intensity I , with an added modulation by the other Stokes parameters, Q, U , and V . The problem of demodulation is to isolate the individual contributions from the superposition of harmonic functions. A transformation of the single terms gives their dependency on frequency :

³Set equal to 1 in the following.

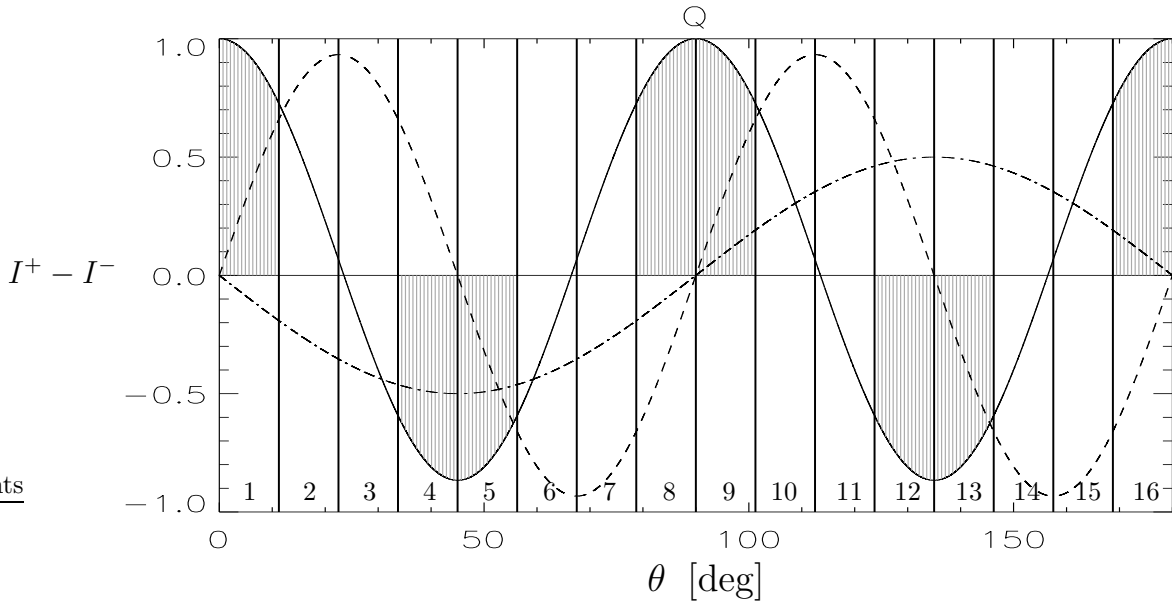


Figure 3.2: The difference of the beams $I^+ - I^-$ for an input of pure Stokes Q (*solid*), U (*dashed*), and V (*dash-dotted*).

The displayed course corresponds to the retarder position angle $\theta \in [0, 180^\circ]$. The vertical lines mark the integration steps. A slight offset of the oscillation from zero can be seen in Q, the modulation frequency is 4θ for Q and U. Only the marked areas contribute to the value of Stokes Q in the demodulation scheme (see the text for more details).

- Q is proportional to $\cos 4\theta + \text{const.}$
- U is proportional to $\sin 4\theta$
- V is proportional to $-\sin 2\theta$.

Fig. 3.2 displays this for the difference, $I^+ - I^-$, and separate input of only one polarization state, i.e. $+Q$, $+U$, and $+V$ ⁴.

There are some methods available to separate the individual contributions. One possibility would be a Fourier analysis, which gives a decomposition into single frequencies. This would need a continuously read out of the detector chips, which is impossible for CCD detectors. The method of choice for POLIS uses an integration scheme, which takes advantage of the specific shape of the modulation for each polarization component.

Using Fig. 3.2 the procedure can quickly be seen. The intensity curve for the position angle of the retarder from 0 to 180° is divided into 16 intervals, over which the intensity is integrated. The integration is done automatically by reading out the CCD chips at the interval limits. To obtain the value of a single polarization component one has to add up the integration values by a demodulation scheme with specific chosen signs.

For example the contribution from Stokes Q is calculated by taking the first and last, the 8th and 9th integration value with a + sign, the 4th and 5th and also 12th and 13th value with a - sign. By comparison with the curves for Stokes U and Stokes V it can be seen, that the integration contributions from these polarization components nullify for that choice, i.e. the value of the integration is proportional only to Stokes Q.

For each polarization a signed addition scheme can be found, in which the other components cancel out. The total intensity I can be derived by an addition of the beams, as can be seen from equation (3.3).

⁴The image was created with a simulation of a dual beam polarimeter. The retardance was set to $\delta = 150^\circ$, the actual value of the retarder used at the ASP.

The order of demodulation and subtraction or addition of the beams is not fixed. In the simulation used for the creation of Fig. 3.2 the beams are first subtracted and then demodulated. Opposite to that the data stored to file for POLIS or the ASP consists of the demodulated beams I^+ and I^- , which have to be added or subtracted afterwards. This allows the removal of individual pixel properties, and reduces the size of information to be saved.

Chapter 4

The vector polarimeter POLIS

"The instrument is presently being built at the KIS and the HAO and will be completed by the end of the year 2000." (Schmidt et al., undated poster)

POLIS stems from a cooperation between the KIS and the High Altitude Observatory (HAO) in the USA. The design of POLIS drew strongly on the heritage of the ASP¹. Due to the delayed setup of POLIS for the testing phase this thesis will have to use ASP data to demonstrate the calibration procedure and expected results. It is therefore necessary to introduce this instrument in more detail.

4.1 The predecessor of POLIS: The Advanced Stokes Polarimeter

The ASP at the Dunn VTT in New Mexico has been in operation for ten years now. Its operation proved that it is possible to achieve a high polarimetric accuracy, even at a telescope with considerable instrumental polarization, by the usage of a telescope model.

The following description refers to Fig. 4.1, displaying the optical setup of the ASP with the inclusion of the telescope tower.

The Dunn VTT differs from the German VTT in Tenerife by two things. The coelostat is mounted in an alt-azimuth configuration, leading to fixed incidence angles of 45° on the coelostat mirrors. Further, all mirrors before the polarimeter calibration unit are inside the vacuum tank. This leads to a simplification in the telescope model, as the mirror properties can be assumed to be identical.

The optical elements discussed in section 3.1, the modulator or measurement retarder, the polarizing beamsplitter, and the intensity detectors are necessary for the measurement of the Stokes parameters. Additionally now devices for spectrally and spatially resolved information are present:

- The grating disperses the modulated polarization spectrally to obtain the variation of the content with wavelength. In the images taken by the detectors the dispersion direction corresponds to columns (cp. Fig. 5.1). The grating can be moved from the wavelength range of observation to a spectral range without strong absorption lines for flat field data (cp. section 5.1.2).
- The slit restricts the area of the solar image under observation. The height in the slit corresponds to rows in the images (also cp. Fig. 5.1). A scan of a region of interest on the solar surface is performed by moving the complete spectrograph unit, including slit and detectors. These elements are all mounted on a separate optical bench, which can be shifted by a motor driven mandrel.

The polarimeter calibration unit after the exit window of the vacuum tank consists of a linear polarizer and a retarder. It is used for the calibration of all optical elements afterwards, exactly like the one of POLIS.

¹Operated by the HAO.

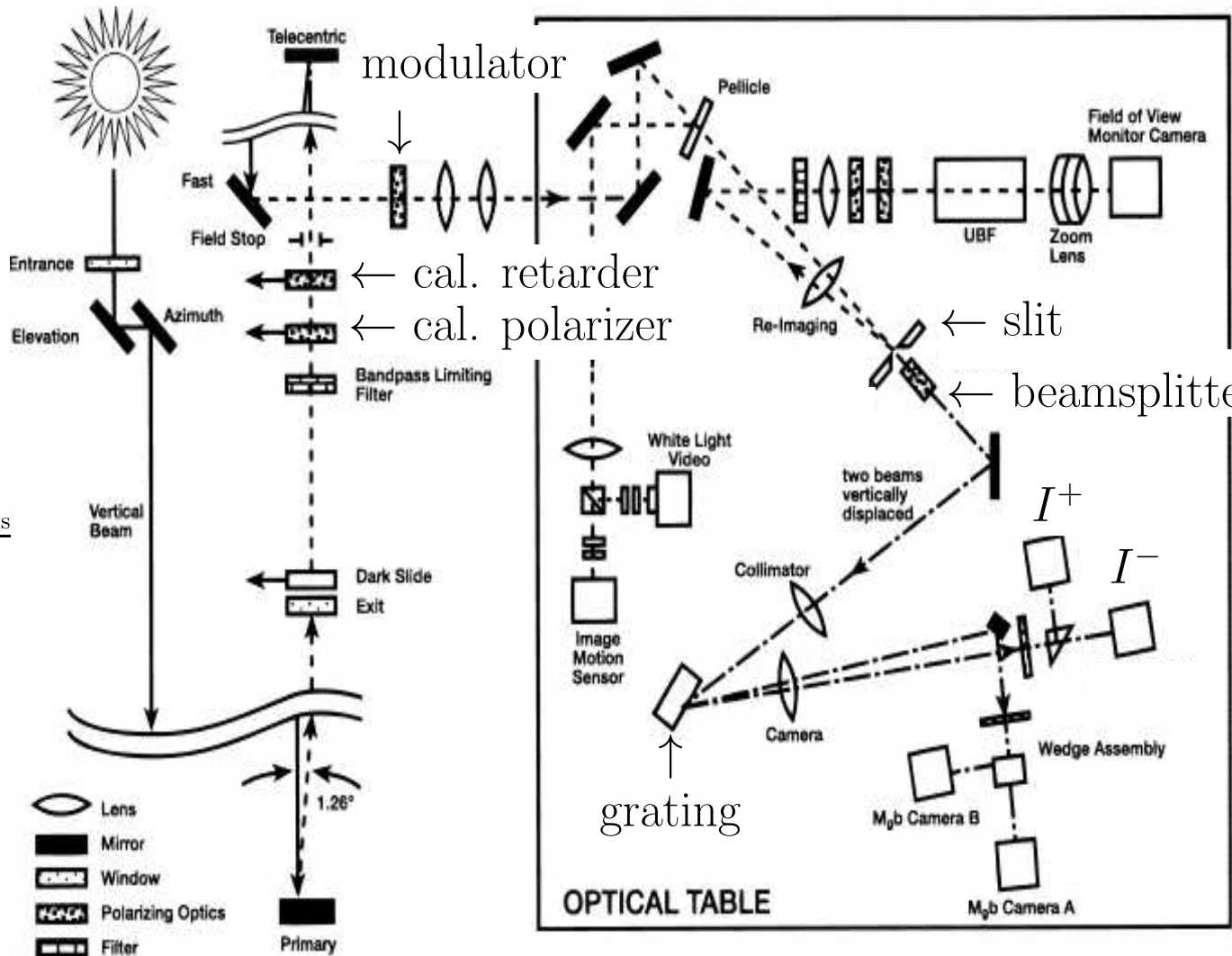


Figure 4.1: Vertical section of the ASP including the light path in the telescope. Original graph taken from [24], Fig. 2, slightly modified. The more important optical devices have been given enlarged labelling.

The optical elements described in section 3.1 are the modulator (=measurement retarder), the beamsplitter, and two CCD-cameras denoted by I^{\pm} . The slit and the grating are necessary for spatially and spectrally resolved data: the grating disperses the modulated signal, while the slit restricts the area of the solar image under observation. The slit, the following spectrograph, and the detectors are on a separate optical bench (not drawn). To scan a region of interest on the solar image it is necessary to move the whole bench by a motor driven mandrel. The mirror labeled 'Fast', directly before the modulator, compensates the image motion caused by the wedge on the modulator (cp. section 4.2.2). The calibration unit consisting of a linear polarizer and a retarder is used for a calibration of all optics between the cameras and its position.

ASP	
wavelength range	630.1-630.3 nm
spectral resolution	225000
dispersion	1.19 pm / detector pixel
scan stepwidth	$\sim 0.4''$
slit width	0.6''
integration time	2.1 s
Dunn VTT	
coelostat mounting	alt-azimuthal
main mirror diam.	152 cm
window diam. (entr./exit)	76.2 / 20 cm

Table 4.1: Instrumental characteristics of the ASP and the Dunn VTT. The telescope uses a coelostat in alt-azimuth mounting inside the vacuum tank. The wavelength range of observation is identical to one of the spectral regions observed at POLIS. The corresponding values for POLIS can be found in table 4.2.

The polarization measurement of the ASP is performed in the same wavelength range around 630 nm as for one of the spectral regions used at POLIS. Therefore the properties of the data, the calibration procedure, and to some extent the results of observations will be comparable.

The main disadvantage of the ASP is its non-permanent installation. The setup on the optical table in the right part of Fig. 4.1 has to be dismantled after an observation campaign. An improved version of the ASP is planned to be installed permanently at the Dunn VTT.

For more technical details the reader should refer to Elmore et al. (1992, [6]), while the calibration procedure is discussed in Skumanich et al. (1997, [24]). Table 4.1 summarizes the instrumental characteristics of the ASP and the Dunn VTT.

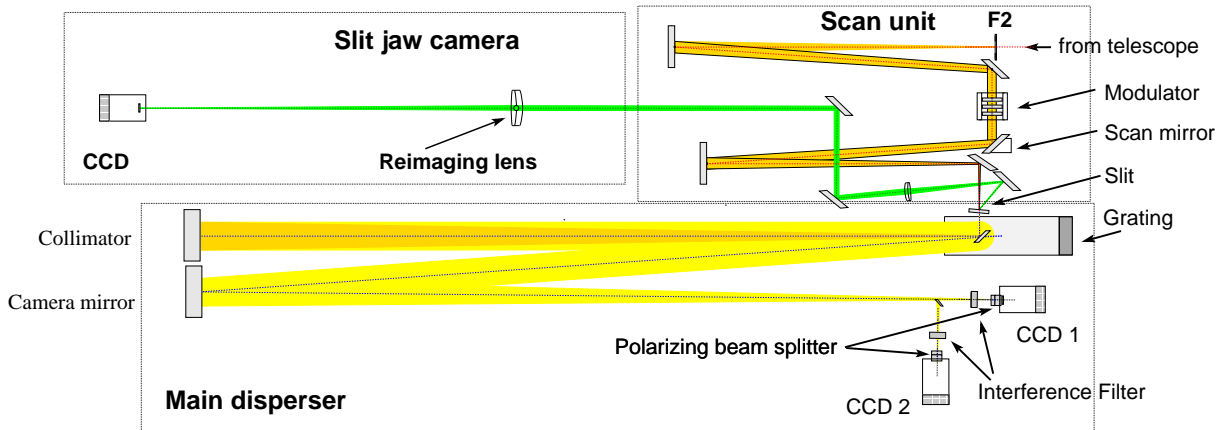


Figure 4.2: Different sections of POLIS. (*top*) Slit jaw camera and scanner unit, side view, (*bottom*) main disperser, top view. The images are combined to give the complete beam path.

As for the ASP (cp. Fig. 4.1) the modulator, beamsplitter and detector are necessary for the measurement of the Stokes parameters. The main differences to the ASP are:

- the design of the scan mirror (see section 4.2.3)
- the 'wobble compensation' included in the modulator device (see section 4.2.2), and most important,
- the simultaneous observation in two spectral ranges.

The beamsplitters are situated after the grating directly in front of the detectors CCD 1/2. Each of these detectors measures the two beams I^+ and I^- for a different wavelength range and such corresponds to both ASP cameras. See the text for a discussion of all elements present.

4.2 The design of POLIS

POLIS was originally intended for a balloon experiment for the 1 m space telescope Solar Lite. This design required to include an increased number -in comparison with the ASP- of components on a L-shaped optical bench of 180 x 50 x 50 cm.

4.2.1 Optical layout

Fig. 4.2 displays the complete beam path in the instrument. It can be separated in three mayor parts, the scan unit (*right top*), the slit-jaw camera (*left top*), and the main disperser (*bottom*).

(1) The scan unit contains:

- A mounting for targets at the focal plane F2 to establish image scaling.
- The modulator, consisting of a retarder and two additional glass wedges. It modulates the polarization content of the incoming beam according to the Mueller matrix in eq. (A.7). The device is described in detail in section 4.2.2.
- The scan mirror. This is a moveable mirror to select the image area of observation in one spatial direction, which was necessary for the balloon experiment. For the ground based version at the VTT it allows to independently point the instrument without changing the telescope orientation. Section 4.2.3 explains the design and operation of this device.

(2) The slit-jaw camera: The back side of the slit is metallized, to reflect the light outside the area covered by the slit. The reflected light is focused on the slit-jaw camera, passing a filter (not drawn). The images obtained in the wavelength selected display the orientation of the slit on the solar image. They are useful for the alignment of POLIS data to simultaneous data from other instruments.

(3) The main disperser consists of:

POLIS		
wavelength range	630.1-630.3 nm	396.7-396.9 nm
spectral resolution	145000	220000
dispersion	0.96 pm / pixel	1.5 pm / pixel
scan stepwidth	0.1"	
slit width	0.1"	
integration time	??	
VTT Tenerife		
coelostat mounting	standard	
main mirror diam.	70 cm	
window diam. (entr./exit)	70 / 10 cm	

Table 4.2: Instrumental characteristics of POLIS and the VTT Tenerife. The telescope uses a standard coelostat on top of the solar tower, outside the vacuum tank. The wavelength range in the visible is identical to the spectral region of the ASP. The corresponding values for the ASP can be found in table 4.1.

- The slit. It transmits the light of only a small region of the solar image. Its metallized back side reflects light to the slit-jaw camera. Across the slit horizontal hairlines can be placed to allow the correct alignment of the images of the two observed wavelengths.
- The grating. Its optical design is a compact combination of an Echelle and reflective Littrow configuration. It disperses the modulated polarization information spectrally. More details can be found in Appendix D.1.
- Interference filters. They prevent light from wavelengths and spectral orders other than the observation ranges to reach the detectors.
- The polarizing beam splitters. At POLIS they are placed directly before the CCD-cameras. They transform the modulated, spectrally dispersed polarization state into varying intensity on the single detector pixels according to eq. (3.3).
- The CCD detectors. On CCD 1 the intensities of the two beams I^+ and I^- for the visible wavelength range at 630 nm are measured on spatially separated detector areas. CCD 2 is used to obtain the polarimetric information of the Ca-line at 400 nm. More details can be found in table D.1.

The performance tests of the scan mirror and the adjustment of the 'wobble compensation' included in the modulator unit were executed by the author and shall be presented more elongated here. For other more technical details refer to Appendix D.

4.2.2 The modulator unit

The measurement retarder consists of a zero-order waveplate of mica/quartz/marmor between two plates of BK7. It has two highly polished parallel surfaces to ensure the same retardance on the full useable area. These parallel surfaces act as a Fabry-Perot-Interferometer, causing a wavelength dependent transmittance (cp. Fig. 5.1 for the size of fringes in ASP data). To prevent this effect, a wedge of 4° inclination has been cemented onto one side of the retarder. As the whole ensemble rotates, also the normal to the wedge changes. This causes the image to move in a circle on the detector, the so called 'beam wobble', because the incoming beam is bent into different directions during one revolution.

To remove this effect at POLIS² a statically scheme was designed that compensates the retarder wedge by two additional wedges. These are mounted above and below the retarder, and are shaped to resemble a wedge of opposite inclination, if they are twisted to $\pm 60^\circ$ relative to the retarder wedge (see Fig. 4.3). No parallel surfaces are present in the final configuration³. The design is currently subject to a patent application.

²At the ASP also a wedge is cemented to the modulator. There a moveable mirror (the one labelled 'fast' in Fig. 4.1) is used to remove the image motion again, requiring an active compensation.

³In difference to the use of only one compensator.

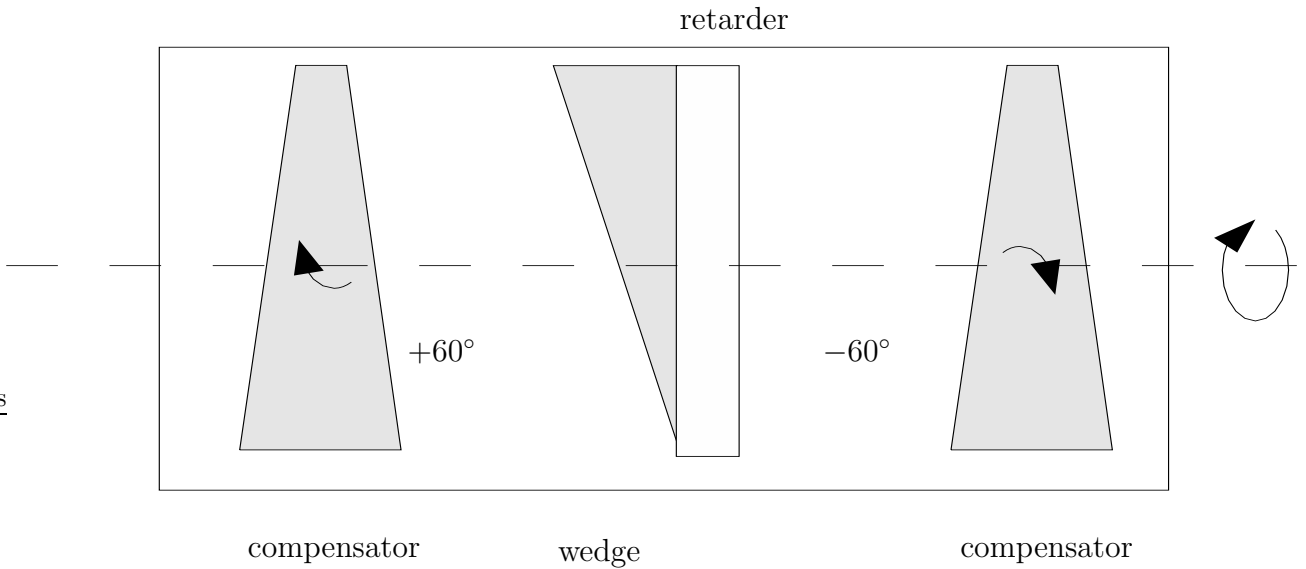


Figure 4.3: Design of the 'wobble compensation' in the modulator unit. The whole unit rotates around the propagation direction.

On one side of the measurement retarder a glass wedge has been cemented. This defeats interference effects due to the highly polished parallel surfaces of the retarder. The introduced circular image motion caused by the rotating wedge is compensated by two additional wedges above and below. The compensator wedges have to be twisted by $\pm 60^\circ$ relative to the wedge on the retarder to give an effective wedge of exactly opposite inclination. No parallel surfaces are present in the final configuration.

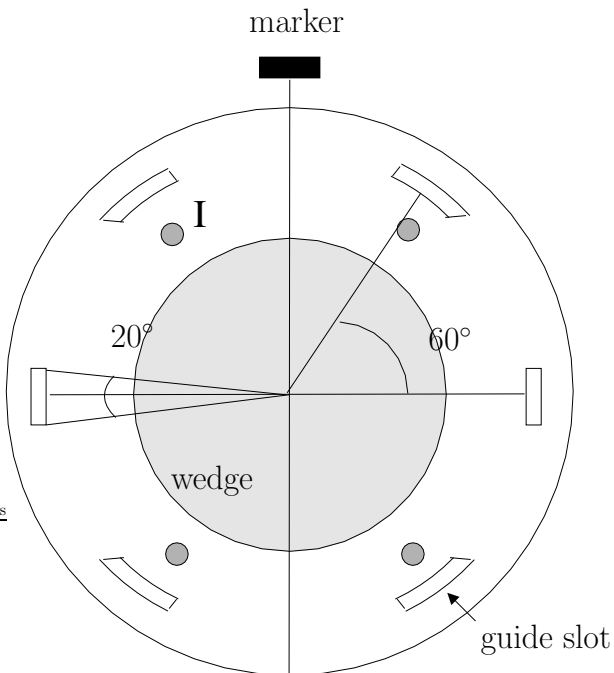


Figure 4.4: Vertical section of one compensator wedge with guide slots. The marker was placed at an arbitrary zero position.

The screwholes are placed with 60° angle separation. The guide slots allow to additionally change the angle by $\pm 10^\circ$. The possibility to rotate the proper wedge in its own mounting by 90° was not needed, but extends the possible angle positions to almost all values.

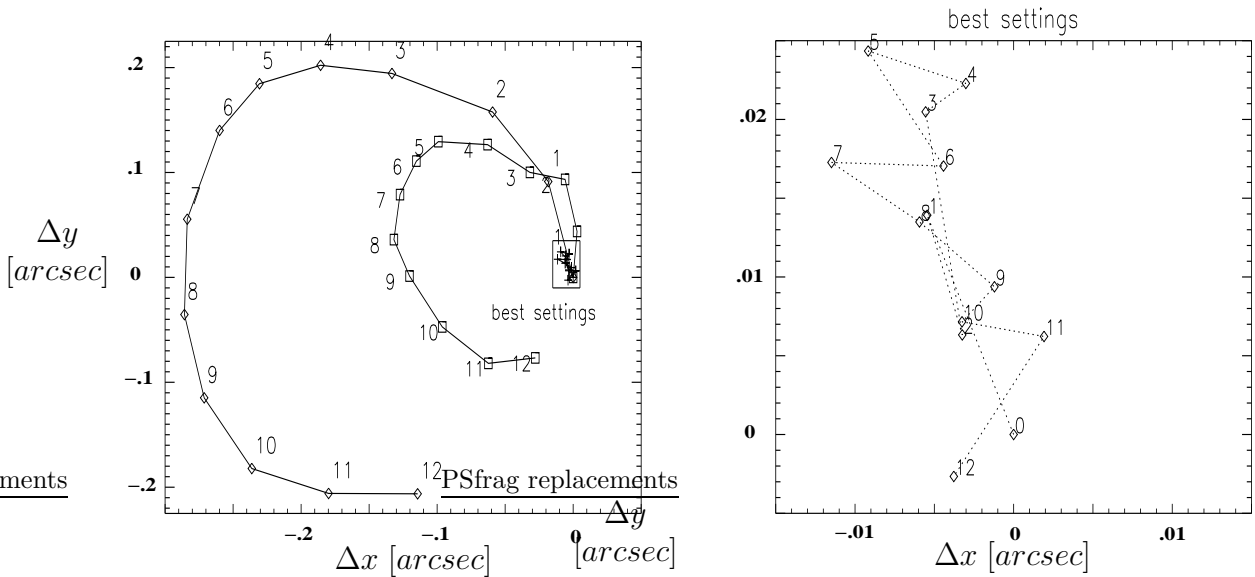


Figure 4.5: The displacement of the image N at the modulator position angle N-24° relative to the first reference image at (0,0) in arcseconds. (left) The improvement through the iterative adjustment of the compensator wedges led to (right) the result of the best setting. Not all intermediate steps are available. The resulting motion at the best setting is more like a random walk, caused by the instability of the measurement setup, than a circle due to a residual 'beam wobbling'. Note that the measurement setup is estimated to be exact only to about 0.007".

A vertical section of the compensator wedges is displayed in Fig. 4.4. The angle position of the compensator wedges can assume almost all values: the fastening screws are set in steps of 60°, the guiding slots give another range of $\pm 10^\circ$, and the wedge can be rotated inside its own mounting by 90°.

It was possible to reach an optimum compensation by using only the different screw holes and guide slots. The adjustment was performed in a reduced setup of POLIS, without the camera CCD 1/2. The displacements of a target, i.e. a glass plate with a regular pattern of grooved lines, placed in F2 were established with the slit-jaw camera mounted after the scan mirror.

To reach the compensation settings it was first necessary to establish the inclination directions of each wedge, which were not marked. To achieve this the compensator wedges were separately inserted in the mounting above the retarder. The resulting radius of image motion for the six main positions, i.e. increasing the position angle of the marker by 60° each time, leads to a minimal value, where the wedges are antiparallel.

As the wedge angles are very small, their actual value may deviate from the design specifications. This means that also the angle of 60°, for which the compensators are supposed to be twisted, is only approximative. The fine tuning of the position angle of both wedges was only practicable by trial and error. The method used was iteratively fixing one of the compensator wedges, and adjusting the second one for minimal radius of image motion.

The last result and some preceding steps are presented in figure 4.5. For the final 'best settings' there is no systematic circular motion in the data. The remaining image motion of about 0.02" is below a) the resolution limit of the telescope, and b) the spectral and spatial size of the detector pixels.

4.2.3 The scan mirror

The scan mirror is intended for positioning the slit on the desired observation area on the solar image along one direction. A graphical user interface⁴ gives access to the different operation modes. The properties

⁴Written by Th. Kentischer.

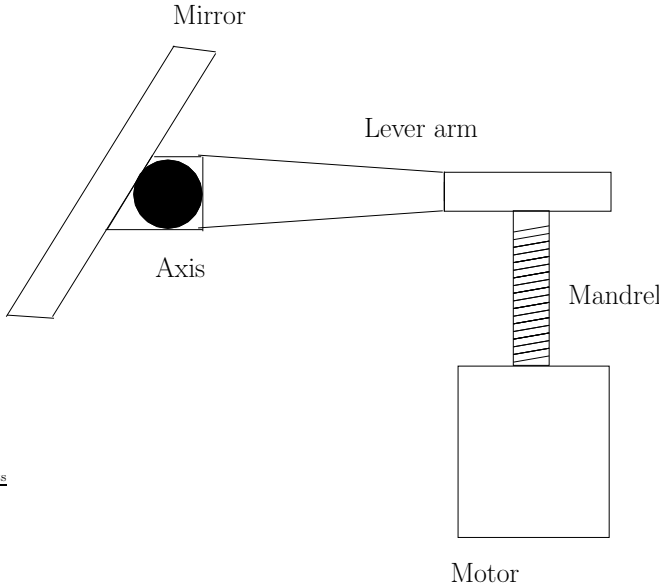


Figure 4.6: Schematic drawing of the scan mirror, side view.

The servo-controlled DC motor changes the height of the mandrel. This tilts the mirror on the other end of the lever arm around the axis drawn. The slit can be moved in one direction on the the solar image. In the performance tests the actual mirror position was checked for various motor positions.

of the scan mirror were established in the same reduced setup as in the preceeding section.

Figure 4.6 gives a side-view of the scan mirror. The proper mirror sits at one end of a lever arm, which can be rotated around the axis drawn. The other end of the lever is moved by a mandrel, whose height can be changed with a servo-controlled DC-motor. The motor position is given in single steps through a contactor. Due to the magnification scale at the VTT 8 motor steps correspond to one scan step of about 0.1" on the sky.

The scan mirror device was checked for three design requirements:

- (1) variation of stepwidth for a single scan step of about 10 %
- (2) variation of the length of a scan of 100 steps of less then 1 step (=1 %)
- (3) 'homing' precision, i.e. the ability to hit a given start position on repetition, of less then one pixel deviation in the data images.

The accuracy of the data acquisition was established through images of the same constellation with no movement of the scan mirror. The routines for the determination of the displacements were checked against an image with a known displacement from a shifting routine. The total error amounted to a value of app. 0.007". The main contribution came from the measurement setup, which was 'unstable'. The whole optical bench was placed on a trolley and the camera itself was not fixed in the only temporarily position.

15 area scans (in the following termed 'runs') of each 200 scan steps with a length of 0.1" over the same region were executed. The settings can be found in table 4.3. This should mimic the later use of POLIS with a repeated scan to obtain a timeseries. For coarser maps the stepwidth can be increased to 0.2" (=16 motor steps) or more.

The data was evaluated in two ways concerning point (1), the variation of stepwidth. Statistically, by the calculation of average value and standard deviation of the 3000 measurement values, which resulted from the comparison of subsequent images. At this straightforward method only 'trigger errors' had to be additionally considered. The camera trigger to take the image was sometimes sent out delayed or in advance, while the scan step was not completed or had not even started. These were easy to identify in the data and could be removed. The relative standard deviation of the length of a step established was $\sigma_{8\ steps} \simeq 14.3\%$.

The second method took advantage of the averaging effect in the comparison of images with N scan steps inbetween. The resulting variance obeys to the equation

$$\sigma_{tot}^2 = \sigma_{offset=const.}^2 + \left(\frac{1}{\sqrt{N}} \cdot \sigma_{8\ steps} \right)^2 . \quad (4.1)$$

stepwidth	start pos.	end pos.	number
8 steps	8500	10100	200
0.1"	0"	20"	

Table 4.3: The settings of the 15 test runs of the scan mirror. The first line is in 'motor coordinates', the second gives the corresponding values in arcseconds on the sky.

The first part contains all contributions not due to the scan mirror, the second is the variance of an average of N scan steps.

Values for two parameters σ_{offset} and $\sigma_{8\ steps}$ were established by a least-square fit of eq. (4.1) to values of the variance calculated from the data set with $N=1,2,3,\dots,50$. The result was slightly greater than the statistical with $\sigma_{scanner} \simeq 16\%$ and $\sigma_{offset} \simeq 6\%$. Summarizing the consistent results the value of about 15 % variation is acceptable, even if above the design requirement.

Point (2), the full length of a run, showed only very little variations. The fluctuations of scan stepwidth average out quickly. The constant offset from above could partly be explained by a systematic dependence of stepwidth on the motor position. This influences all runs over the same range in the same way.

On average over the 15 runs a relative standard deviation of 0.16 % remained, which is well below the required 1 %.

Point (3), the homing precision, was controlled through a statistical evaluation of displacements between images of different runs at an identical motor position. The mean value of about 0.5 pixel displacement should permit an easy alignment of data of repeated scans through sub-pixel shifts.

4.2.4 Observed spectral lines

POLIS is designed for the simultaneous observation of the polarization state in two spectral ranges. The wavelength region from 630.082 nm to 630.318 nm is imaged on CCD 1. This includes four prominent absorption lines. Two of them are telluric O₂-lines formed in the atmosphere of the earth at their rest wavelength. The solar photospheric absorption lines of neutral iron around 630 nm are the main observation target. Table 4.4 gives the properties of the single lines, their appearance in a spectrum can be seen in Fig. 6.1.

CCD 2 records the line core of a CaII line at 396.6 nm. This is a very broad chromospheric absorption line with additional blends of photospheric iron lines. The left panel of Fig. 4.7 shows a image of the spectral range with an identification of different FeI lines.

element	λ [nm]	transition $2S+1L_J$	g_j	Δh^c [km]	h_{max}^c [km]
solar absorption lines, CCD 2					
CaII H	396.649	?	?	> 500	> 500
FeI	396.745	?	?	?	?
FeI	396.682	?	?	?	?
FeI	396.664	?	?	?	?
solar absorption lines, CCD 1					
FeI	630.15091 ^a	$^5P_2 - ^5D_2$	1.67 ^b	300-450	390
FeI	630.25017 ^a	$^5P_1 - ^5D_0$	2.50	260-410	310
telluric absorption lines, CCD 1					
O ₂	630.20005 ^a	-	-	earth atm.	-
O ₂	630.27629 ^a	-	-	earth atm.	-

Table 4.4: Summary of the properties of the observed spectral lines. **a** wavelengths from Pierce & Breckinridge (1973), **b** effective Landé factor from Solanki (1987), **c** height of line core formation and maximum of contribution function above $\tau_{500\text{nm}} = 1$ (H.Schleicher, personal note).

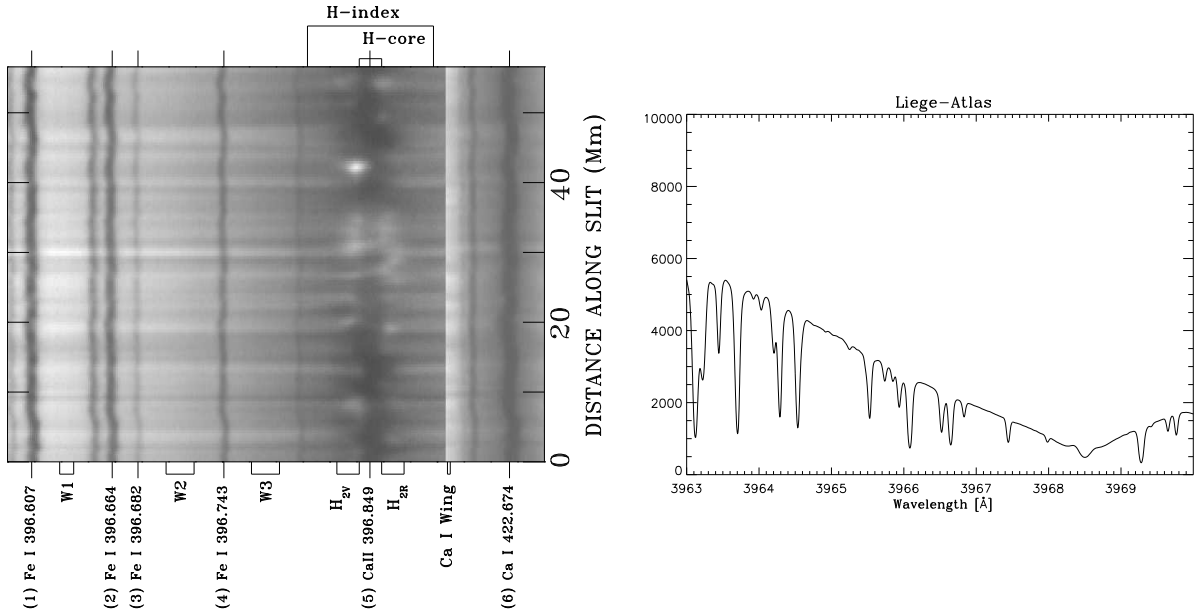


Figure 4.7: (*left*) Spectrum of the wavelength range at 396 nm (B.W. Lites, HAO). (*right*) Corresponding section from the Liege spectral atlas.

The broad chromospheric Ca-line has additional blends of photospheric FeI lines in its wing. The evaluation of the polarization signal is more complicated than for a photospheric line. The contribution to a special wavelength stems from an extended height region in the solar atmosphere. The shape of the spectrum will require more sophisticated methods of data treatment, as no regular continuum or telluric reference lines are available.

4.3 Summary: Characteristics and intended usage of POLIS

POLIS will yield the complete information of the polarization state of light in two wavelength ranges simultaneously. The wavelength ranges include spectral lines formed in different heights in the solar atmosphere. The spatial accuracy of the instrument is of order of 0.1 arcseconds on the sky, to resolve structures of a few 100 km diameter on the solar surface. The spectral resolution allows an inversion of the polarimetric data to retrieve the vector magnetic field. The intended time resolution for a scan step will be of order of seconds. The calibration of the proper polarimeter will be accurate to at least 0.1 % of the continuum intensity.

The following points outline some possibilities of the usage of POLIS:

- The construction of a consistent static model of magnetic field lines from the photosphere to the corona. The strict simultaneity of the polarimetric data is crucial for that.
- Time series of a selected region. The additional information of the chromospheric line allows the detection of vertical motions up- or downwards in the atmosphere. This can help to solve the problem of the heating of the upper solar atmosphere layers by propagating shocks or acoustical waves.
- Total magnetic flux difference. A comparison between the total magnetic flux measured at the two heights can be used to establish the amount of flux returning to the surface.
- Co-observations with the TIP. As another polarimeter in the infrared range is available at the VTT Tenerife, simultaneous observations in a third different spectral line will be possible in the future.
- Studies of effects on small⁵ scales. The spatial accuracy will allow to resolve many solar magnetic

⁵'Small' in solar terms, i.e. of order of some 100 km.

structures. For example, the substructure of the penumbra of a sun spot, or the spatial dependence of the Evershed effect on the magnetic field configuration can be examined in detail.

- Relocation to the planned 1.5m-Gregory-Coudé-telescope. The compact setup and the spatial accuracy allow an installation at the greater telescope under construction.

To repeat the main problem of the examination of solar magnetic phenomena with a polarimeter: the interpretation of the data rests on the unspoken assumption that the polarization signal only stems from the sun. As the following sections will display, POLIS as a polarimeter at the VTT Tenerife will declare a polarization state to be Stokes U, when it actually is Stokes Q, and initially has been Stokes V - before it entered the telescope.

Chapter 5

The calibration of POLIS

” *The beam of sunlight undergoes two reflections on the ... surfaces of the coelostat ..., where elliptical polarization must again be introduced.*” G.E.Hale (1908)

The actual polarimeter output is influenced by a great variety of factors. To give only some examples:

- The usage of the integration scheme requires an exact synchronisation of read out timing and retarder position angle
- The modulation efficiency of the retarder is not equal for the different polarization components, and varies with wavelength.
- The pixels of the two-dimensional detectors are not identical, so their individual response has to be known.
- Intensity variations due to the seeing at the observation site can lead to spurious polarization signals because of the subtraction of intensities¹.

The effects concerning the performance of the *polarimeter* are taken into account by so called **X**-matrix or polarimeter response function. This 4×4 -matrix relates the output Stokes vector of the polarimeter to the input vector at the position of the polarimeter calibration unit.

The other main influence arises from the *telescope* before the proper polarimeter. Reflections under oblique angles change the incoming polarization, which was already taken into consideration for the first polarimetric solar measurements. To quantify these effects a model of the polarization properties of the telescope has to be used. Its result is the so called telescope or **T**-matrix of all optical elements down to the polarimeter calibration unit.

The two matrices are a Mueller matrix of an optical train (**T**) or an equivalent to describe the behaviour of the polarimeter (**X**). They are needed, as the final polarimeter output is always given by

$$\boxed{\mathbf{S}_{\text{out}} = \mathbf{X} \cdot \mathbf{T} \cdot \mathbf{S}_{\text{in,sun}}}, \quad (5.1)$$

where one has to retrieve the Stokes vector of the incident light from the output value.

The determination of these matrices is the crucial point for the polarimetric accuracy, when the optical design of the polarimeter components is decided.

5.1 Polarimeter calibration

The calibration of the polarimeter is performed through the evaluation of the polarimeter calibration data set. The 16 entries of the **X**-matrix calculated in that way give the response of the measurement

¹See B.W. Lites, [13].

instrument to the different polarization states. The \mathbf{X} -matrix is assumed to be constant for hours, it will be established on a daily² base during observation campaigns.

5.1.1 Polarimeter calibration data

The polarimeter calibration data set (in the following referred to as 'cal') has to be taken at the start and/or the end of the measurements. The polarimeter calibration unit is used for the creation of known input polarization states. This unit is located after the deflection mirror inside the vacuum tank (see Fig. 5.3) and consists of a linear polarizer and a retarder. They are placed inside rotateable mounts and can be inserted into the light beam by remote control³. The directions of the transmission axis of the polarizer and the fast optical axis of the retarder have to be established before. The accuracy of the position affects the calculated polarimeter response function. It should be sufficient to fix the positions to $\pm 0.1^\circ$ (M.Collados, personal note). Appendix B describes the method to align the unit correctly. The optical parameters of the two elements can be found in table D.1.

With the directions of the axes known the following equation between created input and polarimeter output is valid:

$$\mathbf{S}_{\text{out}} = \mathbf{X} \cdot \mathbf{M}_{\text{ret}}(\theta_{\text{ret}}) \cdot \mathbf{M}_{\text{pol}}(\theta_{\text{pol}}) \cdot \mathbf{T} \cdot \begin{pmatrix} I_0 \\ 0 \\ 0 \\ 0 \end{pmatrix} = I_0 \cdot \mathbf{X} \cdot \mathbf{M}_{\text{ret}}(\theta_{\text{ret}}) \cdot \mathbf{M}_{\text{pol}}(\theta_{\text{pol}}) \cdot \begin{pmatrix} 1 \\ T_{1,0} \\ T_{2,0} \\ T_{3,0} \end{pmatrix}. \quad (5.2)$$

θ_{ret} and θ_{pol} are the angles to the zero positions of the respective axes, and $\mathbf{M}_i(\theta_i)$ the corresponding Mueller matrices of rotated elements. The telescope matrix \mathbf{T} is intensity normalized, i.e. $T_{0,0} \equiv 1$, and the initial sun light is supposed to be unpolarized⁴ with the intensity I_0 .

To obtain the 16 elements of the matrix the response to four independent⁵ Stokes vectors has to be measured. The problem in choosing the vectors is increased by the unknown values in eq. (5.2). These are the \mathbf{X} -matrix itself, the intensity and the telescope matrix entries. An elegant way to reduce the number of unknowns, and at the same time decouple polarimeter and telescope, is the calibration data set used for the TIP polarimeter, which will be adopted for POLIS. If the linear polarizer is held on a fixed position, for example at $\theta_{\text{pol}} \equiv 0^\circ$, eq. (5.2) transforms to

$$\mathbf{S}_{\text{out}} = I_0 \cdot \frac{1}{2} (1 + T_{1,0}) \cdot \mathbf{X} \cdot \mathbf{R}(\theta_{\text{ret}}) \cdot \begin{pmatrix} 1 \\ 1 \\ 0 \\ 0 \end{pmatrix}. \quad (5.3)$$

The intensity term $I_0 \cdot \frac{1}{2} (1 + T_{1,0})$ can be assumed to be constant, if the variation of $T_{1,0}$ during the measurement of the cal data is negligible⁶. The cal data set will therefore consist of a full revolution of the retarder in 72 steps of 5° for a fixed, but in principle arbitrary, position of the polarizer. The evaluation of the data set is described in section 5.1.4.

5.1.2 Flatfield & dark current data

Before an evaluation of the polarimeter response the properties of the individual detector pixels have to be removed. To this extent an additional data set of flatfield images (in the following referred to as 'flat') has to be available⁴. Only the intensity values of Stokes I are used. The flat data set will contain about 15 images.

²The eventual need for an increased number of calibrations will have to be tested at Tenerrife.

³It is not possible to use them separately, always the combination of first polarizer and then retarder is in the beam path.

⁴The area on the sun during this observation should be at disc center with no visible magnetic activity like sun spots. Additionally the telescope pointing should be varied randomly, to remove all spatial information.

⁵'independent' means in that case, the 4 vectors written in a matrix A have to give $\det(A) \neq 0$, see [24], p. 362.

⁶If seen to be needed, a linear variation of intensity will be included.

The dark current images reflect the number of counts produced by stray light, the electron noise, or read-out effects, when the light path to the sun is blocked. The values have to be compared with the number of counts in an actual observation to obtain the signal-to-noise ratio (S/N). At the beginning of each file a small number of dark images will be taken to ensure a close relationship between the actual and assumed noise level.

5.1.3 Data reduction

The following sections describe the procedure for one detector, for example CCD 1. The data from the second camera will have to be treated analogously, but also separately, in the same way.

The dual beam setup of the polarimeter results in the two beams I^+ and I^- (see section 3.1). They are measured on different detector areas, so before the subtraction or addition of the beams the data has to be corrected for the pixel properties. This concerns all measurement data taken with POLIS, either cal or actual solar measurements. All following images were created from ASP data sets due to the lack of POLIS data. For the wavelength range around 630 nm this data is very similar, the wavelength range around 400 nm will require slightly different methods.

5.1.3.1 Gaintables

The gaintables take into account the individual pixel responses. They are constructed from the averaged flat field data in Stokes I^7 after the subtraction of the dark current. The ASP has two detectors with two gaintables, POLIS will have two set of detectors with four different image areas, i.e. four gaintables.

To remove the spectral information from the data the line cores of one of the telluric⁸ lines along the slit are shifted to a fixed reference position. The average of the shifted image along the spatial direction gives the mean profile. The curvature (or linear variation) of the line core along the slit is established. The gaintable results from the division of the averaged flat by the mean profile, which is shifted in λ according to the curvature. Fig. 5.1 shows a gaintable constructed for one of the ASP cameras with this procedure.

At first look the procedure may appear to be not satisfying. This is mainly caused by the small number of flat field images (only 4) in an ASP cal file. Flat field data for the ASP is created by rotating the grating to a spectral range without strong absorption lines. As this option is not available for POLIS, the intensity images from the ASP cal file were chosen as most similar to flat field data of POLIS. The residual spectral information is enhanced by the displayed range of the gaintable. The visible spectral information corresponds only to app. 1% variation. The interference fringes present in ASP data can be identified as periodic variations along the wavelength dimension. The treatment of fringes for POLIS will depend on their shape and size in actual data.

5.1.3.2 Balancing, coaligning and merging

After the subtraction of the dark current and the application of the gaintables the pixel properties of the detectors are not yet fully removed. The gaintable can be interpreted as a comparison of the intensity on single pixels to the mean intensity on the respective detector area. This does not account for differences in the mean detector intensities due to the different light path in the beam splitter. To balance the detectors the mean intensity in Stokes I of an arbitrary chosen beam, say I_{mean}^+ , is normalized to the intensity I_{mean}^- .

The two images of Stokes I from I^+ and I^- should then contain the same spectral information, with identical intensities, i.e. number of counts. In the next step they have to be coaligned in spectral and spatial dimension. Again the position of the line core of one telluric O₂-line can be used. One of the images is shifted row by row, until the line cores in both images lie on the same column in each row⁹. The alignment along the slit can be performed with the horizontal hairlines inserted in the slit. These hairlines will be especially useful for the correct alignment of images of the chromospheric and photospheric lines.

⁷Remark: the stored data is the already demodulated Stokes vector, consisting of (I,Q,U,V) (λ).

⁸For the 630 nm wavelength range, see the discussion for the co-alignment procedure below for other possibilities.

⁹cp. Fig. 5.1 for the definition of column and rows of the image

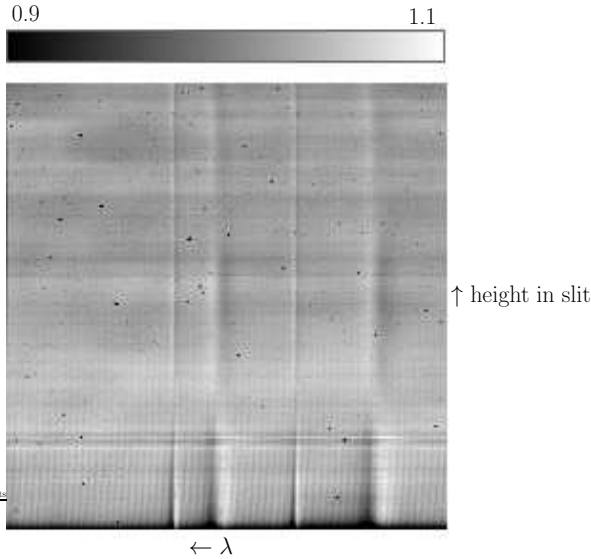


Figure 5.1: Gaintable for one of the ASP detectors (camera B), in the range of 0.9 to 1.1.

The spectral information is not fully removed, as can be seen by the residual spectral lines. The single black spots correspond to pixels with greatly reduced intensity response. The periodic variation in the image along the wavelength dimension are the interference fringes present in ASP data. See text for a discussion of the quality of the gaintable. The wavelength dimension λ corresponds to columns of the image, the height in the slit to rows.

The values of the intensity normalization, and the respective shifts in spatial and spectral direction are established from Stokes I, but have of course to be applied to Stokes Q,U and V as well.

For the coaligning of images a number of possibilities exist, the one cited using line cores is only an example. The actual program code here needs to consider mainly two things. First, quality of the calculation of the shifts, second, stability under complicated conditions, i.e. intensity profiles distorted by gradients or fully split lines. Especially for the Ca-line a correlation method using an extended image area may be the only stable option.

After balancing and co-aligning the data from the two beams the components of the Stokes vector can be merged according to eq. (3.3) by:

$$\mathbf{S}(\lambda) = \begin{pmatrix} I_+ + I_- \\ Q_+ - Q_- \\ U_+ - U_- \\ V_+ - V_- \end{pmatrix} (\lambda), \quad (5.4)$$

where the subscript + or - indicates the information from the beam I^+ or I^- , and λ is identical to the column number.

Summary:

The polarimeter calibration data consists of three types, calibration, flat field, and dark current images. The individual pixel response of the detectors is established from dark and flat and stored in the gaintables. The data images from I^+ and I^- have to be gain-corrected separately, balanced, and co-aligned before merging.

5.1.4 Determination of the polarimeter response function

After the calibration data has been treated in the way described in the preceding sections, a data set consisting of 73 images remains, corresponding to the number of input vectors from the calibration unit. Along the wavelength dimension the polarimetric value should be constant, whereas along the slit it may vary¹⁰. The polarimeter response function is therefore established at four different heights in the slit.

¹⁰Along the slit spatial inhomogeneties of the calibration unit or in the later beam path may cause variations, while the grating only spectrally disperses the incoming modulated polarization state.

5.1.4.1 Intensity normalization

As the input intensity $I_0 \cdot \frac{1}{2} (1 + T_{1,0})$ from eq. (5.3) is unknown, the data set has to be normalized. If the slit heights are set to r_i ($i=1,2,3,4$), the normalization is given by:

$$\int_{\Delta\lambda, \Delta x_i} \frac{\mathbf{S}_{\text{out}}(\lambda)}{I(\lambda)} d\lambda dx \cdot \frac{\int_{\Delta\lambda, \Delta x_i} I(\lambda) d\lambda dx}{\langle \int_{\Delta\lambda, \Delta x_i} I(\lambda) d\lambda dx \rangle_{\text{cal}}} \equiv \frac{\int_{\Delta\lambda, \Delta x_i} \mathbf{S}_{\text{out}}(\lambda) d\lambda dx}{\langle \int_{\Delta\lambda, \Delta x_i} I(\lambda) d\lambda dx \rangle_{\text{cal}}}.$$

$\Delta\lambda$ (=columns) is the restriction on the useable wavelength range, excluding eventual image distortions at the borders. The Δx_i (=rows) are a decomposition of the slit height into four non-overlapping intervals, each centered around the value r_i . $\langle .. \rangle_{\text{cal}}$ indicates the average over all images in the calibration file. Note that the normalization retains the information on the intensity variations in the cal file, which are necessary to establish the first row of the \mathbf{X} -matrix.

5.1.4.2 Matrix inversion

For a single slit height r_i the data is reduced to 73 output Stokes vectors with this method. The corresponding input vectors can be calculated from the position angles of the polarizer and retarder of the calibration unit, using the right side of eq. (5.2). The resulting linear problem can be written in the form

$$(\mathbf{S}_{\text{out}})_{\text{cal}} = (\mathbf{S}_{\text{in}})_{\text{cal}} \cdot \mathbf{X}^T, \quad (5.5)$$

where $(\mathbf{S}_{\text{out, in}})_{\text{cal}}$ are 73×4 -matrices and $\mathbf{X} \in \mathbb{R}^{4 \times 4}$. With the substitutions of $(\mathbf{S}_{\text{out}})_{\text{cal}} = \mathbf{y}$ and $(\mathbf{S}_{\text{in}})_{\text{cal}} = \mathbf{M}$ the problem can be solved through

$$\begin{aligned} \mathbf{y} &= \mathbf{M} \cdot \mathbf{X}^T \\ \mathbf{M}^T \cdot \mathbf{y} &= \mathbf{M}^T \cdot \mathbf{M} \cdot \mathbf{X}^T = \mathbf{D} \cdot \mathbf{X}^T \quad \text{by} \end{aligned}$$

$$\boxed{\mathbf{X}^T = \mathbf{D}^{-1} \cdot \mathbf{M}^T \cdot \mathbf{y}} \quad (5.6)$$

^T denotes transposition, and ⁻¹ the inverse of the matrix. The errors can be calculated from the matrix $\mathbf{A} = \mathbf{D}^{-1} \cdot \mathbf{M}^T$ in the following way:

$$\sigma_{X_i}^2 = \sum_j A_{ij}^2 \sigma_{y_j}^2 = \bar{\sigma}^2 \sum_j A_{ij}^2, \quad \text{where} \quad (5.7)$$

$$\bar{\sigma}^2 = \frac{1}{N} \cdot \sum_{\text{cal}} (\mathbf{y} - \mathbf{M} \cdot \mathbf{X}^T)^2. \quad (5.8)$$

The errors of the single measurements, σ_{y_i} , are approximated by the total deviation of the fit, $\bar{\sigma}$. As the same A_{ij} ($j=1, \dots, 73$) are used for the calculation of X_{ik}^T ($k=0, 1, 2, 3$), the procedure results in identical errors for each column of the polarimeter response function \mathbf{X} . The matrix is normalized in intensity by division through X_{00} at the end of the calculation.

5.1.4.3 Properties of the calibration unit

The matrix inversion relates polarimeter input and measured output by the \mathbf{X} -matrix. To ensure the correct inclusion of the properties of the calibration unit three additional parameters are introduced in the construction of the input $(\mathbf{S}_{\text{in}})_{\text{cal}}$. The polarizer is assumed to be ideal¹¹ and aligned correctly. For the wave plate it is useful to use the retardance, δ_{ret} , the dichroism, $b = r_x - r_y$, and a position error of its fast axis, $\theta_{\text{ret, pol}}$, as free parameters. The resulting matrix of the retarder is identical to eq. (5.10). The values of θ_{ret} , b , and $\theta_{\text{ret, pol}}$ are established by minimizing $\bar{\sigma}^2$ in eq. (5.8) with regard to the parameters through a gradient method.

¹¹The transmission coefficient of light polarized linear in the blocking direction is app. 10^{-5} .

r_i	δ_{ret}	b
15	81.7352	0.0067
85	82.0277	0.0034
155	82.1160	-0.0003
200	81.7162	-0.0030

Table 5.1: The parameters of the retarder of the calibration unit for four slit heights r_i . They were established with the procedures described in this section from a data set of the ASP. The retardance δ is almost constant along the slit, while the value of the dichroism b systematically decreases.

5.1.4.4 Final result and evaluation

The determination of the polarimeter finally gives the following values for each slit height r_i :

- \mathbf{X} -matrix
- retardance δ_{ret} , dichroism b , and position error $\theta_{ret,pol}$.

The entries of the \mathbf{X} -matrices are interpolated linearly to obtain the \mathbf{X} -matrix for an arbitrary slit height. The values describing the properties of the wave plate can be used to control the consistency of the evaluation. The variation should be rather small for one cal data set.

The following values, which resulted from an application of the procedures on a calibration data set of the ASP, can also serve as a good example for the values to be expected for POLIS.

The \mathbf{X} -matrix for $r_4 = 200$ and its error were calculated to be

$$\mathbf{X} = \begin{pmatrix} 1.0000 & -2.7 \cdot 10^{-8} & 2.8 \cdot 10^{-8} & 3.8 \cdot 10^{-9} \\ -0.0004 & 0.1022 & 0.4108 & 0.1696 \\ -0.0017 & -0.4459 & 0.0975 & 0.0299 \\ 0.0011 & -0.0088 & -0.1624 & 0.3979 \end{pmatrix}, \text{ error: } \pm \begin{pmatrix} 0.0013 & 0.0037 & 0.0037 & 0.0019 \\ 0.0013 & 0.0037 & 0.0037 & 0.0019 \\ 0.0013 & 0.0037 & 0.0037 & 0.0019 \\ 0.0013 & 0.0037 & 0.0037 & 0.0019 \end{pmatrix}. \quad (5.9)$$

Here each image of the polarimeter output was normalized separately with the average intensity of the image itself. This causes the information about the first row to get lost. The values of the diagonal elements clearly reflect the necessity of the polarimeter calibration. A measured signal of Stokes Q is mainly caused by an input of U, and vice versa. Only for Stokes V the matrix element $X_{33} \equiv V \rightarrow V$ is the greatest contribution. Table 5.1 displays the results for the properties of the calibration retarder¹², with the expected result of almost uniform retardance.

5.2 Telescope calibration

The polarimeter response function takes into account all optical elements behind the calibration unit, and the performance of the proper measurement instrument itself. The application of the inverse matrix \mathbf{X}^{-1} on measurement data results in the Stokes vector of the light beam at the position of the calibration unit. This vector is not identical to the polarization signal incident in the telescope.

The various elements in the beam path up to this point, the coelostat mirrors, the windows of the vacuum tank, or the main and deflection mirror change the polarization to a certain degree. These effects are usually summarized in the term 'instrumental polarization' of the telescope. Some telescope designs are suited to minimize the instrumental polarization due to their layout, for example a Gregory-Coudé optic system¹³. Unfortunately a coelostat does not belong to that category. Nonetheless, the ASP demonstrated how to successfully operate a polarimeter at a telescope, which is in principle not suited for polarimetry (cp. section 4.1).

It is necessary to first introduce the telescope model, because the calibration data set is adjusted its specific shape.

5.2.1 The telescope model of the vacuum tower telescope in Tenerife

The telescope model has to include all optical elements before the calibration unit of the polarimeter to give effective values for the polarimetric properties of the VTT. In the description of a mirror the specific

¹²The position error was not included in this calculation.

¹³M.Stix, [26], p. 76f

geometry of the reflection enters (section 5.2.1.2). This requires an explicit calculation of the beam path for every moment of time, as the coelostat orientation and the beam path are permanently changing (section 5.2.1.4). The main aim of the model is to give an accurate estimation of the instrumental polarization from an only small number of parameters. Opposite to the \mathbf{X} -matrix no constancy in time can be assumed, thus one has to deal with 16 variable entries in the \mathbf{T} -matrix.

Each mirror is represented in the model by a separate Mueller matrix, whose entries depend on the physical properties of the mirror, and geometrical factors of the beam path like the incidence angle. The matrices are only valid for a specific set of reference frames (RFs) for each mirror. It is necessary to additionally include rotation matrices to switch between the different RFs.

A semianalytical approach is used to calculate the incidence and rotation angles in the telescope model. It uses analytical solutions and some numerical procedures. One of the advantage of this method is that one can control all actual directions, i.e. the different reference frames, the mirror normals, the sun position and the position of the second coelostat mirror, as they are given in a fixed coordinate system as unit vectors. It is further possible to choose different reference frames as input or intermediate systems. This is important for the calibration of the telescope by inserting a sheet polarizer at different places in the light path. The input created depends on the orientation of the polarizer and has to be described in a suited reference frame.

Another advantage is that the procedure developed is not restricted to the specific design of the coelostat, but applicable on other optical setups as well. If the beam path and the respective optical elements are known, it is possible to calculate the polarimetric properties according to the equations given in the following sections¹⁴. This concerns for example an examination of a single mirror through polarized light under different incidence angles.

The accuracy of the numerical part of the routines can be checked by the comparison of axes, which are supposed to coincide after a rotation. The numerical errors introduced corresponded to less than $6 \cdot 10^{-4}$ degrees in all cases.

The results for the telescope model are equivalent to the analytical set of equations for a coelostat given by Cap. et al. (1989), [3], which will be discussed in Appendix C for comparison. The model was developed in cooperation with members¹⁵ of the Instituto de Astrofísica de Canarias (IAC¹⁶).

5.2.1.1 Geometry of the Vacuum Tower Telescope

The telescope is built primarily from two separate parts: the coelostat on the top of the tower, which reflects the sunlight vertically downwards, and the main and deflection mirror in the vacuum tank, which produce an image of the solar disc in the focal plane.

The coelostat of the german VTT at Tenerife consists of the two mirrors labelled C1 and C2 (see Fig. 5.2). The primary coelostat mirror C1 can has two degrees of freedom:

- The footpoint of its mounting can be moved on a circle of rails with a radius of 1.55 m laid around the center of the entrance window. The necessity of an adjustable footpoint arises to avoid C1 being shaded by C2 at noon, or to reduce the pillar height, when the sun has a negative declination (cp. section 5.2.1.4 for the connection between these parameters). The position on the circle is measured with the so-called mirror azimuth, by convention positive from N to E.
- C1 can be rotated around an axis pointing to the celestial north pole to reflect the sun light on the second mirror C2. This feature defines the optical design of a coelostat opposite to for example a

¹⁴To take the worst possible case, for a randomly oriented light beam no analytic solution is possible, but the numeric method will work.

¹⁵Thanks to M.Collados for his patience at this point.

¹⁶The IAC operates the Tenerife Infrared Polarimeter at the VTT Tenerife, and some other telescopes at Izaña, Tenerife, and at the Roque de los Muchachos, La Palma.

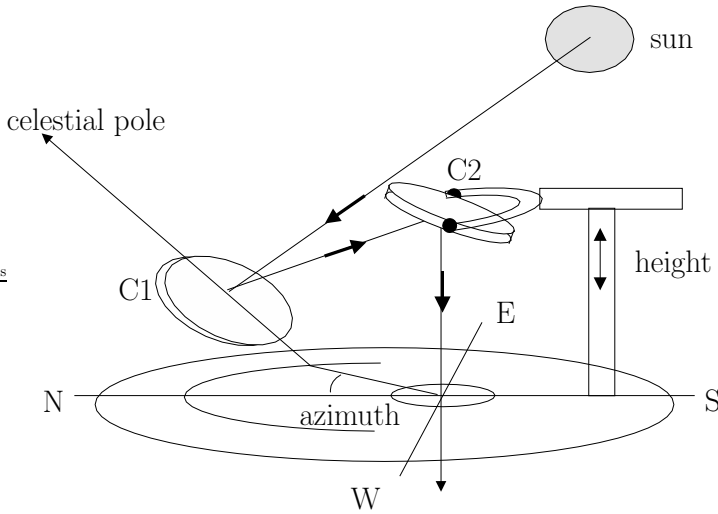


Figure 5.2: Scheme of the coelostat at the VTT Tenerife.

The coelostat consists of two mirrors C1 and C2. The mirror C1 can be moved on a circle of 1.55 m radius around the center of the entrance window. The position on the circle is the mirror azimuth angle, which is by convention positive from N to E. The rotation axis is inclined 28° (= geographical latitude of Tenerife) to the horizontal plane and points to the celestial north. C2 is mounted on a pillar with variable height and can be tilted along two axes to deflect the incoming light vertically downwards to the main mirror in the vacuum tank.

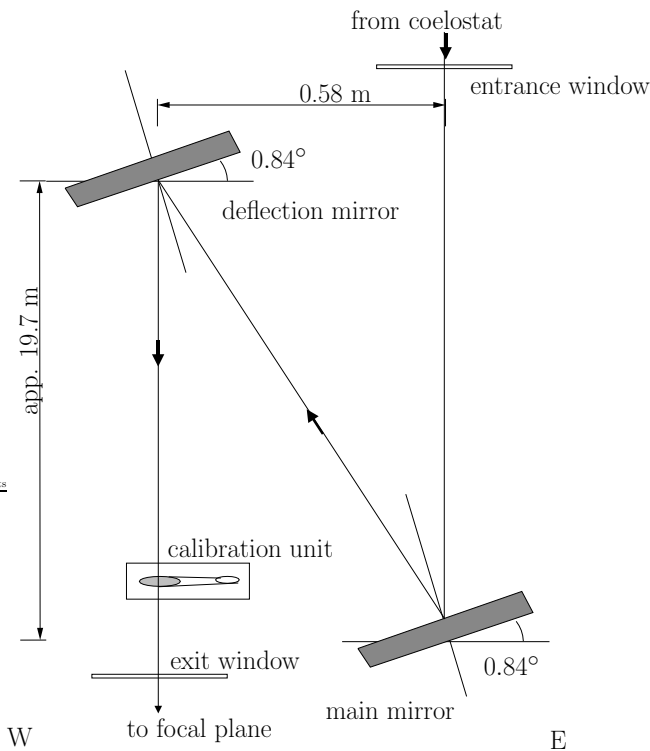


Figure 5.3: The contents of the vacuum tank.

The light enters vertically downwards from the second coelostat mirror C2 through the entrance window. The main mirror is inclined by 0.84° (drawing strongly exaggerated) to the W and reflects the light to the deflection mirror app. 19.7 m above it. The deflection mirror is inclined by the same amount and can be moved ± 1 m in height to adjust the position of the focal plane. The calibration unit of the polarimeter is positioned before the exit window, if the correlation tracker tank (not drawn) is also evacuated. After passing the window the light reaches instrumentation like the spectrograph or POLIS.

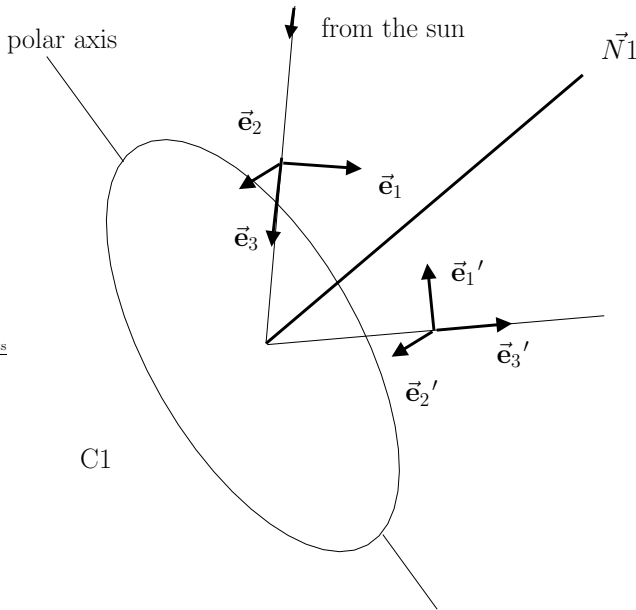


Figure 5.4: Reference frames of a single mirror for the incoming and reflected beam (here for C1). The RF for the incoming beam ($\vec{e}_1, \vec{e}_2, \vec{e}_3$) is defined by \vec{e}_3 in the propagation direction, \vec{e}_1 in the incidence plane of mirror normal $\vec{N}1$, orthogonal to \vec{e}_3 , and pointing to the mirror normal. \vec{e}_2 is orthogonal on both, forming a right-handed RF. The RF of the reflected beam is constructed analogously from the respective directions. Note that \vec{e}_2 and \vec{e}_2' are identical and parallel to the mirror surface.

heliostat¹⁷.

The vacuum tank contains the main and the deflection mirror (see Fig. 5.3). These are fixed in their position with an inclination angle of about 0.84° to the W direction. The height of the deflection mirror above the main mirror can be changed by ± 1 m to adjust the position of the focal plane, but this affects the incidence angles important for the polarimetric properties only slightly. It is therefore assumed that the default values can be used.

The combination of Fig. 5.2 and 5.3 gives the complete beam path inside the telescope down to the polarimeter calibration unit. If the correlation tracker (CT) tank (not shown) is evacuated, the calibration unit sits before the exit window. If the CT is not in vacuum, the window will be before the calibration unit (cp. section 5.2.1.2 for the implications).

5.2.1.2 Mueller matrices in the model

There are two kinds of Mueller matrices used in the calculation. One are matrices describing the polarizing properties of single mirrors or other optical active media like the entrance window, the other are rotation matrices between different reference frames.

Mirror matrices & reference frames

For the description of a mirror with a simple expression, a special set of RFs has to be chosen explicitly. The Stokes vector of the incoming and reflected beam are described in two different RFs. The following definition of the RF is sometimes labelled 'canonical'¹⁸.

The RF consists of the vector \vec{e}_3 , parallel to the propagation direction of the light beam. The vector \vec{e}_1 lies in the incidence plane defined by \vec{e}_3 and the mirror normal. It is orthogonal to \vec{e}_3 , and points from \vec{e}_3 to the normal. \vec{e}_2 must be orthogonal on both to form a right-handed RF. The output Stokes vector is given in the RF of the reflected beam, which is constructed analogously from the propagation direction and the mirror normal. This is depicted in Fig. 5.4 for the first coelostat mirror C1 and a positive declination of the sun.

The following discussion will concentrate on the more general optical thin aluminium coatings¹⁹. The

¹⁷see M.Stix, [26], p. 69f

¹⁸[24], p.361

corresponding formulation for optically thick coatings can be found in Appendix C.

The mirror matrix \mathbf{M} in this case is given by²⁰

$$\mathbf{M}_{\text{mirror}} = \mathbf{M}(\tilde{\mathbf{e}}_1, \tilde{\mathbf{e}}_2, \tilde{\mathbf{e}}_3 \mid \tilde{\mathbf{e}}_1', \tilde{\mathbf{e}}_2', \tilde{\mathbf{e}}_3') = \begin{pmatrix} (r_x + r_y)/2 & (r_x - r_y)/2 & 0 & 0 \\ (r_x - r_y)/2 & (r_x + r_y)/2 & 0 & 0 \\ 0 & 0 & \sqrt{r_x r_y} c \delta & \sqrt{r_x r_y} s \delta \\ 0 & 0 & -\sqrt{r_x r_y} s \delta & \sqrt{r_x r_y} c \delta \end{pmatrix}. \quad (5.10)$$

The conventions used are²¹:

- (1) The electromagnetic wave is described by $\mathbf{E} = \mathbf{E}_0 \cdot \exp i(\mathbf{k} \cdot \mathbf{r} - \omega \cdot t)$.
- (2) The components E_i are defined in the canonical RF / RF' as given above.
- (3) The reflectivities are defined by $E_i^{ref} = R_i \cdot E_i^{in}$.
- (4) The given values are the incidence angle, η , the refractive index, n , the absorption coefficient, k , the thickness of the mirror coating in wavelength fractions, d/λ , and the refractive index, ν , of the substrate below the coating.

Under this conditions the matrix entries can be calculated by the following equations²²:

$$R_{\parallel} = \frac{r_{\parallel} + s_{\parallel} t}{1 + r_{\parallel} s_{\parallel} t}, \quad R_{\perp} = \frac{r_{\perp} + s_{\perp} t}{1 + r_{\perp} s_{\perp} t} \quad (5.11)$$

where

$$\begin{aligned} r_{\parallel} &= \frac{(n + ik)^2 \cos \eta - u - iv}{(n + ik)^2 \cos \eta + u + iv}, & r_{\perp} &= \frac{(\cos \eta - u) - iv}{(\cos \eta + u) + iv} \\ s_{\parallel} &= \frac{\nu(u + iv) - (n + ik)^2 \cos \alpha}{\nu(u + iv) + (n + ik)^2 \cos \alpha}, & s_{\perp} &= \frac{(u + iv) - \nu \cos \alpha}{(u + iv) + \nu \cos \alpha} \\ t &= e^{4\pi(d/\lambda)(u+iv)i} \end{aligned} \quad (5.12)$$

and

$$\begin{aligned} u &= \sqrt{\frac{1}{2}[n^2 - k^2 - \sin^2 \eta + \sqrt{n^2 - k^2 - \sin^2 \eta + 4n^2 k^2}]} \\ v &= \sqrt{\frac{1}{2}[-n^2 + k^2 + \sin^2 \eta + \sqrt{n^2 - k^2 - \sin^2 \eta + 4n^2 k^2}]} \\ \cos \alpha &= \sqrt{1 - \frac{\sin^2 \eta}{\nu^2}} \end{aligned}$$

Taking $R_{\parallel} = R_x e^{i\epsilon_x}$ and $R_{\perp} = R_y e^{i\epsilon_y}$ with real R_x, R_y , the entries of the matrix are

$$\begin{aligned} r_x &= R_x^2, & r_y &= R_y^2 \\ \sqrt{r_x r_y} \cos \delta &= \text{Re}(R_{\parallel} \cdot R_{\perp}^*), & \sqrt{r_x r_y} \sin \delta &= -\text{Im}(R_{\parallel} \cdot R_{\perp}^*) \end{aligned} \quad (5.13)$$

For optical thick coatings the substrate below the coating can be neglected, and the equations simplify (see Appendix C).

It is assumed, that a sufficient polarimetric accuracy of the telescope model can be achieved also with the simpler equations (M.Collados, personal note). The resulting values for the refraction indices would in that case have to be interpreted more as effective than as physical values. Both sets of equations will be used to check the consistency. If the coating thickness d/λ is used as free parameter in a least-square-fit to telescope calibration data, its value should allow the decision, which equations are best suited to describe the telescope.

¹⁹i.e., the value of the thickness of the coating $d/\lambda \ll 1$

²⁰Jaeger & Oetken, [10]

²¹Almost literally from Skumanich et al., [24], p.379f.

²²The equation were also taken from [24], p. 380. A derivation is possible from Born & Wolf, *Principle of optics*, [2], chapters 1.5, 13.2, and 13.4.

Summary:

The Mueller matrices of the single mirrors have to be calculated for each point in time with the momentaneous incidence angles, while the other parameters entering are constant physical mirror properties.

Rotation matrices

To transform between different RFs, in general a base transformation has to be performed. This is simplified by the fact that the beam directions of subsequent optical elements are identical, i.e. for example the reflected beam of C1 (\vec{e}_3' from Fig. 5.4) is the incoming beam of C2 (\vec{e}_3 of C2).

Only the axes orthogonal to the beam direction can be different and the transformation can be established by a rotation around the \vec{e}_3 -axis. The matrix of a rotation is given in Appendix A.6. The only thing to be considered additionally is the direction of the rotation: the rotation angles are to be measured by convention counter-clockwise from \vec{e}_1 to \vec{e}_1' , when looking towards the light source. The primed vector is from the RF to be transformed to²³. Neglecting of the convention can easily lead to sign errors in the calculated angles, which are very difficult to track down.

Window matrix

The windows of the vacuum tank can exhibit stress induced birefringence. The entrance window is modelized as pure retarder with an arbitrary, but fixed, position angle of the fast and slow axis²⁴. Its properties can be included by the two parameters retardance, δ , and position angle, θ . The exit window is assumed too small to show polarizing effects at all. Values for the parameters result from the least square fit to the telescope calibration data.

The paper of Owner-Petersen, [17], gives a derivation for this modelization. If the telescope model is seen to give an insufficient fit, a more rigid approach for the entrance window will be tried following the considerations in the paper. Additionally the possibility to exclude the window will be investigated. Then the main effect caused by the window, an increased retardance, should be included in the effective physical values of the main and deflection mirror. The way of treatment in this case is still an open issue, depending on actual measurements at Tenerife.

5.2.1.3 Additional reference frames

In addition to the RFs of the single mirrors, which are defined by the beam path and the mirror normals, three other RFs are needed. The first is a RF, which stays fixed on the sun. Into this RF the measurement result has to be transformed at the end. The second one is the actual measurement RF of the polarimeter, while the third one is the coordinate RF ('main RF') for all following calculations of vectors.

- The main RF has its origin in the center of the first mirror C1 and is defined by:

$$\vec{x} = \begin{pmatrix} 1 \\ 0 \\ 0 \end{pmatrix} \text{ points from N to S, } \vec{y} = \begin{pmatrix} 0 \\ 1 \\ 0 \end{pmatrix} \text{ from W to E, and } \vec{z} = \begin{pmatrix} 0 \\ 0 \\ 1 \end{pmatrix} \text{ from nadir to zenith.}$$

Its orientation can be seen by moving the coordinate directions in Fig. 5.2 from the center of the entrance window to the center of C1. Four different ways are used later to describe a vector in the main RF :

- (1) Horizontal plane coordinates: the horizontal angular height, h , equal to 90° - zenith distance, and the azimuth, A , given by the angular distance between S and the projection of the vector to the x-y-plane, increasing from S to W²⁵.

²³Capitani et al., [3], p. 177

²⁴As in Skumanich et al., [24], p.362 .

²⁵H.-H. Voigt, *Abriss der Astronomie*, [28], p.1f

- (2) Equatorial coordinates: declination, δ , the angular distance from the equatorial plane. This plane is inclined by (90° - geographical latitude) to the horizontal plane. The second coordinate is the hour angle, t , in the equatorial plane, which also is increasing from S to W. This is not identical to the azimuth A because of the angle between these two planes²⁶.
- (3) Spherical coordinates: θ , the angle to the \vec{z} -axis (equal to zenith distance), and ϕ , the angle in the \vec{x} - \vec{y} -plane, this time increasing from \vec{x} to \vec{y} , i.e. from S to E, therefore equal to $-A$.
- (4) Cartesian coordinates x, y and z as given by the definition of the axes.

Transformations between these coordinate systems are:

– for $\delta, t \rightarrow h, A$ ²⁷:

$$\cos h \cdot \sin A = \cos \delta \cdot \sin t \quad (5.14)$$

$$\sin h = \sin \phi \cdot \sin \delta + \cos \phi \cdot \cos \delta \cdot \cos t \quad (5.15)$$

$$-\cos h \cdot \cos A = \cos \phi \cdot \sin \delta - \sin \phi \cdot \cos \delta \cdot \cos t. \quad (5.16)$$

– for $h, A \rightarrow \theta, \phi$:

$$\theta = 90^\circ - h, \quad \phi = -A \quad (5.17)$$

– for $\theta, \phi \rightarrow \vec{r} = (x, y, z)$:

$$\begin{pmatrix} x \\ y \\ z \end{pmatrix} = \begin{pmatrix} \cos \phi \cdot \sin \theta \\ \sin \phi \cdot \sin \theta \\ \cos \theta \end{pmatrix}. \quad (5.18)$$

- For the solar RF it is sufficient to fix one axis. This reference axis is the tangent to the equatorial plane at the hour angle of the sun. If this vector is moved in angular height to the sun center, it bisects the sun from W to E. This direction is given in the cartesian main RF by

$$\vec{x}_0 = \begin{pmatrix} -\sin \phi \cdot \sin t_{sun} \\ -\cos t_{sun} \\ -\cos \phi \cdot \sin t_{sun} \end{pmatrix}, \quad (5.19)$$

where ϕ denotes the geographical latitude and t_{sun} the hour angle.

- The measurement RF of the polarimeter is defined through the zero position of the transmission axis of the linear polarizer of the calibration unit as \vec{e}_1 . The rotation between telescope and polarimeter at the end of the optical train will be used as free parameter, to compensate errors in the initial positioning of the calibration unit.

5.2.1.4 Calculation of the telescope matrix

To calculate the polarimetric properties of the complete telescope, consisting of the four mirrors C1, C2, main and deflection mirror, and the entrance window of the vacuum tank, the following parameters²⁸ are needed:

- mirror properties : refraction index, n , absorption coefficient, k , thickness of the aluminium coating in wavelength fractions, d/λ , refraction index of substrate, ν
- window properties : retardance, $\delta_{entrance}$, position angle, $\theta_{entrance}$,

which are constant properties of the system, and

- position angle of C1 on the circle of rails (azimuth)

²⁶Voigt, [28], p.2

²⁷Voigt, [28], p.5

²⁸Remark: for optically thin coatings.

- sun position,

which define the beam path.

With the last two parameters the path of the light beam in the telescope can be constructed, also the mirror normals and the RFs of the single mirrors. This gives the values needed for the calculation of the Mueller matrices of the optical train, namely

- incidence angles on the mirrors : i_1, i_2, i_3, i_4
- rotation angles between RFs : θ_1 (sun→C1), θ_2 (C1→C2), θ_3 (C2→main), θ_4 (defl. mirror→polarimeter).

The actually used input parameters of the routine are the constant physical properties, which will be stored in a separate file, and the azimuth of the first mirror, date, and time of the measurement.

The construction of the beam path

The beam path is defined by three direction vectors, corresponding to the bold arrows in Fig. 5.5 :

- The position of the sun as seen from C1. The program `r_frame_asp` of the ASP-library returns the sun position for Tenerife in equatorial coordinates, δ, t . These can be transformed to the cartesian vector \vec{r}_{sun} with the equations (5.14)-(5.18).
- The position of the second mirror C2 as seen from the center of C1. The coordinates of C2 are -unfortunately in two different coordinate systems- given by

$$\begin{aligned} \text{declination in equ. plane coordinates} & : \delta_{C2} = -\delta_{sun} \\ \text{azimuth in hor. plane coordinates} & : A_{C2} = \text{azimuth} . \end{aligned}$$

The first stems from the fact that the mirror normal on the first mirror, $\vec{N}1$, always is in the equatorial plane. Due to the law of reflection C2 then must have the value opposite to the sun with regard to the equatorial plane (see the lower part of Fig. 5.5). The second coordinate, A_{C2} , can easily be derived from the definition of the azimuth in section 5.2.1.1.

The value, which needs to be established here, is the horizontal height, h_{C2} . To solve the equations (5.14)-(5.16) in this case a numerical solution is used. Multiplication of Eq. (5.15) with $\sin \phi$ and of Eq. (5.16) with $\cos \phi$, and addition of the modified equations gives:

$$\sin \phi \cdot \sin h - \cos A_{C2} \cdot \cos \phi \cdot \cos h = \sin \delta_{C2} , \quad (5.20)$$

with the known values δ_{C2}, ϕ and A_{C2} , the only unknown parameter is the angular height h .

The left half of equation (5.20) is calculated for values of $h \in [0, 90^\circ]$. The angular height h_{C2} sought is the intersection point of this curve with the constant value $\sin \delta_{C2}$. With eq. (5.17) and (5.18) the vector \vec{r}_{C2} is obtained.

- The vertical beam path after C2. This direction simply is (0,0,-1) in the main RF.

The mirror normals

The direction of the mirror normal on C2 is easy to construct. The incoming beam has the direction \vec{r}_{C2} , the reflected beam must be vertically downwards. The mirror normal therefore has to be inbetween $-\vec{r}_{C2}$ and (0,0,-1). As these directions have the same length (both are normalized), the mirror normal $\vec{N}2$ is given by²⁹:

$$\vec{N}2 = \frac{-\vec{r}_{C2} + (0, 0, -1)}{|\vec{r}_{C2} + (0, 0, -1)|} . \quad (5.21)$$

²⁹ A proof is simple, this follows from the properties of an isosceles triangle.

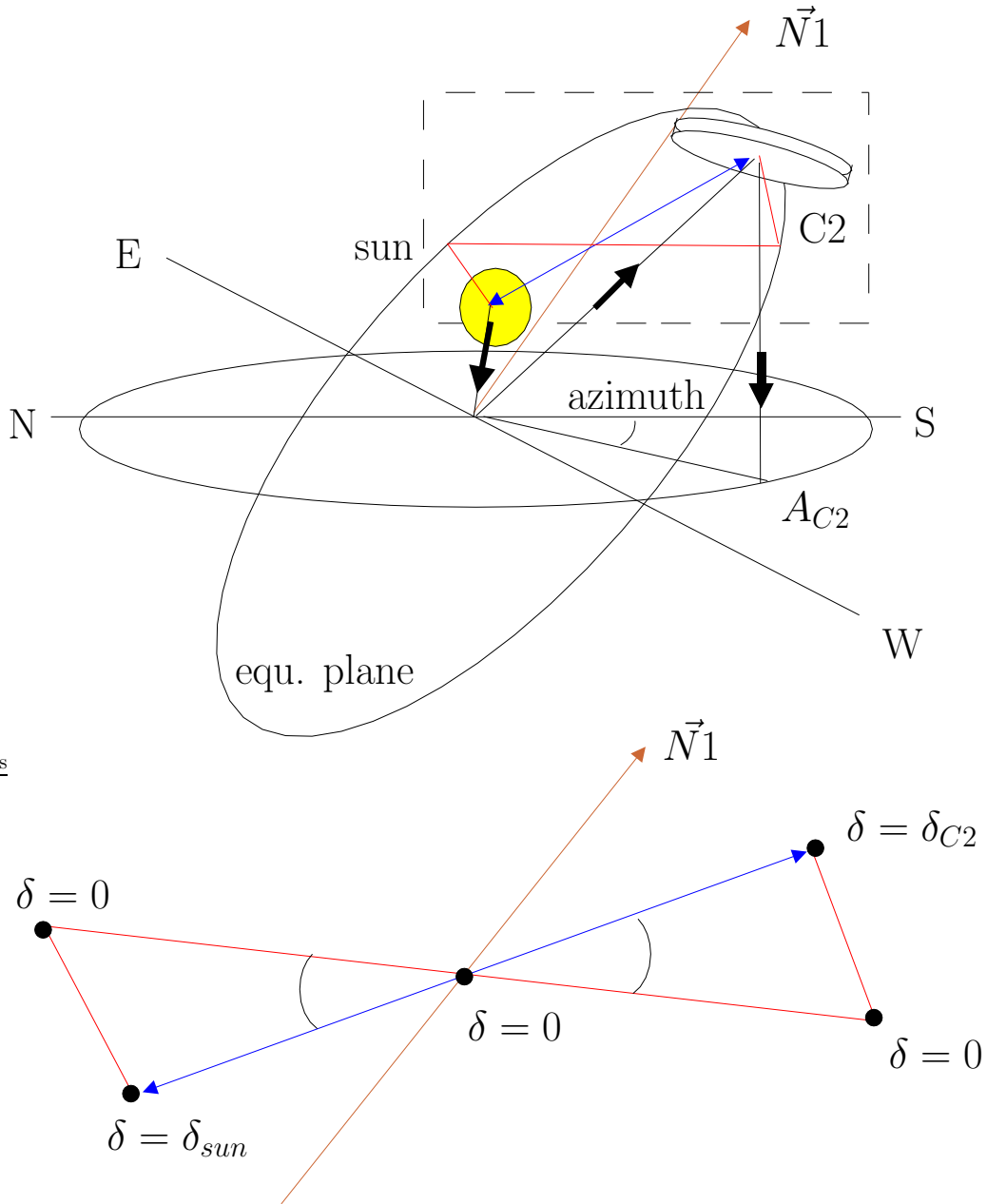


Figure 5.5: (*top*) The position of the second coelostat mirror $C2$ relative to $C1$. The origin lies in the center of $C1$. The position angle A_{C2} in the horizontal plane is fixed by the azimuth of the first mirror. The mirror normal on $C1$, $\vec{N}1$, is in the equatorial plane, which is inclined $90^\circ - \phi$ to the horizontal plane. Bold arrows denote the beam path. The declination of the sun is negative. The entrance window would be vertically below $C2$.

The declination of the second mirror, δ_{C2} , is the negative of the declination of the sun, δ_{sun} , as the (*bottom*) part displays. There the line with the arrows connects the centers of the sun and the second mirror. From the law of reflection it follows, that it is exactly bisected by the mirror normal $\vec{N}1$, and is orthogonal to it. The triangles built by the footpoints in the equatorial plane, the intersection point and the positions of sun or $C2$ are identical, therefore $\delta_{C2} = -\delta_{sun}$.

The mirror normal of C1, $\vec{N}1$, is constructed in the same way from \vec{r}_{C2} and \vec{r}_{sun} :

$$\vec{N}1 = \frac{\vec{r}_{C2} + \vec{r}_{sun}}{|\vec{r}_{C2} + \vec{r}_{sun}|}. \quad (5.22)$$

The incidence angles

The incidence angles on the respective mirrors can be calculated from the standard scalar product, $\langle \vec{a}, \vec{b} \rangle = \sum_i a_i b_i = |\vec{a}| |\vec{b}| \cos(\alpha)$, between mirror normal and the direction of the incoming or reflected beam. So each i_j can be calculated in two ways³⁰:

$$i_1 = \text{acos}(\langle \vec{r}_{sun}, \vec{N}1 \rangle) = \text{acos}(\langle \vec{N}1, \vec{r}_{C2} \rangle), \text{ and} \quad (5.23)$$

$$i_2 = \text{acos}(\langle -\vec{r}_{C2}, \vec{N}2 \rangle) = \text{acos}(\langle \vec{N}2, (0, 0, -1) \rangle). \quad (5.24)$$

The incidence angles on main and deflection mirror are constant with $i_3 = i_4 = 0.84^\circ$, which can be derived from Fig. 5.3.

Construction of the reference frames

The RFs of the single mirrors are determined by beam directions and mirror normals. An example will be executed for an incoming beam (see Fig. 5.6).

The axis \vec{z} , equal to the inverse direction of the incoming beam, the mirror normal \vec{N} and the x-axis \vec{x} lie in the same plane (incidence plane). The two vectors \vec{x} and \vec{z} are an ONB for every vector in the incidence plane, thus \vec{N} can be decomposed by

$$\vec{N} = \langle \vec{z}, \vec{N} \rangle \cdot \vec{z} + \vec{\beta}, \quad (5.25)$$

where $\langle \vec{\beta}, \vec{z} \rangle = 0$.

With

$$\vec{x} = \frac{\vec{\beta}}{|\vec{\beta}|} = \frac{\vec{N} - \langle \vec{z}, \vec{N} \rangle \cdot \vec{z}}{|\vec{N} - \langle \vec{z}, \vec{N} \rangle \cdot \vec{z}|} \quad (5.26)$$

a direction is obtained, which is orthogonal to the propagation direction, points from it to the mirror normal, and lies in the incidence plane, the requirements for the x-axis in section 5.2.1.2.

The y-axis can be calculated by:

$$\vec{y} = \vec{x} \otimes \vec{z}, \quad (5.27)$$

where \otimes denotes the standard vector crossproduct.

Calculation of the rotation angles

Two different subsequent RFs have one axis in common, that is the propagation direction, \vec{e}_3' (RF1) = \vec{e}_3 (RF2). One needs to establish the rotation angle around this axis, arbitrarily oriented in space, that moves \vec{e}_1' (RF1) onto its counterpart \vec{e}_1 (RF2). This can be done numerically for the calculated unit vectors of the RFs, which shall not be disussed in detail³¹.

³⁰For control one can calculate $i_2 = (\pi/2 - h_{C2})/2$, which is also valid.

³¹The condition of counter-clockwise rotation unfortunately excludes the use of the scalar product.

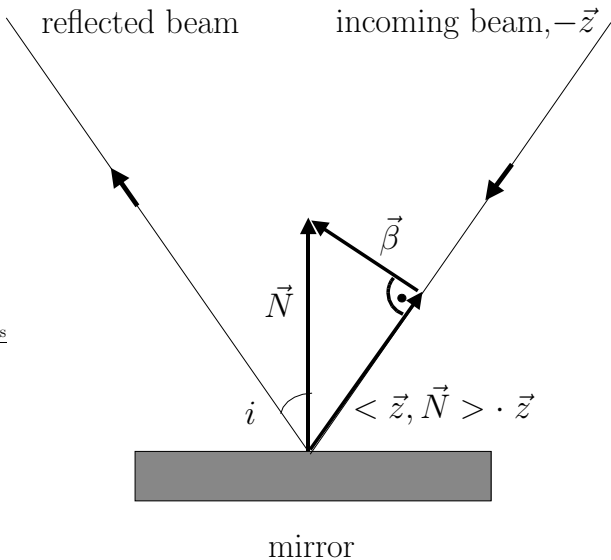


Figure 5.6: Construction of the RFs.

The mirror normal can be decomposed into two orthogonal parts. One is parallel to the propagation direction, \vec{z} . It is given by $\langle \vec{z}, \vec{N} \rangle \cdot \vec{z}$.

The other, $\vec{\beta}$, is parallel to the unknown x-axis in the incidence plane. The x-axis direction can be calculated by normalizing $\vec{\beta} = \vec{N} - \langle \vec{z}, \vec{N} \rangle \cdot \vec{z}$.

The final matrix product

Now the complete optical train can be calculated:

$$\mathbf{T} = \mathbf{R}_{\text{tel,pol}} \cdot \mathbf{M}_{\text{defl}} \cdot \mathbf{M}_{\text{main}} \cdot \mathbf{M}_{\text{entrance}} \cdot \mathbf{R}_{C2,\text{main}} \cdot \mathbf{M}_{C2} \cdot \mathbf{R}_{C1,C2} \cdot \mathbf{M}_{C1} \cdot \mathbf{R}_{\text{sun},C1} \quad (5.28)$$

$$= \mathbf{T}(n, k, d/\lambda, \nu, \delta_{\text{entr}}, \theta_{\text{entr}}, \text{azimuth}, \text{time}, \text{date}) \quad (5.29)$$

\mathbf{R} are rotation matrices according to eq. (A.6) with the corresponding angles, \mathbf{M} the Mueller matrices of the optical elements like eq. (5.10) for the mirrors, and according to eq. (A.7) for the entrance window.

5.2.2 Telescope calibration data

The principle of the telescope calibration is identical to the polarimeter calibration. It consist of the creation of known input Stokes vectors, and the measurement of the corresponding polarimeter output. After the application of the inverse of the \mathbf{X} -matrix the properties of the polarimeter can be assumed to be removed from the data. The difference is the time dependence of the \mathbf{T} -matrix, which makes a fit of constant matrix entries like for the polarimeter impossible.

The main problem of the telescope calibration unit is the size needed. It has to cover the full area of the first coelostat mirror or the entrance window. This can not be achieved with a single sheet polarizer of sufficient quality. Large sheet polarizers are subject to spatial inhomogeneties due to deformations of the surface. The telescope calibration unit therefore consists of an array of sheet polarizers. The single sheets are placed in separate mountings and can be aligned individually. The whole array is rotateable to create different linear polarizations (see Fig. 5.7). Unfortunately the calibration unit is too heavy to be placed freely in the beam path above the first mirror³². The possible positions of the calibration unit are on top of the first mirror, which also solves the problem of accurate co-motion to guarantee an input constant in time, and on top of the entrance window after the coelostat mirrors.

The telescope calibration unit thus allow two different sets of data to be created. Each set will consist of a full (half) revolution of the calibration unit with a stepsize of 10° (5°). The data sets include different optical elements of the telescope and will have to be evaluated in correct order, but not fully separately.

5.2.2.1 Calibration unit on top of the entrance window

Fig. 5.8 shows the corresponding telescope calibration unit of the TIP with polarizer sheets in the infrared wavelength range on that position.

³²This would additionally require a larger covered area, and an accurate co-motion with the mirror.

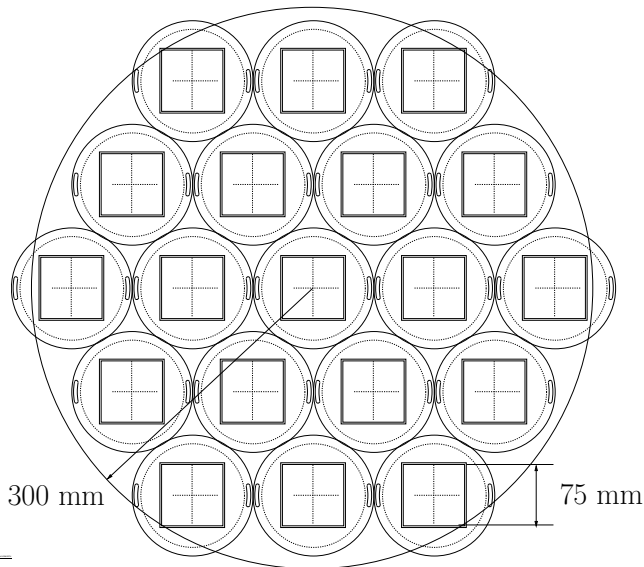


Figure 5.7: Section of the telescope calibration unit.

The covered area corresponds to the diameter of the first mirror. The 19 quadratic sheet polarizers can be separately aligned. The array can be rotated as a whole to create different linear polarizations. It can be placed either on top of the first coelostat mirror C1 (Fig. 5.10) or on the entrance window (Fig. 5.8).

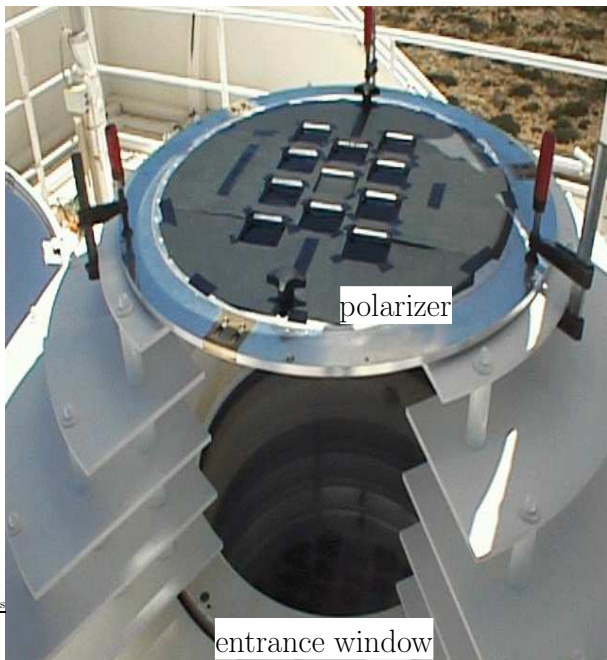


Figure 5.8: The array of sheet polarizers in the infrared for the TIP on top of the entrance window. Only 10 of the 19 polarizing sheets were delivered to that time. The whole array can be rotated to create different linear polarizations.

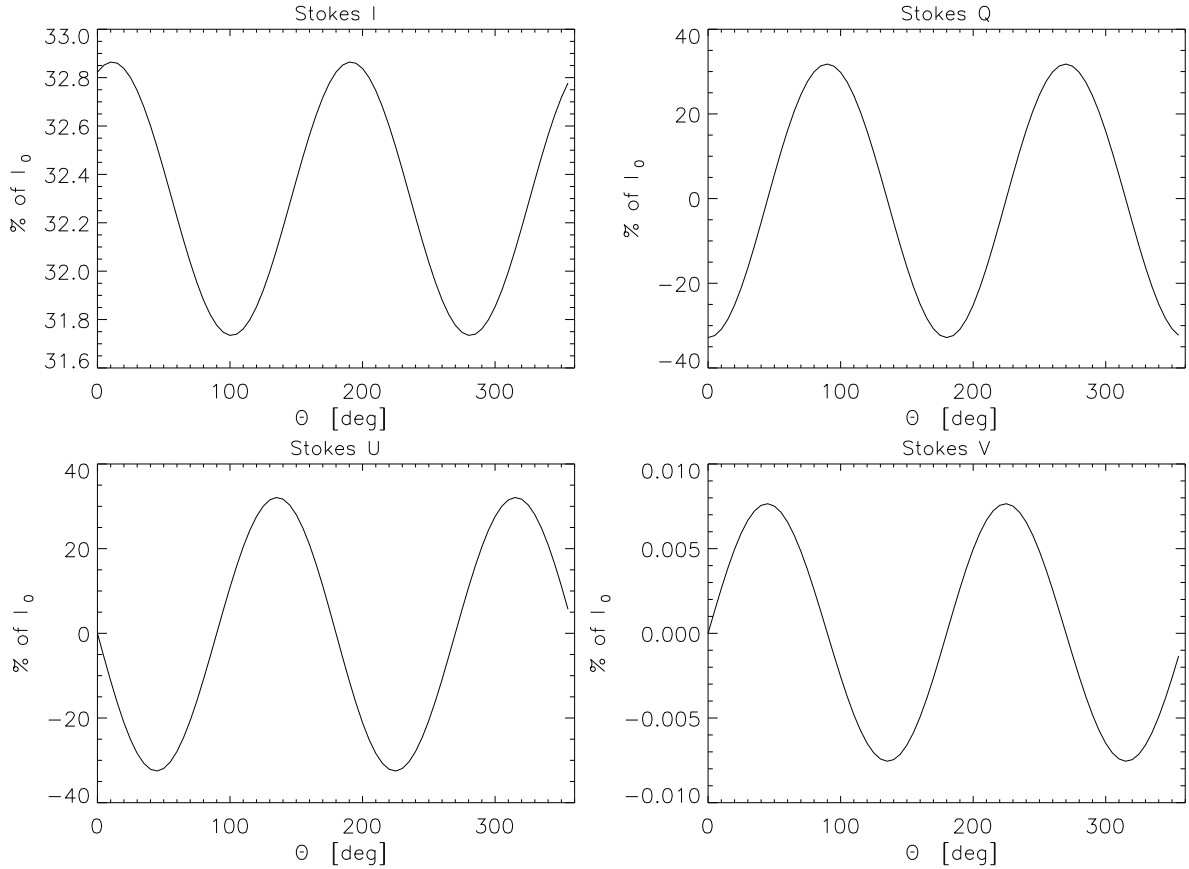


Figure 5.9: Stokes vector for a full rotation of the telescope calibration unit on the entrance window in the model. Date: 21.07.02, 12:00 UT, azimuth = 0° . Mirror parameters $(n, k, d/\lambda, \nu) = (0.30, 3.63, 0.094, 1.54)$, taken from an ASP telescope calibration. The window is excluded, $\theta_{tel, pol} = 90^\circ$.

The array of polarizers is placed on top of the entrance window and rotated for an angle $\theta \in [0, 360^\circ]$ in already polarized light. The resulting matrix $(\mathbf{T})_{pol, window}$ is applied on unpolarized sunlight with the intensity I_0 . The transmitted intensity is given in % of the incident intensity. See text for more details.

If the telescope calibration unit is placed on top of the entrance window, the optical elements below are the entrance window, the main and the deflection mirror. The zero position of the polarizer is the W direction ($=\vec{e}_1$ of the main mirror RF), the array has to be rotated from W to N to give a counter-clockwise rotation.

Both mirrors are usually coated at the same time. Their polarimetric properties can be assumed to be identical, and should exhibit only small changes on longer time scales due to their evacuated environment.

With the inclusion of the entrance window as optical element and using the description of optical thin mirrors (see section 5.2.1.2 above) the following parameters are open in the reduced model:

- $n_{vac}, k_{vac}, d/\lambda$ for the mirrors. The label 'vac' indicates that these values are supposed to be valid only for the mirrors in the vacuum tank.
- $\theta_{entrance}, \delta_{entrance}$ for the entrance window.
- $\theta_{tel, pol}$ between telescope and polarimeter.

Even if it seems that the coelostat mirrors can be neglected for this part, they still have an influence. The polarizer array is rotated in already polarized light. This leads to intensity variations like already

discussed in section 5.1. The equation connecting input and output is:

$$\mathbf{S}_{\text{out}} = \mathbf{I}_0(t) \cdot \mathbf{X} \cdot \mathbf{T}_{\text{vac}} \cdot \mathbf{L}(\theta_{\text{pol}}) \cdot \begin{pmatrix} 1 \\ \alpha(t) \\ \beta(t) \\ \gamma(t) \end{pmatrix}. \quad (5.30)$$

\mathbf{T}_{vac} is the restriction of the telescope model on the elements after the polarizer. The time dependence of $\mathbf{I}_0(t)$, $\alpha(t)$, $\beta(t)$, and $\gamma(t)$ takes into account small variations in total intensity and the polarization content resulting from the motion of the first coelostat mirror. The values of α , β , and γ , i.e. the polarization introduced by the coelostat mirrors, are of order of some %. If the polarizer now is rotated, the intensity in \mathbf{S}_{out} may vary by the same amount, with the total intensity \mathbf{I}_0 also unknown. The intensity variation can be seen in Stokes I in Fig. 5.9. The maxima and minima in the curve occur, if the polarizer is aligned parallel or anti-parallel to the linear polarization produced by the two coelostat mirrors. For an azimuth of C1 $\neq 0^\circ$ the order of the intensity variations increases strongly.

To remove this intensity variation the following procedure may be used³³. The left side of eq. (5.30) is normalized with the intensity after the application of the inverse \mathbf{X} -matrix:

$$\mathbf{S}'_{\text{out}} = \begin{pmatrix} 1 \\ \delta \\ \eta \\ \nu \end{pmatrix} = \frac{\mathbf{X}^{-1} \cdot \mathbf{S}_{\text{out}}}{(\mathbf{X}^{-1} \cdot \mathbf{S}_{\text{out}})_0}, \quad (5.31)$$

where δ , η , and ν is the polarization information.

The right side is constructed from an unit intensity input, and the final input vector is also normalized:

$$\mathbf{S}_{\text{in}} = \frac{\mathbf{T}_{\text{vac}} \cdot \mathbf{L}(\theta_{\text{pol}}) \cdot (1 \ 0 \ 0 \ 0)^T}{(\mathbf{T}_{\text{vac}} \cdot \mathbf{L}(\theta_{\text{pol}}) \cdot (1 \ 0 \ 0 \ 0)^T)_0} \stackrel{!}{=} \begin{pmatrix} 1 \\ \delta \\ \eta \\ \nu \end{pmatrix}. \quad (5.32)$$

This should allow to perform a least square fit of the free parameters n_{vac} , k_{vac} , d/λ , θ_{entrance} , δ_{entrance} , and $\theta_{\text{tel,pol}}$. The intensity information lost by the normalization is not needed for the fit of the model parameters, as the \mathbf{T} -matrix is intensity normalized anyway, i.e. divided by \mathbf{T}_{00} . See the discussion on additional intensity variations due to geometrical effects in the following section.

5.2.2.2 On top of the mirror C1

In this case the light passes the polarizer twice. After the second transmission through the calibration unit the beam path includes all remaining elements in the telescope model. The properties of the entrance window and the subsequent mirrors can assumed to be known. The open parameters now are n_{coel} , k_{coel} , and d/λ , where the label 'coel' refers to the two coelostat mirrors only. The thickness of coating may be dropped for optical thick coatings, see the discussion in 5.2.1.2.

This seems to be easy to achieve, but the setup causes a mayor problem. The polarizers of the calibration unit are assumed to be ideal, and they are passed again after the first mirror. The only way to retain the information on the properties of this mirror is to use here a non-normalized \mathbf{T} -matrix, contrary to the section above and the application on observational data. It seems necessary to explicitly derive how the information is still available, even with an ideal polarizer.

To simplify the calculation a 'quasi-ideal'³⁴ mirror, i.e. the assumption of a retardance of $\delta = 180^\circ$ in eq. (5.10), is used. Its Mueller matrix is:

$$\mathbf{M}_{\text{mirror,ideal}} = \begin{pmatrix} \alpha & \beta & 0 & 0 \\ \beta & \alpha & 0 & 0 \\ 0 & 0 & -\gamma & 0 \\ 0 & 0 & 0 & -\gamma \end{pmatrix}, \quad (5.33)$$

³³Keeping the polarizer fixed as for the polarimeter calibration data is no option here

³⁴'ideal' would additionally require $r_x = r_y = 1$.

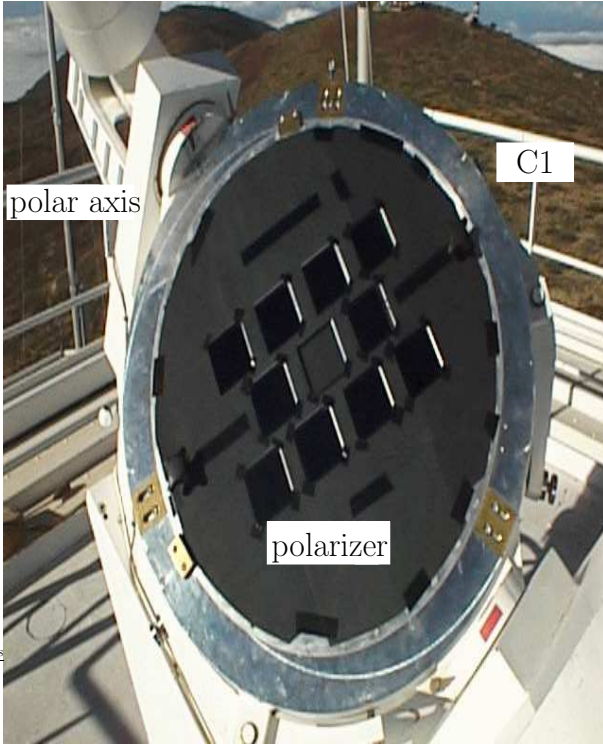


Figure 5.10: The array of sheet polarizers in the infrared for the TIP on top of the first mirror. Only 10 of the 19 polarizing sheets were delivered to that time. The whole array can be rotated on the mirror to create different linear polarizations.

where $\alpha = (r_x + r_y)/2$, $\beta = (r_x - r_y)/2$, and $\gamma = \sqrt{r_x r_y}$.

If the optical train for the rotated polarizer with the angle θ before and $-\theta$ ³⁵ after the mirror is calculated, the transmitted intensity is:

$$I(\theta) = \frac{1}{4} \cdot (\alpha \cdot (1 + \cos^2 2\theta) + 2 \cdot \beta \cdot \cos 2\theta + \gamma \cdot \sin^2 2\theta) \quad (5.34)$$

For $r_x = r_y$ the intensity I is constant. In all other cases a modulation of the intensity dependent on the mirror properties remains.

It should thus be possible to extract the properties of the first coelostat mirror from the intensity I in the data set. Fig. 5.11 displays a result for eq. (5.34) predicted from the telescope model. The non-normalized matrix $(\mathbf{T})_{\text{pol},C1}$ with the inclusion of the polarizer array on C1 is applied on unpolarized sunlight with the intensity I_0 . The physical mirror parameters were taken from an ASP telescope calibration and can be found in the caption. The variables in eq. (5.34) here are $\alpha = 0.897$, $\beta = -0.0079$, and $\gamma = 0.893$, calculated from eqs. (5.11)-(5.13)³⁶. The total transmitted intensity drops to about 16 % of the incident intensity, which will require longer integration times. Note that the position of the extrema in Stokes I (=extrema of eq. (5.34)) are not directly related to the extrema of the polarizations (dependent on angle θ_{pol}).

From observational data taken with a calibration unit of similar design in the infrared range (see Fig. 5.10) an additional complication seems to be present. The array of polarizers does not cover the full area of the mirror. There are strong hints that in the rotation of the array an intensity modulation appears due to a cross-mounting holding a folding mirror in the vacuum tank. This mirror reflects light out of the beam path to the telescope guiding system. A rotation of the structure of Fig. 5.7 over this cross-like pattern of non-neglectible extension leads to a variation in intensity of an order similar to the one due

³⁵The minus arises due to the counter-clockwise definition of the angle. The x-axis of the mirror is assumed to coincide with the zero position of the array of polarizers.

³⁶The calculated retardance of the first mirror is $\delta = 175.16^\circ$, which motivates the neglect of the off-diagonal terms $\propto \sin \delta$ in the lower right corner of the mirror matrix.

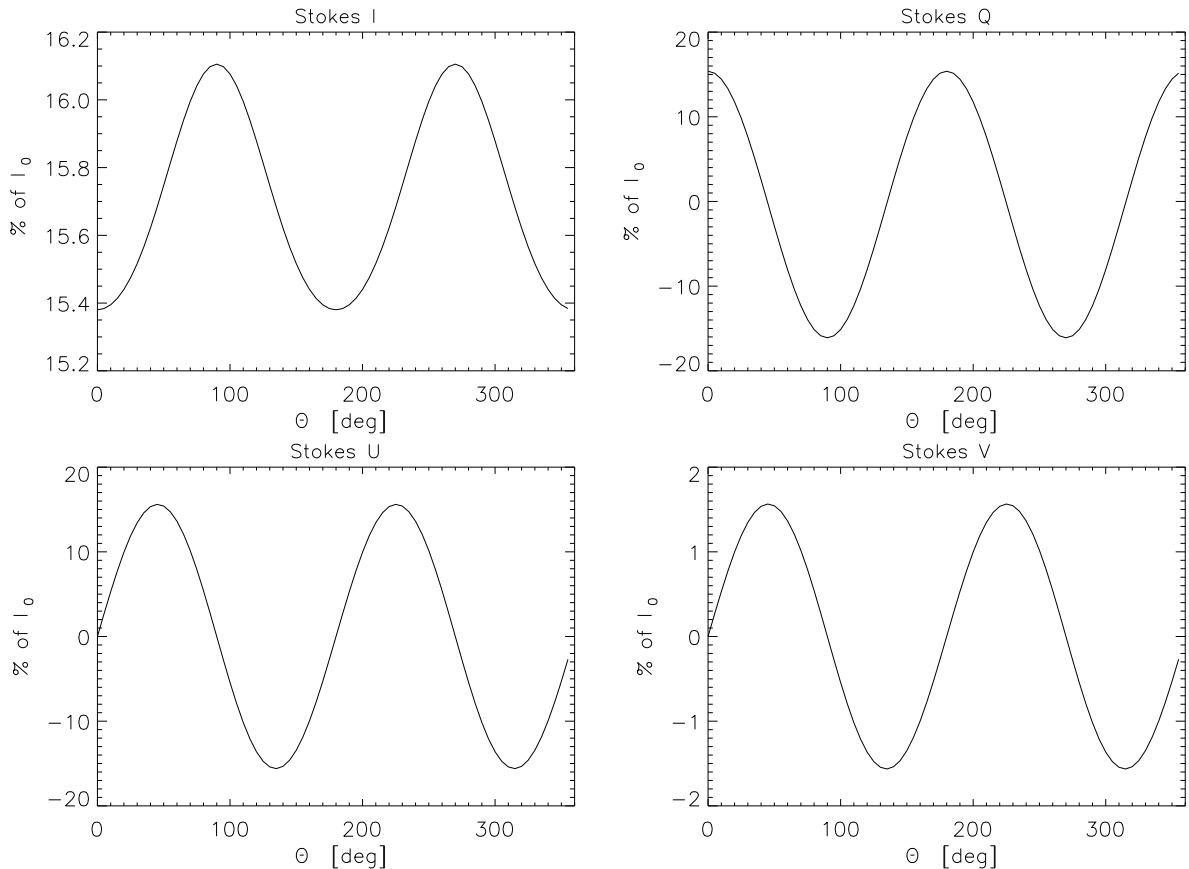


Figure 5.11: Stokes vector for a full rotation of the telescope calibration unit on the first mirror C1 in the model. Date: 21.07.02, 12:00 UT, azimuth = 0° . Mirror parameters $(n, k, d/\lambda, \nu) = (0.30, 3.63, 0.094, 1.54)$, taken from an ASP telescope calibration. The window is excluded, $\theta_{tel, pol} = 90^\circ$. The array of polarizers is placed on top of C1 and rotated for an angle $\theta \in [0, 360^\circ]$. The resulting matrix $(\mathbf{T})_{pol, C1}$ is applied on unpolarized sunlight with the intensity I_0 . The transmitted intensity is given in % of the incident intensity. See text for more details.

to eq. (5.34). It may be necessary to remove this purely geometrical effect by a calculation of the area shaded for each angle θ to obtain the information important for the polarimetric properties.

5.2.2.3 Additional possibilities for the telescope calibration

There are some other methods to establish the instrumental polarization of the telescope. They mainly differ in the way used to create the known polarization input of the incoming beam.

- The usage of the presumably unpolarized sun light from a non-magnetic region at disc center, corresponding to a Stokes vector of $(I, 0, 0, 0)$. This has some disadvantages:
 - The application of the telescope matrix on unpolarized light only uses the first column. No direct control of the entries of the cross-talk between polarization states is possible.
 - The window properties will most likely not be well determined, as they are more important for the polarized states than intensity.

This input of unpolarized light should only be used in addition to other data in the determination of the instrumental polarization, but is well suited as a control value for predictions of the telescope model.

- The usage of a sunspot with a magnetic field aligned parallel to the LOS. The magnetic field lines are assumed to be vertically upwards, with regard to the solar surface, in the center of the umbra of a sunspot. Depending on the position of the spot on the solar disk a point may contain field lines parallel to the LOS. The emerging light of this point then is polarized only circularly, corresponding to a Stokes vector of $(I,0,0,V)$. This has the only drawback to find a suited sunspot near disk center at the day of the calibration measurements. As this coincidence can not be planned, this possibility should also be seen as an addition.
- The usage of mirror parameters measured in a laboratory from samples. These samples always must be kept under the same environment conditions as the telescope mirrors. This method seems to have too many error sources to be used. The results for the mirror parameters at the Dunn VTT strongly deviate from literature values for aluminium coatings, which were measured in optical laboratories. The mirrors are part of a complicated optical setup, where not all polarization-sensitive elements in the beam path may have been explicitly included in the telescope model. Most likely this will lead to effective values for the physical parameters only weakly connected to, for example, the actual refraction index of a single mirror.

Chapter 6

Observations with the ASP: evaluation of polarimetric data

"Forget about the ASP for a moment..."

M.Collados Vera (2002, in a discussion)

The evaluation of two data sets from the ASP was performed prior to the diploma thesis as preparation to the calibration of POLIS. It was intended as a preliminary examination of the quality of the data, and to get used to polarimetric data. All interpretations and conclusions drawn stem from the limited knowledge of the author on the discussed subjects¹. Again here actual data from POLIS was planned to be used, but this was impossible due to the delayed setup.

The section shall demonstrate the properties and some evaluation possibilities of polarimetric data. Some of the effects mentioned in section 2.1 can be displayed.

6.1 Measurement data: size and content

The data sets available were a scan of 239 scan steps over a magnetic active region with emergent flux, and a single sunspot with 120 scan steps. The polarimetric data measured by the ASP is the intensity and the polarization content for the wavelength range from about 630.0 nm to 630.4 nm (cp. table 4.1). Fig. 6.1 gives the profiles in one row of a data image from the active region. There are four spectral lines included in the intensity spectrum of Stokes I:

- two telluric O_2 -lines, which are formed in the atmosphere of the earth at their rest wavelength. They can be used as reference for absolute velocity calibrations or to measure the spectral dispersion per detector pixel.
- two FeI lines of solar origin. These may show Dopplershifts due to relative motions, between earth and sun, the solar rotation and finally motions of material in the photosphere of the sun. The displacement from their rest wavelength gives the LOS velocity. In the profiles of Fig. 6.1 the magnetic field strength is sufficient to produce a visible splitting of the line with the greater Landé factor in the intensity profile. The intensities of the linear polarizations Stokes Q and U give information on the horizontal field component, while the signal in Stokes V is proportional to the LOS component.

More information on the spectral lines can be found in table 4.4. Along the slit height corresponding to 74 arcsecs on the solar image 229 rows of (I,Q,U,V) profiles are available for each scan step. A reduction to two-dimensional maps of selected parameters is shown in for example Fig. 6.6 and 2.1.

¹And may be wrong.

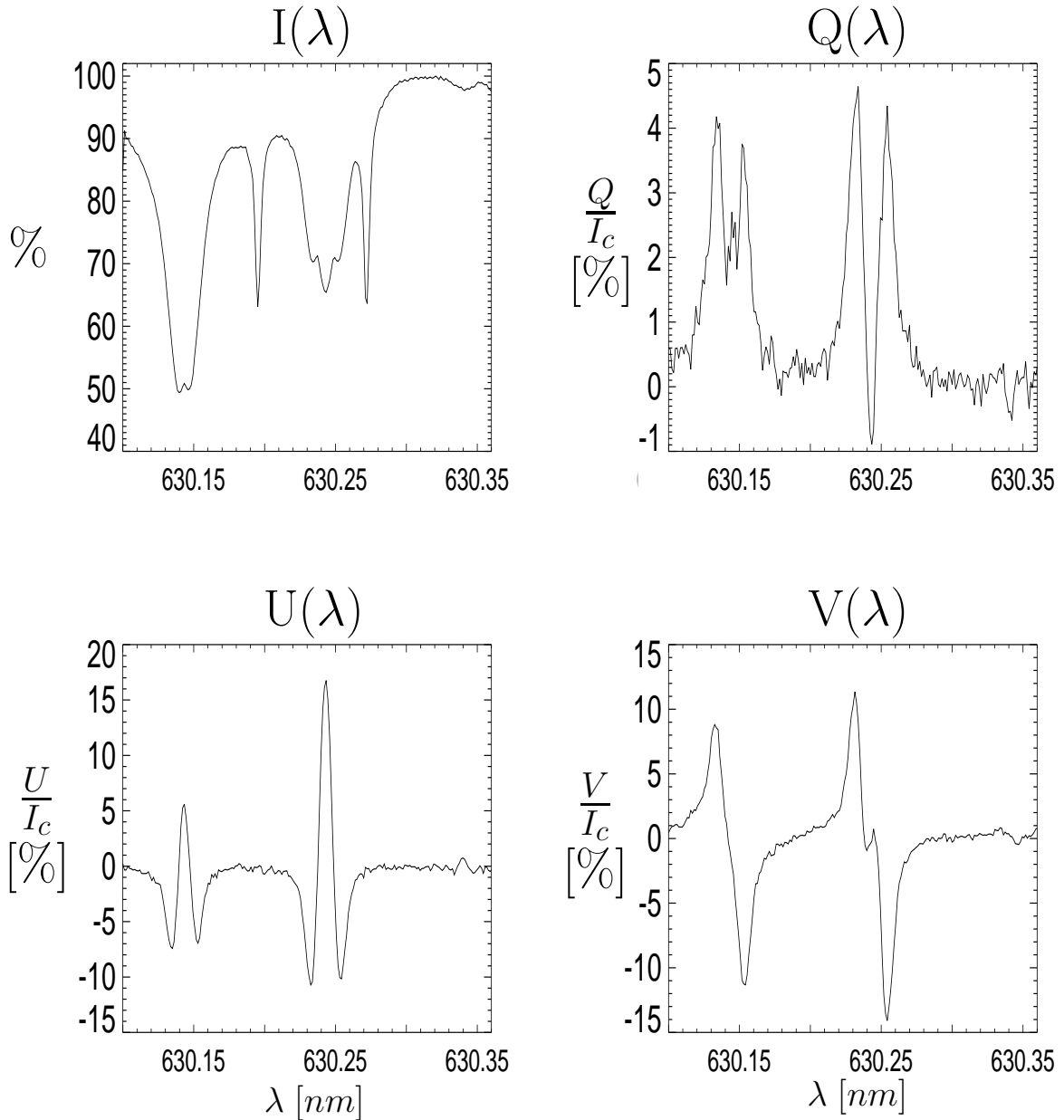


Figure 6.1: Stokes spectra (I, Q, U, V) (λ) of the wavelength region around 630 nm. All profiles are normalized by the continuum intensity I_c calculated from the spectral range around 630.30 nm.

In Stokes I four spectral lines can be identified. The sharp lines at 630.20 nm and 630.27 nm are telluric O_2 -lines formed in the atmosphere of the earth. They can be used for a calibration of velocities, as they show no systematic Dopplershift due to any systematic motion. The two FeI lines at 630.15 and 630.25 nm are of solar origin. The line with the greater Landé factor shows a visible splitting.

The linear polarizations Q and U correspond to the case depicted in Fig. 2.4, bottom right.

The observation direction is not perpendicular to the magnetic field, so also a vertical component is present as proven by the signal in Stokes V. These profiles were taken from the data set of an active region and show a great amount of linear polarization, while in the sun spot data set the magnetic field is mainly vertical.

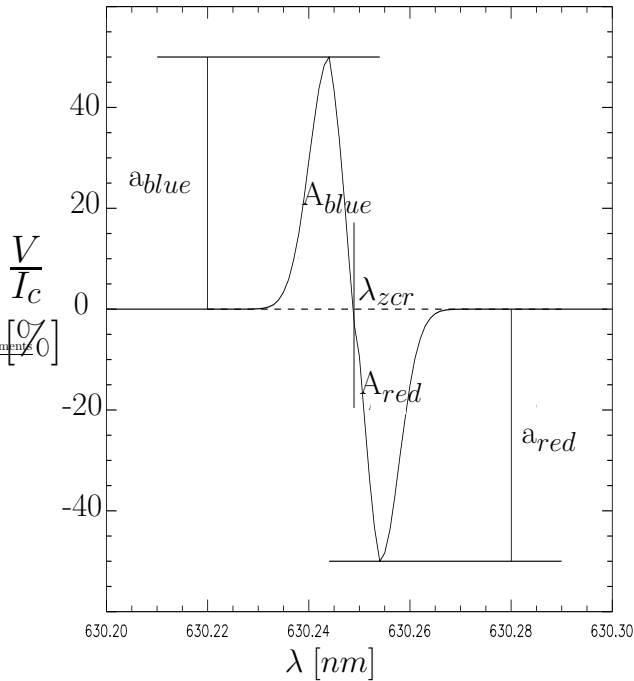


Figure 6.2: Artificial Stokes-V profile for the FeI line at 630.25 nm.

The amplitudes $a_{blue/red}$ can be used for the construction of magnetograms. The positions of minimum and maximum exchange when the magnetic field lines are of opposite direction. Subtraction of the areas under the single peaks, $A_{blue/red}$, gives the net circular polarization (NCP). The wavelength of the zero-crossing, λ_{zcr} , is the position of the π -component, which is not influenced by the magnetic field. The calculation of the zero-crossing velocity from λ_{zcr} gives the velocity of material inside the magnetic field. This can be compared to the velocity derived from the intensity profile, containing mostly the non-magnetic environment.

6.2 Evaluation of the Stokes V signal

An accurate measurement is easiest for the Stokes V signal for two reasons: the magnetic fields on the sun are usually more vertical than horizontal with regard to the solar surface, thus they are more or less oriented parallel to the LOS. Therefore the signal in V is usually the strongest. Secondly, the polarization effects of mirrors or other optical devices in the beam path are smaller for circular polarization. Before the use of vector polarimeters so-called magnetographs (cp. the introduction to chapter 3) were mainly in operation for solar magnetometry, which measure the amount of circular polarization only.

Fig. 6.2 gives an idealized Stokes V profile for a magnetic sensitive spectral line. It is useful to define the following quantities for an evaluation:

- $a_{red/blue}$ are the maximal amplitudes of the signal at the position of the left or right circular component. A magnetic field with the opposite direction exchanges the position of the peaks, i.e. then the minimum would precede. The amplitude can be used for the construction of magnetograms like in Fig. (6.6) or (2.1). They give an estimation of vertical strength and the direction, sometimes called polarity, of the field.
- $A_{red/blue}$ is the area under the single peaks. Their subtraction results in the net circular polarization (NCP).
- The zero-crossing wavelength λ_{zcr} is the position of the transition (π -component) of the spectral triplet, that is not influenced by the magnetic field (cp. Fig. 2.3).

6.2.1 The zero-crossing velocity

The last item, the zero-crossing wavelength, is important to establish the LOS velocity of material in the magnetic field, v_{zcr} . This may be different to the velocity derived from the intensity line profile, which contains contributions from non-magnetic areas. Examples of velocity maps are displayed in Fig. 6.3 for the sunspot data. The pattern of velocities towards and away from the observer, roughly anti-symmetric to the direction to the center of the solar disk (not drawn), is caused by the Evershed effect. This is assumed to be a radial outflow from the sunspot center, where the different viewing angle on the spot

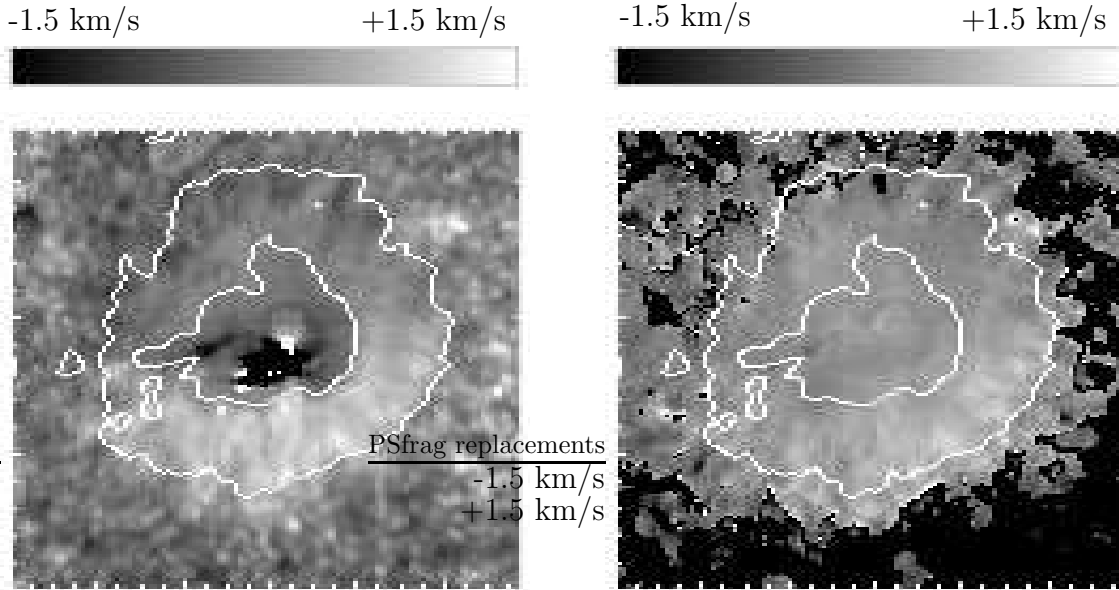


Figure 6.3: Dopplergram (*left*) and zero-crossing map (*right*) of the sun spot from Fig. 2.1. The Doppler shift caused by the relative movement of earth and sun and the sun rotation has been subtracted. Outside the spot single granulation cells can be identified, in which hot material is rising, then cooling and sinking down at their borders. The anti-symmetrical pattern of motions towards (lower hemisphere) and away from the observer (upper hemisphere) in the spot is caused by the Evershed effect. The radial outflow of material from the spot center has an effective LOS component depending on the azimuthal position in the spot. For the area in the central umbra, where the line profile splits up, the evaluation method with a parabola fit is not suited, as the artifacts in the left panel display. The zero-crossing map of the velocity in the magnetic field shows the same general structure. Here the central umbra with strong Stokes V signals presents no difficulties for the calculation of the zero-crossing wavelength. In the uniform black area outside the spot no zero-crossing can be established (insufficient V signal). The magnetic field extends over the boundary of the penumbra in the continuum (outer white line). The limit for the evaluation of a Stokes V profile was a minimal polarization content of 1 %, which is exceeded in the outer regions as well.

changes the measured LOS velocity². The diagnostic importance of the zero-crossing velocity is shown in Fig. 6.4. The difference between the LOS velocity from the intensity profile, v_{dop} , and v_{zcr} displays some features:

- Single magnetic elements outside the spot may show up as well as down flows relative to their environment.
- The Evershed effect can still be seen in the two images, which give the difference of the velocities, $v_{dop} - v_{zcr}$, for $v_{zcr} > v_{dop}$ and $v_{zcr} < v_{dop}$ separately. Above the spot the filling factor, i.e. the fraction of area covered by magnetic fields, can assumed to be 100 %. Therefore no velocity differences should be seen at all, as all material is inside magnetic fields. Single unresolved, concentrated magnetic structures with a small filling factor inside a detector element would contribute to the Stokes V signal, but only little to the intensity due to the small area covered. If these structures have a significantly differing mass velocity, they may cause an additional shift of the zero-crossing wavelength relative to the intensity line core. The clearly visible remaining velocity differences therefore hint to unresolved magnetic elements in the penumbra.

²see Westendorp et al. (2001), [29], or Schlichenmaier and Schmidt (2000, [20] and [21]) for a detailed examination of LOS-velocities in a sunspot

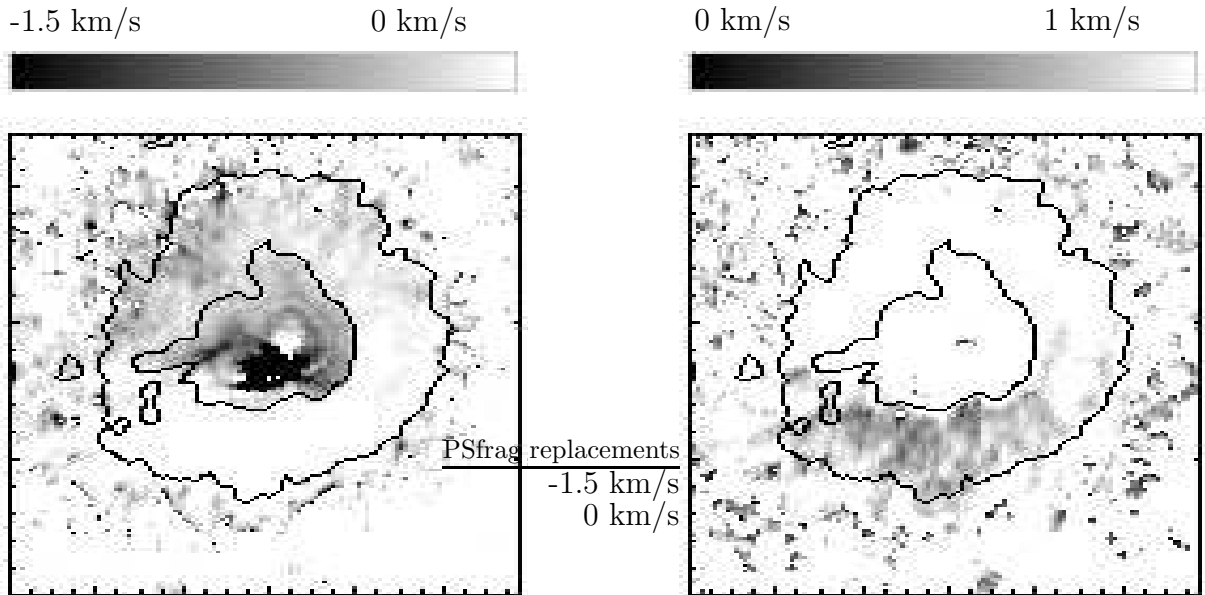


Figure 6.4: The difference between dopplergram and zero-crossing velocity from Fig. 6.3, (left) $v_{zcr} > v_{dop}$, (right) $v_{zcr} < v_{dop}$.

Outside the spot the velocity in isolated magnetic elements shows up as well as down flows relative to the non-magnetic environment. The Evershed effect remains even after the subtraction of both images. The white rectangle marks a feature in the outer penumbra, where in an extension of a brightening in the intensity a radial oriented region with a velocity difference of about 1 km/s can be seen.

- The rectangle in the left image highlights a substructure inside the penumbra. In an extension of a brightening in the continuum intensity a radially oriented region shows v_{zcr} to be greater than the doppler velocity by about 1 km/s. Such a feature can be explained by the model of single flux tubes embedded in the background field of a sun spot (Schlichenmaier, [19], 1997). This model predicts nearly horizontal flux tubes in the outer penumbra, inside which flows of up to 15 km/s can appear. If one assumes the remaining velocity difference to be caused by a horizontal flow in a single flux tube, and a viewing angle of about 10° , the horizontal speed would need to be here app. 6 km/s greater than in its environment.

6.2.2 Net circular polarization

The area under the single wings of the Stokes V profile, A_{blue} and A_{red} , should be equal for a static atmosphere in local thermal equilibrium. Fig. 6.5 displays, that this is very often not the case in the sunspot. In the upper hemisphere the complete penumbra shows net circular polarization (NCP), i.e. an integration along the wavelength dimension leads to a residual value not equal to zero. The NCP value changes abruptly at the border of penumbra and umbra from the continuum image, in difference to the magnetogram, where the transition is smooth. This behaviour can be also be explained by the model of moving flux tubes on the background field of the sunspot (Schlichenmaier, [19], 1997, and Schlichenmaier et al., 1998). The existence of more horizontal, isolated flux tubes in the outer penumbra, in which the plasma moves radially outwards with a speed of about 15 km/s, leads to gradients in either the velocity and the magnetic field strength along the LOS. If gradients in both environment parameters are present, the produced Stokes V signal has a non-vanishing NCP. Inside the umbra no isolated elements appear.

The particular shape of the NCP, being roughly symmetric to an axis from the top to the bottom of the image, is predicted by the thesis of Müller, [16], 2001. In this thesis synthetic NCP maps of axialsym-

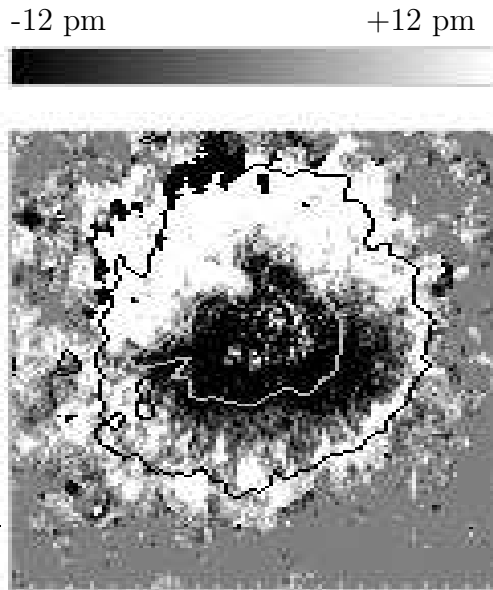


Figure 6.5: Map of the net circular polarization (NCP). The value is calculated as in Schlichenmaier et al. (2001), $NCP = \int V(\lambda)d\lambda$, with V in % of I_c . The NCP gives the difference between the areas A_{red} and A_{blue} , if the V signal is zero outside the magnetic sensitive spectral line. If the NCP is not equal to zero for the whole profile, the Stokes V signal is not fully anti-symmetric. The NCP abruptly changes at the border between umbra and penumbra in the upper hemisphere. This indicates quite different environment conditions, mostly in material velocities, as the magnetogram in Fig. 2.1 shows a smooth transition.

metric sunspots for different spectral lines were examined, which were constructed by placing the final results of the moving tube simulations into a three-dimensional background field. The calculation of the NCP of the Stokes V profile along the LOS around the spot resulted in a symmetric shape for the iron line at 630.25 nm. For another iron line at 1564 nm the NCP should be anti-symmetric. This could be confirmed by observations with the Tenerife Infrared Polarimeter (TIP) (Schlichenmaier et al., 2001). To give one additional example of polarimetric data, Fig. 6.6 shows some maps of the other data set taken with the ASP. This active region is dominated by the increased appearance of opposite polarities, i.e. magnetic fields with opposite directions, opposite to the sun spot data with mainly a single polarity. A time series was taken for the area in the center of the image, where the dopplergram shows the disturbance of the granulation pattern by the magnetic fields, to study the evolution of this emerging magnetic flux. A complete evaluation of the data set requires an inversion. An extended discussion of the data can be found in the report on the 'Hauptpraktikum',[1].

Summary:

Polarimetric data of the Stokes vector allows to calculate the vector magnetic field, i.e. field strength and direction. The zero-crossing wavelength gives the velocity of material inside magnetic elements, which may differ from the Doppler velocity of the intensity profile. The NCP hints to gradients in velocity and field strength. It can be used to test theoretical models. The environment conditions in umbra and penumbra of sunspots are different. Last, but not least: every interpretation of polarimetric data rests on the assumption, that the effects are of solar origin only. The calibration of the data should be better than the order of the observed effect, especially for the correct interpretation of weak polarization signals.

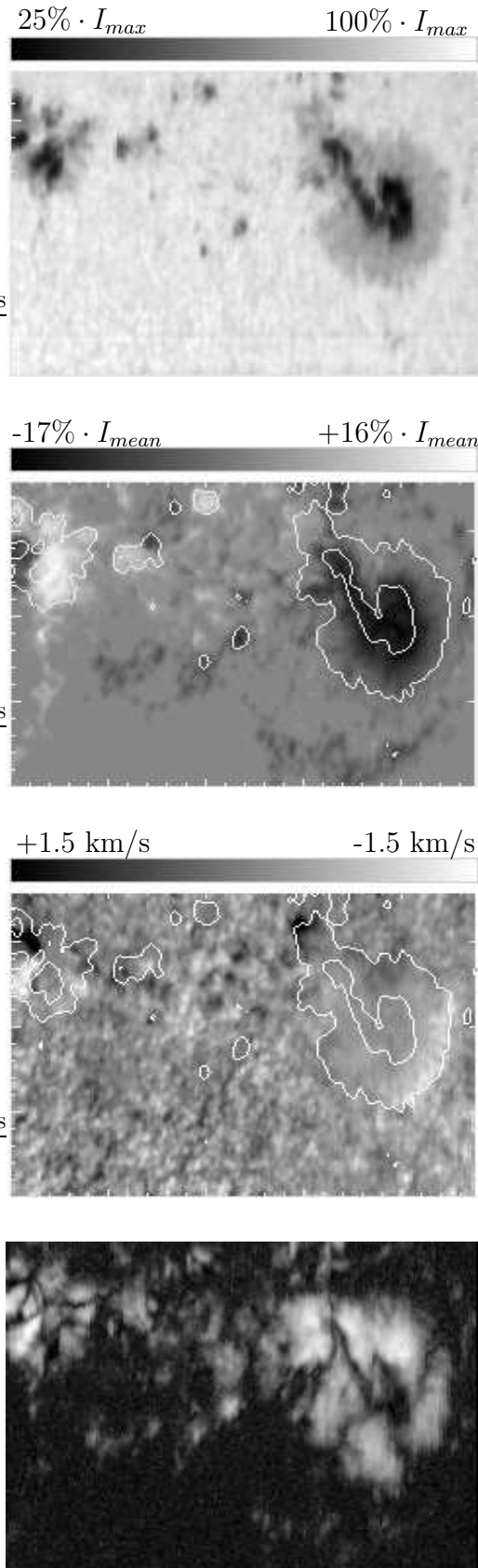


Figure 6.6: Data set of the ASP of an active region, taken on 29.09.00 (courtesy W.Schmidt), preliminary evaluation by the author. The image area is $90'' \times 63''$, consisting of 240 steps of $0.375''$ stepwidth. The spectral line is FeI at 630.25 nm.

The continuum intensity drops to 25 % of the maximum intensity in the sunspots and pores. The spot itself can be divided in dark umbra and brighter penumbra. In comparison with Fig. 2.1 the minimal intensity is higher, while the Stokes-V amplitude is lower.

The signed amplitude of the Stokes-V signal in % of the mean intensity with superimposed borders of the umbra and penumbra.

The amplitude is proportional to the magnetic field strength, while its sign distinguishes the field direction to or away from the observer. Some of the pores and the sunspot at the left border of the area can be seen to be of opposite polarities. The region in the center of the image shows additional magnetic activity, which is not visible in the continuum intensity above.

A Dopplergram of the LOS velocities relative to the solar surface with superimposed borders of the umbra and penumbra.

The velocity pattern outside the strong magnetic fields reflects the movements of the granulation, hot material rising and cooler sinking. The *Evershed flow* can be seen in the greater sunspot. The granulation pattern between the two spots is slightly distorted, presumably due to the presence of magnetic field in that area.

A logarithmic map displaying $\log(\int |Q(\lambda)| d\lambda)$.

The Stokes parameter Q measures linear polarization, which corresponds to more horizontal magnetic fields. These are strongest in the area between the two pores of different polarity at the left border. This can be explained by field lines connecting the opposite polarities in a loop, where at the top of the loop the field is horizontal. The cross-like structure in the greater sunspot is caused by the axialsymmetric field of a spot, where the angle between LOS and magnetic field lines is the same for different positions around the spot center.

Bibliography

- [1] **C. Beck** , *Kalibration und Auswertung von ASP-Daten (Hauptpraktikumsbericht)*, April 2001, KIS library, in german

The report on the 'Hauptpraktikum' gives a slightly shortened translation into german of the theory as described in [4]. Further the calibration of an ASP data set is discussed as well as results of a preliminary evaluation.

- [2] **M. Born, E. Wolf** , *The Principles of optics* , Pergamon, New York, 1970
- [3] **C. Capitani, E. Landi degl'Innocenti, F. Cavallini, G. Ceppatelli, M. Landi degl'Innocenti** , *Polarization properties of a 'Zeiss-type' coelostat - The case of the solar Tower in Arcetri* , Solar Physics, vol. 120, no. 1, 1989, p. 173-191

A theoretical description of the polarizing properties of a 'Zeiss-type' coelostat which can be transferred on other coelostats as well by considering the different geometrical design.

- [4] **Edward Collett** , *Polarized light : fundamentals and applications* , Marcel Dekker Inc., New York, 1993

The book of Collett gives a very extensive derivation of the Stokes and Mueller calculus and also other theoretical descriptions of polarized light. Its primary strong point are the many examples used to demonstrate the theory and the interesting remarks on the historical evolution in this field.

- [5] **W. Demtröder** , Band 3 : *Atome, Moleküle und Festkörper* , Springer, Berlin, 1994
- [6] **D.F. Elmore, B.W. Lites, S. Tomczyk, A.P. Skumanich, R.B. Dunn[†], J.A. Schuenke, K.V. Streander, T.W. Leach, C.W. Chambellan, H.K. Hull, L.B. Lacey[†]** , *The Advanced Stokes Polarimeter : A new instrument for solar magnetic field research* , AAS, 1992

A full description of the ASP dual beam polarimeter, only the part about the nonlinearity of the cameras has become obsolete.

- [7] **G.E. Hale** , *On the probable existence of a magnetic field in sun-spots* , ApJ **28** , 1908
- [8] **U. Grossmann-Doerth** , *Height of formation of solar photospheric spectral lines* , Astron. Astrophys., 285, p. 1012-1018, 1994
- [9] **U. Grossmann-Doerth, B. Larsson, S.K. Solanki** , *Contribution and response functions for Stokes line profiles formed in a magnetic field* , Astron. Astrophys., 204, p. 266-274, 1988
- [10] **F.W. Jaeger, L. Oetken** , *Zur Theorie und Praxis der instrumentellen Polarisierung I & II* , Publ. des Astrophys. Observatoriums Potsdam, Band 31, Nr. 103 & 107, Akademie-Verlag Berlin, 1963 & 1968
- [11] **A. Kučera, H. Balthasar, J. Rybák, H. Wöhl** , *Heights of formation of Fe I photospheric lines* , Astron. Astrophysics, 332, p. 1069-1074, 1998

- [12] **E. Landi Degl’Innocenti** , *Magnetic field measurements* , in: Solar Observations: techniques and interpretation, Sánchez, Collados, Vázquez (Eds.), Cambridge Univ. Press, 1992
- [13] **B.W. Lites** , *Rotating waveplates as polarization modulators for Stokes polarimetry of the sun : evaluation of seeing-induced crosstalk errors* , Applied Optics **26** , 3838, 1987

Also includes details on the demodulation scheme.

- [14] **P. Magain** , *Contribution functions and the depths of formation of spectral lines* , Astron. Astrophys., 163, p. 135-139, 1986
- [15] **Mayer-Kuckuck** , *Atomphysik* , Teubner, Stuttgart, 1997, 5.Auflage
- [16] **D. Müller** , *Polarisation von Linien im Spektrum einer Sonnenflecken-Penumbra (Dipl. thesis)* , Freiburg, 2001
- [17] **M. Owner-Petersen** , *On the polarization effects of stress induced birefringence of the entrance window of solar telescopes* , LEST Foundation, Technical report No. 49, 1991
- [18] **J. Sánchez Almeida, B. Ruiz Cobo, J.C. del Toro Iniesta** , *Heights of formation for measurements of atmospheric parameters* , Astron. Astrophys. 314, p. 295-302, 1996
- [19] **R. Schlichenmaier** , *Die Dynamik magnetischer Flußröhren im Sonnenfleck (Diss.)* , LMU München, 1997
- [20] **R. Schlichenmaier, W. Schmidt** , *Flow geometry in a sunspot penumbra* , Astron. Astrophys. 358, p. 1122-1132, 2000
- [21] **W. Schmidt, R. Schlichenmaier** , *Small-scale flow field in a sunspot penumbra* , Astron. Astrophys. 364, p. 829-834, 2000
- [22] **William A. Shurcliff** , *Polarized light* , Harvard University Press, 1962

For questions of more technical nature the older book of Shurcliff still can be used, it includes details on the production and classification of polarizers.

- [23] **M. Sigwarth** , *Dynamik solarer Magnetfelder (Diss.)* , Februar 1999
- [24] **A. Skumanich, B.W. Lites, V. Martínez Pillet, P. Seagraves** , *The calibration of the Advanced Stokes Polarimeter³* , ApJ Suppl. **110** , 357, 1997

A detailed description of the telescope model, calibration procedure and results of it for the ASP.

- [25] **J.O. Stenflo** , *Solar magnetic fields* , Kluwer Academic Publishers, 1994

Strongly theoretical inclined book describing mainly the radiation transport equations and ways to a solution. The short experimental chapter is nonetheless sufficient for a quick overview on polarimetry.

- [26] **M. Stix** , *The sun* , Springer-Verlag, 1989
- [27] **K.G. Strassmeier** , *Aktive Sterne : Laboratorien der solaren Astrophysik* , Springer-Verlag Wien/New York, 1997

The book uses the sun, whose activities are best known and are described in detail, to mark differences and commons to active stars. It highlights some not understood features of the solar dynamo in comparison with other stars, mainly the dependence on rotation, as stars require certain conditions before getting active at all.

³Available in a translation into german by the author

- [28] **H.-H. Voigt** , *Abriss der Astronomie*, Bibliographisches Institut, Mannheim, 1969
- [29] **C. Westendorp Plaza, J.C. del Toro Iniesta, B. Ruiz Cobo, V. Martinez Pillet** , *Optical tomography of a sunspot. III. Velocity stratification and the Evershed effect* , ApJ, V 547, 2001

Appendix A

The Mueller matrices

In the Stokes formalism the effects of optical active elements can be formulated as matrices $\mathbf{M} \in \mathbb{R}^{4 \times 4}$, which are applied on the Stokes vector $\mathbf{S} \in \mathbb{R}^4$ as defined in equation (2.8). The matrix elements are determined from the electrical field components before (E_x, E_y) and after (E'_x, E'_y) the transmission through the element from the equation

$$\mathbf{S}' = \mathbf{M} \cdot \mathbf{S} . \quad (\text{A.1})$$

For this calculations an equivalent definition of the Stokes parameters with complex field amplitudes is very useful. It is given by substituting equation (2.4) with

$$\begin{aligned} E_x(t) &= E_{x,0} \cdot \exp [i (\omega t + \delta_x)] \\ E_y(t) &= E_{y,0} \cdot \exp [i (\omega t + \delta_y)] \end{aligned} \quad (\text{A.2})$$

and changing the definition of the Stokes parameters to

$$\begin{aligned} S_0 &= E_x E_x^* + E_y E_y^* \\ S_1 &= E_x E_y^* - E_y E_x^* \\ S_2 &= E_x E_y^* + E_y E_x^* \\ S_3 &= i (E_x E_y^* - E_y E_x^*) . \end{aligned} \quad (\text{A.3})$$

An explicit calculation and also the proof of equivalency can be found in [4]. Here shall only the results for the different optical elements being used be presented.

The polarizer

A polarizer is an optical element with a transmission dependent on the oscillation direction of the electrical field and can be described by

$$\begin{aligned} E'_x &= p_x \cdot E_x \\ E'_y &= p_y \cdot E_y , \end{aligned}$$

with $0 \leq p_x, p_y \leq 1$.

Inserting the electrical field amplitudes into equation (A.1) one obtains the Mueller matrix of a linear polarizer as

$$\mathbf{M}_{\text{pol}} = \frac{1}{2} \begin{pmatrix} p_x^2 + p_y^2 & p_x^2 - p_y^2 & 0 & 0 \\ p_x^2 - p_y^2 & p_x^2 + p_y^2 & 0 & 0 \\ 0 & 0 & 2 \cdot p_x \cdot p_y & 0 \\ 0 & 0 & 0 & 2 \cdot p_x \cdot p_y \end{pmatrix} . \quad (\text{A.4})$$

The retarder

A retarder has different propagation velocities for the two directions (x,y). It changes the relative phase between the field components. Here is

$$\begin{aligned} E'_x &= e^{+i\Phi/2} \cdot E_x \\ E'_y &= e^{-i\Phi/2} \cdot E_y, \end{aligned}$$

and the Mueller matrix resulting is

$$\mathbf{M}_{\text{ret}} = \begin{pmatrix} 1 & 0 & 0 & 0 \\ 0 & 1 & 0 & 0 \\ 0 & 0 & \cos \Phi & \sin \Phi \\ 0 & 0 & -\sin \Phi & \cos \Phi \end{pmatrix}. \quad (\text{A.5})$$

The rotator

A rotator rotates (as its name says) the field components by a fixed angle θ . Here is

$$\begin{aligned} E'_x &= E_x \cdot \cos \theta + E_y \cdot \sin \theta \\ E'_y &= -E_x \cdot \sin \theta + E_y \cdot \cos \theta, \end{aligned}$$

and the matrix is

$$\mathbf{M}_{\text{rot}}(2\theta) = \begin{pmatrix} 1 & 0 & 0 & 0 \\ 0 & \cos 2\theta & \sin 2\theta & 0 \\ 0 & -\sin 2\theta & \cos 2\theta & 0 \\ 0 & 0 & 0 & 1 \end{pmatrix}. \quad (\text{A.6})$$

Rotated optical elements

The Mueller matrix of the rotator is especially important as it also allows one to determine the effects of rotated optical elements, which often occur in optical designs. The rotation can be included by two rotator matrices around the optical element itself by

$$\mathbf{M}_{\text{elem}}(\theta) = \mathbf{M}_{\text{rot}}(-2\theta) \cdot \mathbf{M}_{\text{elem}} \cdot \mathbf{M}_{\text{rot}}(2\theta).$$

One example is the rotating retarder used by either the ASP or POLIS :

$$\mathbf{M}_{\text{ret}}(\theta) = \begin{pmatrix} 1 & 0 & 0 & 0 \\ 0 & c^2 + s^2 d & sc(1-d) & -se \\ 0 & sc(1-d) & s^2 + c^2 d & ce \\ 0 & se & -ce & d \end{pmatrix}, \quad (\text{A.7})$$

with $c = \cos 2\theta$, $s = \sin 2\theta$, $d = \cos \delta$ and $e = \sin \delta$. δ is the retardance of the modulator and θ the angle between its fast axis and the x-direction, as always counter-clockwise when looking at the light source¹.

¹I really like that definition.

Polarizing beam splitter

The Mueller matrix of the polarizing beam splitter is²

$$\mathbf{M}_{\text{beamsplitter}}^{\pm} = \frac{r^{\pm}}{2} \begin{pmatrix} 1 & \pm 1 & 0 & 0 \\ 1 & \pm 1 & 0 & 0 \\ 0 & 0 & 0 & 0 \\ 0 & 0 & 0 & 0 \end{pmatrix}. \quad (\text{A.8})$$

The matrix multiplication with the rotated retarder above, application on a Stokes vector (I,Q,U,V) and the selection of the first vector entry gives the intensities of the two beams labelled + respectively - as

$$I^{\pm}(\theta, \delta) = \frac{r^{\pm}}{2} \{ I \pm Q \cdot (c_{2\theta}^2 + s_{2\theta}^2 c_{\delta}) \pm U \cdot s_{2\theta} c_{2\theta} (1 - c_{\delta}) \mp V \cdot s_{2\theta} s_{\delta} \}, \quad (\text{A.9})$$

on which the measurement scheme relies.

²No derivation given.

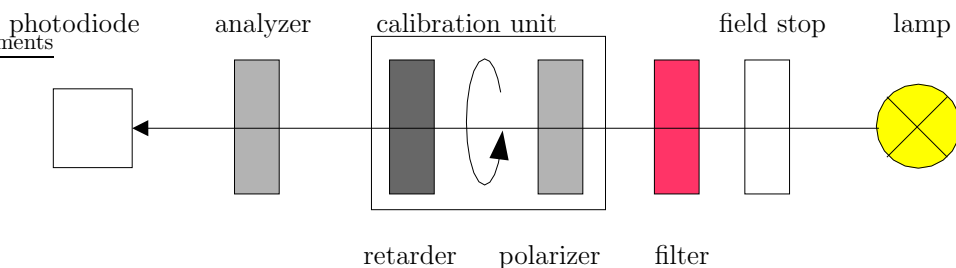
Appendix B

Alignment of the polarimeter calibration unit

In the polarimeter calibration unit two elements have to be aligned correctly, i.e. the direction of the transmission axis of the linear polarizer, and the direction of the fast axis of the retarder have to be established. The measurement setup used is shown in Fig. B.1. In addition to the optical elements under examination a second polarizer as analyzer, a light source, and an intensity detector, in this case a photo diode, are needed. The usage of a wavelength filter for 630 nm is optional to increase the resemblance to the conditions of operation in Tenerife. The field stop reduces the stray light.

Figure B.1: Measurement setup for the alignment of the polarimeter calibration unit.

The optical train consists of an artificial light source, a field stop, a wavelength filter for 630 nm (optional), the polarimeter calibration unit, a second polarizer as analyzer, and a photo diode as intensity detector. The elements of the calibration unit can separately be rotated clockwise, when looking at the light source, for 180°.



The axis of the polarizer is established with the use of the second polarizer, the analyzer. The method introduced in Fig. B.2 works without any axes known beforehand. Note that all position angles derived may be off by 90°, i.e. the axes marked on the polarizers may be the blocking instead of the transmission axes, and the retarder may get the slow instead of the fast axis marked. This can be simply cross-checked with a light source of known polarization, for example reflection under the Brewster angle.

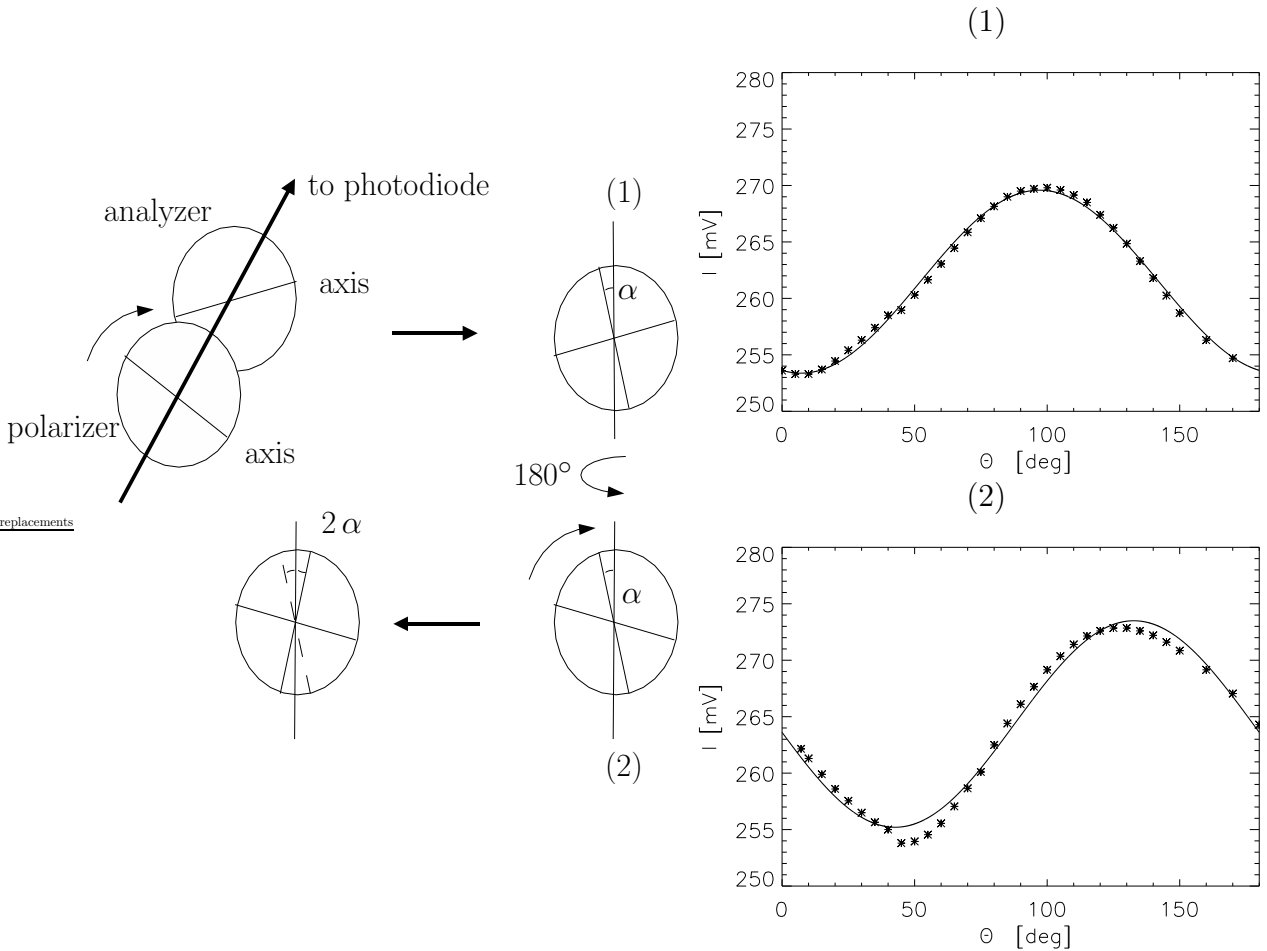


Figure B.2: The transmission axes of the polarizer and the analyzer have arbitrary, and unknown directions. If the polarizer is rotated around the propagation direction, the resulting curve of transmitted intensity, (1), shows a minimum, when polarizer and analyzer are crossed. In the crossed position, $\theta_{pol,min} \sim 7.3^\circ$, the axis of the polarizer forms an unknown angle, α , with the vertical.

Now the analyzer is rotated by 180° around the vertical axis. This causes its transmission axis to jump by 2α . The polarizer is rotated again for 180° , resulting in curve (2).

The minimal intensity now occurs at the angle $\theta_{pol,min} + 2\alpha \sim 40.3^\circ$. The value was established from a least square fit to the intensities for $\theta_{pol} > 45^\circ$ only. The motor seems to have positioning problems around 45° , but it is the spare unit hopefully never to be used.

Half the difference between the angles of minimal intensity is the angle to the vertical, α . Thus the transmission axis of the polarizer is 16.5° off the vertical in the first minimal position, i.e. it is at -23.8° for $\theta_{pol} = 0$. The analyzer can then also be marked.

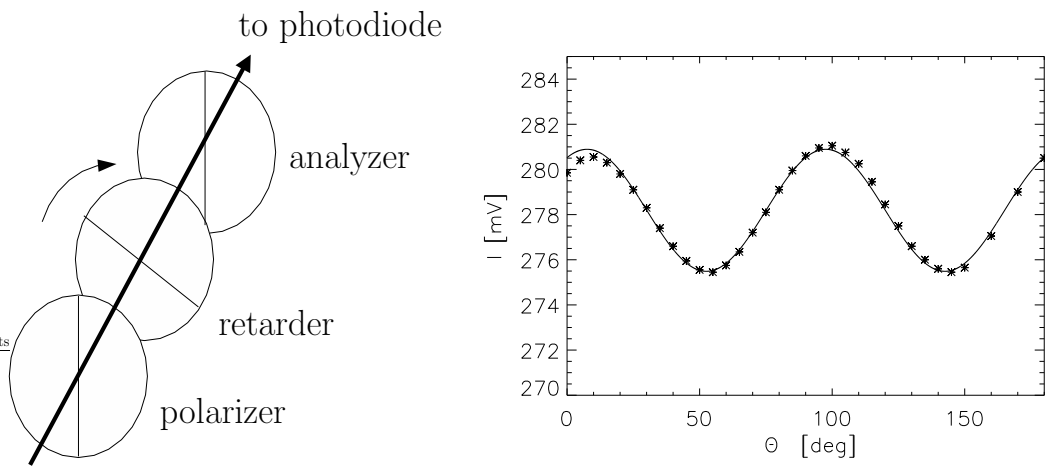


Figure B.3: The axis of the retarder is established by inserting it between the polarizers, now both vertically oriented. The intensity curve for a rotation of the retarder shows maxima, when the fast axis is parallel to the transmission axes of the polarizers. The first maximum appears for $\theta_{ret} = 7.92^\circ$. The axis of the retarder therefore is off the vertical by -7.92° at $\theta_{ret} = 0$.

Appendix C

The analytical telescope model: discussion and comparison

Section 5.2.1 describes a way for the construction of the telescope model that relies on some numerical procedures. The developed procedure can be applied to optical setups other than a coelostat as well, if the beam path is known. For the restriction on the polarimetric properties of a coelostat it is possible to find an analytical solution. Section C.1 presents the formulae of this solution, section C.2 the mirror matrix for optical thick coatings, and section C.3 a discussion on the plausibility of results from the model, and a comparison between the analytical and the numerical method.

C.1 The analytical solution of the telescope model

The paper by Capitani et al, [3], derives analytically the rotation and incidence angles needed for the description of the instrumental polarization of a coelostat. Only the resulting equations for the important parameters $i_1, i_2, \theta_1, \theta_2$ will be presented here.

C.1.1 Position of the second coelostat mirror

This is identically to the discussion in section 5.2.1.4. The position of C2 is fixed by its azimuth A_{C2} , and the horizontal angular height, h_{C2} . For the VTT Tenerife this in fact is easier to establish due to the motion of the first mirror C1 on a circle, while for the solar tower in Arcetri described by Capitani the mirror moves on two orthogonal set of rails (Cap., eqs. (13a)-(13d)). This complicates the calculation of the azimuth due to another degree of freedom.

C.1.2 Analytical equations

The equations derived by Capitani, listed in the required order of calculation, now are:

$$\sin H_{C2} = \frac{\cos h_{C2} \sin A_{C2}}{\cos \delta_{sun}} \quad (C.1)$$

$$\cos H_{C2} = \frac{\sin h_{C2} + \sin \phi \sin \delta_{sun}}{\cos \phi \cos \delta_{sun}} \quad (C.2)$$

$$H = \frac{1}{2} (H_{C2} - H_{sun}) \quad (C.3)$$

$$\sin 2\theta_1 = \frac{2 \sin \delta_{sun} \sin H \cos H}{\sin^2 \delta_{sun} \cos^2 H + \sin^2 H} \quad (C.4)$$

$$\cos 2\theta_1 = \frac{\sin^2 \delta_{sun} \cos^2 H \cos H - \sin^2 H}{\sin^2 \delta_{sun} \cos^2 H + \sin^2 H} \rightarrow \theta_1 \quad (C.5)$$

$$\sin \theta_1 \sin i_1 = -\sin H \quad (C.6)$$

$$\cos \theta_1 \sin i_1 = -\sin \delta_{sun} \cos H \quad (\text{C.7})$$

$$\cos i_1 = \cos \delta_{sun} \cos H \rightarrow i_1 \quad (\text{C.8})$$

$$i_2 = \frac{1}{2} (90^\circ - h_{C2}) \quad (\text{C.9})$$

$$A = A_{C2} - A_{sun} \quad (\text{C.10})$$

$$\sin \theta_2 = -\frac{\cos h_{sun} \sin A}{\sin 2i_1} \quad (\text{C.11})$$

$$\cos \theta_2 = \frac{\sin h_{C2} \cos 2i_1 - \sin h_{sun}}{\cos h_{C2} \sin 2i_1} \rightarrow \theta_2 \quad (\text{C.12})$$

These equations were mainly used to check the results of the numerical routines, but of course they allow the construction of the telescope model by themselves. For the agreement between the two methods see section C.3 below.

C.2 Mirror matrix for optical thick coatings

The mirror matrix for the description of optical thick coatings is in principle identical to eq. 5.10, but the equations for the calculation of the entries simplify. The matrix is:

$$\mathbf{M}_{\text{mirror}} = \frac{r_{\perp}^2}{2} \begin{pmatrix} X^2 + 1 & X^2 - 1 & 0 & 0 \\ X^2 - 1 & X^2 + 1 & 0 & 0 \\ 0 & 0 & 2 \cdot X \cdot \cos \delta & 2 \cdot X \cdot \sin \delta \\ 0 & 0 & -2 \cdot X \cdot \sin \delta & 2 \cdot X \cdot \cos \delta \end{pmatrix}, \quad (\text{C.13})$$

with $X^2 = \frac{r_{\parallel}}{r_{\perp}}$.

The entries can be calculated with

$$f^2 = \frac{1}{2} \left(n^2 - k^2 - \sin^2 i + \sqrt{(n^2 - k^2 - \sin^2 i)^2 + 4n^2 k^2} \right) \quad (\text{C.14})$$

$$g^2 = \frac{1}{2} \left(k^2 - n^2 + \sin^2 i + \sqrt{(n^2 - k^2 - \sin^2 i)^2 + 4n^2 k^2} \right) \quad (\text{C.15})$$

by

$$X^2 = \frac{f^2 + g^2 - 2 \cdot f \cdot \sin i \tan i + \sin^2 i \tan^2 i}{f^2 + g^2 + 2 \cdot f \cdot \sin i \tan i + \sin^2 i \tan^2 i}, \text{ and} \quad (\text{C.16})$$

$$\tan \delta = \frac{2 \cdot g \cdot \sin i \tan i}{\sin^2 i \tan^2 i - (f^2 + g^2)}. \quad (\text{C.17})$$

i is the incidence angle on the mirror, n and k refraction and extinction coefficient. The thickness of the coating and the properties of the substrate do not enter in the calculation.

C.3 Discussion and comparison of model results

The best test of the telescope model is the comparison with actual measurement data from the telescope, but some consistency checks are possible with the model alone.

- image rotation of the coelostat:

If the first mirror C1 is not on the zero azimuth position, the coelostat will perform a rotation of the sun image of

$$p = -\text{asin} \left(\frac{\cos \phi \cdot \sin(\text{azimuth})}{\cos \delta_{sun}} \right) + \text{azimuth}. \quad (\text{C.18})$$

This can be checked with the model in the following way:

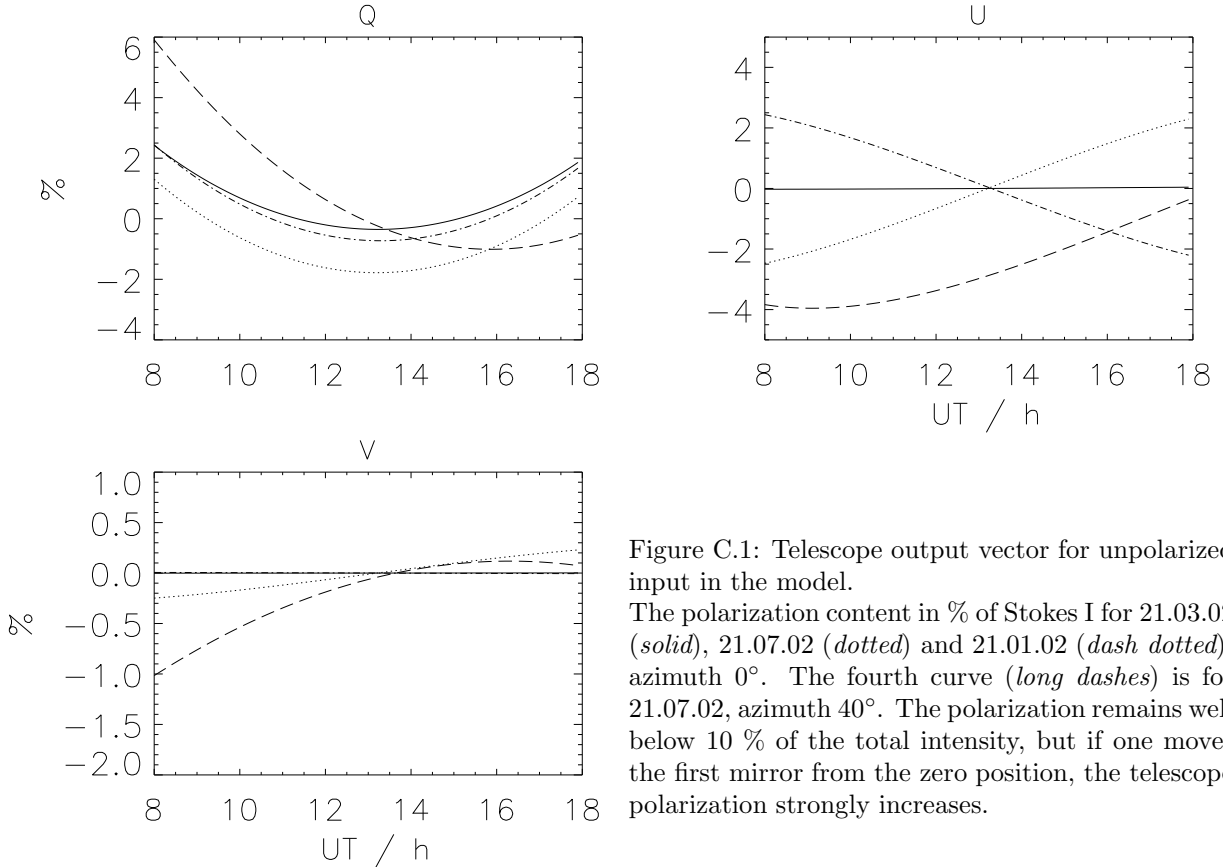


Figure C.1: Telescope output vector for unpolarized input in the model.

The polarization content in % of Stokes I for 21.03.02 (*solid*), 21.07.02 (*dotted*) and 21.01.02 (*dash dotted*), azimuth 0° . The fourth curve (*long dashes*) is for 21.07.02, azimuth 40° . The polarization remains well below 10 % of the total intensity, but if one moves the first mirror from the zero position, the telescope polarization strongly increases.

- the definition of an angle of the linear polarization by

$$\tan \alpha = \frac{Q}{U}, \quad (\text{C.19})$$

which can be calculated for \mathbf{S}_{in} , and also $\mathbf{S}_{out} = \mathbf{T} \cdot \mathbf{S}_{in}$.

- the usage of ideal mirrors, i.e. the mirror matrices are set to $\text{diag}(1,1,-1,-1)$. This corresponds to mirror reflectivities of 100 % regardless of the oscillation direction of the incoming light and no cross talk terms $Q \leftrightarrow U$.

The rotation of the defined polarization axis can be shown by the difference $\alpha_{in} - \alpha_{out}$. This has to be compared to the value of p predicted by Eq. (C.18). An example is displayed in Fig. C.2 for the date 21.07.02 and an azimuth setting of C1 of 50° for 8:00-18:00 UT. The remaining differences between theoretical value and the output from the modelized coelostat are of order of 0.005° and arise from the used numerical procedures.

- comparison with the results in Cap. et al., [3]:
 - symmetry properties: the matrix entries plotted in Fig. (C.3) for three dates show either a symmetric or antisymmetric course with regard to noon. The resulting pattern is in accordance with the properties given in Cap., [3], eq. (14).
 - telescope output for unpolarized input: Fig. C.1 displays the Stokes vector, which leaves the telescope optics according to the model for an unpolarized input. Comparing with Cap., [3], Fig. (9 a-c), which show measurements at the Donati Solar tower in Arcetri, one can see a similar range of values for the polarization content. The long-dashed curve is for an azimuth position of 40° on 21.07.02. The polarization created in the telescope increases, if the first mirror is moved away from the zero azimuth position.

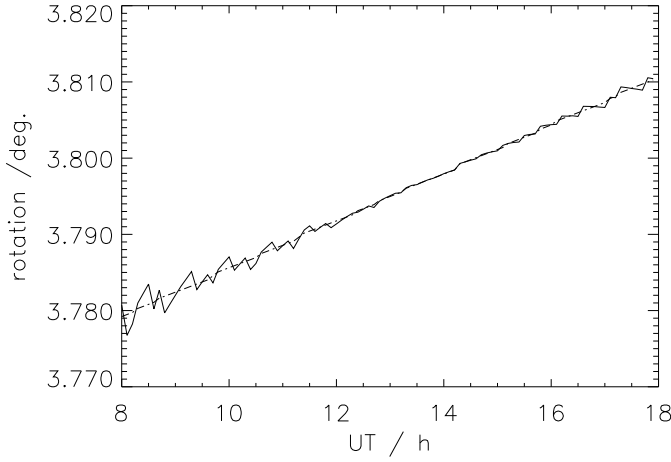


Figure C.2: Image rotation produced by the modelized coelostat in degrees.

Shown is the difference of the angles $\alpha_{in} - \alpha_{out}$ for the date 21.07.02 and an azimuth setting of C1 of 50° for 8:00-18:00 UT (solid line). The dash-dotted line is the prediction of Eq. (C.18) for the rotation angle. The increase of the rotation angle is caused by the changing declination of the sun.

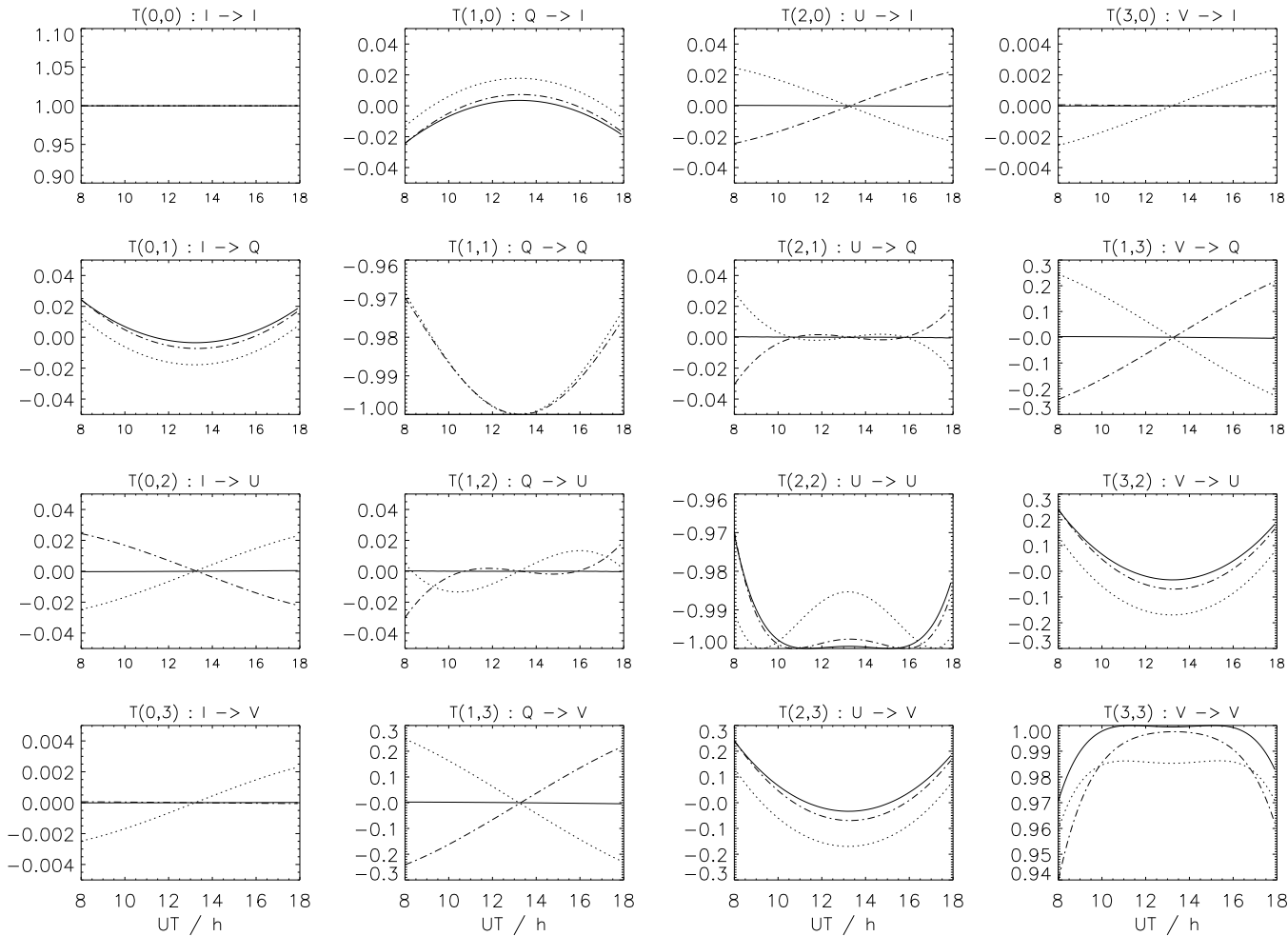


Figure C.3: Normalized telescope matrix for three dates.

The 16 entries of the telescope matrix resulting from the model are plotted for 8:00-18:00 UT. The azimuth of C1 was always set to 0° . (solid) 21.03.02, (dotted) 21.07.02, (dash-dotted) 21.01.02. The matrix entries are either symmetric or antisymmetric to noon. A comparison of absolute values is more difficult, as this depends on the parameter set used for the physical properties of the mirrors. The cross talk between different polarizations has contributions from geometrical effects (image rotation) and the mirror properties.

Appendix D

Technical characteristics

D.1 The grating

The optical design of the grating is a combination of an Echelle and a reflective Littrow configuration. As the entrance pupil with the central obscuration of the telescope is imaged onto the grating, the central part of the grating is not illuminated. This area is used for a small folding mirror that feeds the light beam to the collimator (cp. Fig. 4.2). The grating is slightly tilted about a horizontal axis and the imaging mirror is located above the collimator. The final image plane is formed above the grating. The configuration has only small reflection angles and thus a high optical quality across a large field of view.

Grating		
79 grooves / mm	blaze angle: 63.4°	dispersion: 12 pm/mm @ 400 nm
CCD		
652×488 pixels	12μ × 12μ pixel size	frame rate: max. 40 Hz
Modulator		
$\delta = 3/8\lambda$ @ 630 nm	$\delta = 5/8\lambda$ @ 400 nm	zero-order
Interference filters		
5 nm FWHM @ 630 nm	1 nm FWHM @ 400 nm	
Demodulation		
15 Hz frame rate	synchronized with retarder rotation	
Computer control		
PC-based with Windows NT		

Table D.1: Technical characteristics.

Appendix E

Many thanks to

In no special order:

Wolfgang Schmidt for the topic, the assistance during the work, the scientific background, etc.

My parents for their unlimited sponsorship all the time

Manolo Collados for his great patience, and a very important visit to Tenerife

Bruce Lites for his great patience, and the help in the calibration of the ASP data sets

Michael Sigwarth for exactly the same

Kai Langhans for the introduction into IDL

Thomas Kentischer for the work on POLIS, the opportunity to smoke inside, and his great patience

Tayeb Aiouaz for a great time, and much fun with negative pressure

Helmold Schleicher, Jo Bruls for the new calculations of formation heights - when only asked if the old values were correct

Carsten Baur, Stefan Henninger, Michael Engler for the weekly 'Skatrunde'

Everybode else I forgot

Appendix F

Zusammenfassung (in german)

In dieser Arbeit wird die Kalibration des neuen Spektropolarimeters POLIS beschrieben. Das Gerät resultiert aus einer Kooperation zwischen dem Kiepenheuer Institut für Sonnenphysik (KIS), Freiburg, und dem High Altitude Observatory (HAO), Boulder (USA). Es soll am deutschen Vakuum-Turm-Teleskop (VTT) des KIS in Teneriffa betrieben werden.

Das Gerät bestimmt den Polarisationszustand des Sonnenlichtes in zwei verschiedenen Wellenlängenbereichen bei 400 und 630 nm. Zur Messung wird eine rotierende Verzögerungsplatte verwendet, die den Polarisationszustand des einfallenden Lichtes moduliert. Durch einen polarisierenden Strahlteiler wird die modulierte Polarisation in eine Intensitätsmodulation umgewandelt. Die Demodulation zur Bestimmung des Stokes-Vektors erfolgt über ein gewichtetes Integrationschema.

Um eine ausreichende polarimetrische Genauigkeit von 0.1 % der Kontinuumsintensität zu erreichen, muss das eigentliche Messgerät kalibriert werden, um seine Antwort auf verschiedene Polarisationszustände festzustellen. Weiterhin muss die instrumentelle Polarisation des Teleskops bestimmt werden, die den Polarisationszustand des einfallenden Sonnenlichtes verändert.

Zur Kalibration des Polarimeters steht eine spezielle Kalibrationseinheit zur Verfügung, die aus einem Linear-Polarisator und einer Verzögerungsplatte besteht. Die Kalibrationseinheit wird sich innerhalb des Vakuumtanks des Teleskop befinden, wo der Strahldurchmesser des Lichtbündels bereits auf einen Durchmesser von 6 cm verringert ist. Mit dieser Einheit lassen sich durch Rotation der beiden optischen Elemente verschiedene bekannte Polarisationszustände erzeugen, die im Kalibrations-Datensatz gemessen werden. Aus einem Vergleich zwischen dem erzeugten Input und dem gemessenen Output lässt sich die Polarimeter-Antwort-Funktion \mathbf{X} durch einen Least-Square-Fit bestimmen. Mit dieser 4×4 -Matrix kann man aus dem eigentlichen Messwert den zutreffenden Stokes-Vektor der Polarisation am Ort der Kalibrationseinheit rekonstruieren.

Die vollständige Kalibration erfordert mehrere zusätzliche Datensätze. Um die Detektoreigenschaften der verwendeten CCD-Kameras zu bestimmen, werden Dunkelstrom- und Flatfield-Daten gewonnen. Aus diesen beiden Datensätzen lässt sich die Antwort der einzelnen Detektorpixel auf einfallende Intensität ermitteln. Diese Detektoreigenschaften werden in Gaintables für die jeweiligen Detektorbereiche gespeichert. Der eigentliche Kalibrations-Datensatz zur Bestimmung der Polarimeter-Antwort wird danach mit den Gaintables korrigiert, um die Detektoreigenschaften zu entfernen.

Die korrigierten Daten werden über die Wellenlängen gemittelt, da der polarimetrische Gehalt im Kalibrationsdatensatz konstant sein sollte. Entlang des Spaltes können jedoch durch Verunreinigungen oder räumliche Inhomogenitäten der Kalibrationseinheit Schwankungen auftreten. Deshalb wird die Antwort-Funktion an vier Positionen entlang des Spaltes durch eine Matrix-Inversion des linearen Problems $\mathbf{S}_{\text{out}} = \mathbf{X} \cdot \mathbf{S}_{\text{in}}$ bestimmt.

Um die Eigenschaften der Kalibrationseinheit zu erfassen, werden zusätzliche freie Parameter verwendet, wie z.B. die tatsächliche Verzögerung δ der Wellenplatte. Die Anwendung der inversen Polarimeter-Antwort-Funktion \mathbf{X}^{-1} auf Messdaten ergibt den tatsächlichen Stokes-Vektor des Lichtes am Ort der Kalibrationseinheit.

Der Strahlengang im Teleskop vor der Kalibrationseinheit umfasst vier Spiegel und das Eintrittsfenster des Vakuumtanks. Um die polarimetrischen Eigenschaften dieses komplexen optischen Systems zu bestimm-

men, werden die einzelnen Komponenten durch Mueller-Matrizen modelliert. Bei den Spiegeln benötigt man die spezifische Geometrie der Reflexion zur Berechnung der Spiegelmatrix. Die Mueller-Matrix des Spiegels ist jeweils nur in speziellen Koordinatensystemen gültig. Zur Berechnung des Gesamtsystems muss man daher sowohl die Spiegelmatrizen als auch die Koordinatentransformationen bestimmen.

Das Eintrittsfenster steht unter grossem Druck und kann deswegen spannungsinduzierte Doppelbrechung zeigen. Es wird als Verzögerungsplatte mit einer beliebigen, aber festen, Ausrichtung der Achse modelliert.

Das Teleskopmodell ergibt die polarimetrischen Eigenschaften des Systems durch Berechnung des jeweiligen Strahlenganges als Funktion folgender Parameter:

- Spiegel: Brechungsindex n , Absorptionskoeffizient k . Die beiden Coelostatenspiegel werden als gleich angenommen, ebenso Haupt- und Umlenkspiegel im Vakuumtank (insgesamt 4 Parameter)
- Fenster: Verzögerung, Ausrichtung der Achse (2)
- Ausrichtung der Kalibrationseinheit: zusätzliche Rotation am Ende des Strahlenganges (1).

Diese 7 Parameter werden aus Teleskop-Kalibrationsdaten bestimmt. Zu diesem Zweck steht eine drehbare Fassung zur Verfügung, in der Linear-Polarisatoren angebracht sind. Die Fassung kann auf dem ersten Coelostatenspiegel oder dem Eintrittsfenster befestigt werden. Durch eine Rotation um 180° lassen sich verschiedene linear polarisierte Zustände erzeugen. Der Polarisationszustand nach dem Teleskop wird mit dem kalibrierten Polarimeter bestimmt. Danach werden die Parameter im Teleskopmodell ebenfalls mittels eines iterativen Least-Square-Fits an die Messdaten angepasst.

Nach erfolgter Kalibration von Polarimeter und Teleskop lässt sich mittels

$$\mathbf{S}_{\text{solar}} = \mathbf{T}^{-1} \cdot \mathbf{X}^{-1} \cdot \mathbf{S}_{\text{gemessen}} \quad (\text{F.1})$$

der Stokes-Vektor des eingefallenen Sonnenlichtes aus dem Messergebnis bestimmen.

Im letzten Kapitel der vorliegenden Arbeit wird ein Datensatz eines bereits existierenden Vektorpolarimeters untersucht. Selbst bei dieser nur vorläufigen Auswertung lassen sich Phänomene wie der Evershed-Effekt in Sonnenflecken wiederfinden.

Glossary

chromosphere

the chromosphere is blue, until it turns grey at the borders of reality

convection / convective zone

energy transport mainly by mass movement

corona

the corona is the part of the sun most intensively revered in Bavaria by such immortal songs as 'Corona Bavariae, deep unter the stary night...'

differential rotation

the sun as a ball of gas does not behave as a solid body, so the rotation speed on the surface is different depending on solar latitude. The values range from 26 to 30 days on the poles

Doppler effect

The principal effect is a change of frequency if a source or an observer of radiation are moving relative to each other along their line-of-sight (LOS). In solar physics the Doppler effect is used to established the material movements on the sun by measuring the wavelength of *absorption* and *emission lines*, as the relative movement of earth and sun is known

flux tube

a magnetic flux tube is assumed to be a highly evacuated bundle of magnetic field lines held stable against the gas pressure from outside by the internal magnetic pressure of the increased magnetic field. The field strength rises to values of kG

granulation

the convective energy transport in the outer atmosphere leads to more or less stable convection cells. The pattern of the borders of these cells is called the *granulation*, while a single cell is called a *granule*. The material is supposed to rise up in the middle and flow down at the borders

line

emission \sim : light of a certain wavelength emitted by an electron transition between atomic energy levels, $E = h \cdot \nu = h \cdot \lambda/c$

absorption \sim : lowered intensity at a certain wavelength in a continuum spectrum caused by absorption and undirected reemission, in the sun the outer atmosphere produces the *Fraunhofer lines* in this way

magnetic

\sim **field** : the second component of the electromagnetic field, appearing in the sun on greater scale in the form of *sun spots* and smaller *flux tubes*, supposed to be produced by the *solar dynamo*

\sim **loops** : loops of magnetic field lines as suggested mostly in images taken in the H_{α} wavelength

\sim **reconnection** : the annihilation of magnetic field lines with antiparallel directions, supposed to take part on small scales and producing the energy visible in *flares* or other short time features, where a great amount of energy is set free

photosphere

the photosphere is green for the most part, at least where it's not red

plasma

ionized atoms lead to a gas of electrons and ions, which is highly conductive, a situation

prevalent almost everywhere in the sun

polarimetry

in general the measurement of the polarization state of light. Today polarimetry has a great number of applications in science (magnetic fields, saccharimetry, biology,...) and technics (stress tests, quality control of surfaces,...). In solar physics one can divide into vector polarimetry with measurement of the full *Stokes vector* and 'simple' polarimetry, using only one polarization state

pore

a small sunspot without any visible penumbra

quiet sun

region on the sun with no solar activity, i.e. no sunspots or flares, but only the diffuse small scale magnetic background

radiative core

in the inner regions of the sun the energy is transported mainly by radiation, whereas after a small transient zone the outer atmosphere is *convective*

resolution

spatial \sim : the distance which two for example intensity features must have at least on the sun to be detectable seperately

spectral \sim : the minimal distance in wavelength which can be separated

solar cycle

the changing of the polarity of the solar magnetic activity with a periode of about 11 years, coupled with the intensity of activity as can be seen in for example the number of sun spots. A theoretical description of the *solar dynamo* would have to include an explanantion of this fact

solar dynamo

the magnetic fields on the sun are supposed to be generated by the solar dynamo. It works on the mass movements of the ionized *plasma*, which constitutes a current and so gives rise to a *magnetic field*. The main factors are the *convective* movement caused by the radial temperature differences and the *differential rotation*. The exact working principle and for example the *solar cycle* are still far from being well understood

sun spot

larger area on the surface of the sun with lower temperature than the surroundings. The drop in temperature is caused by the *magnetic field*, which suppresses *convection*. Greater sun spots can be divided in the dark *umbra* and the brighter *penumbra*. Smaller spots without penumbrae are called *pores*

Stokes vector

the Stokes formalism developed by G.Stokes about 1850 gives an easy way to describe the polarization properties of light. It uses the four Stokes parameters to include all necessary information on the polarization state, which most times are grouped into the Stokes vector for convenience